Carbon-supported Pt-based alloy electrocatalysts for the oxygen reduction reaction in polymer electrolyte membrane fuel cells: particle size, shape, and composition manipulation and their impact to activity

Wang, Yan-Jie; Zhao, Nana; Fang, Baizeng; Li, Hui; Bi, Xiaotao T.; Wang, Haijiang

Publisher's version / Version de l'éditeur:
https://doi.org/10.1021/cr500519c
Chemical Reviews, 115, 9, pp. 3433-3467, 2015-04-15

CHEMICAL REVIEWS

Review

pubs.acs.org/CR

Carbon-Supported Pt-Based Alloy Electrocatalysts for the Oxygen Reduction Reaction in Polymer Electrolyte Membrane Fuel Cells: Particle Size, Shape, and Composition Manipulation and Their Impact to Activity

Yan-Jie Wang,[†,‡] Nana Zhao,[‡] Baizeng Fang,[†] Hui Li,[*,§] Xiaotao T. Bi,[*,†] and Haijiang Wang[*,§]

[†]Department of Chemical and Biological Engineering, University of British Columbia, 2360 East Mall, Vancouver, BC Canada V6T 1Z3

[‡]Vancouver International Clean-Tech Research Institute Inc., 4475 Wayburne Drive, Burnaby, Canada V5G 4X4

[§]Electrochemical Materials, Energy, Mining and Environment, National Research Council Canada, 4250 Wesbrook Mall, Vancouver, BC, Canada V6T 1W5

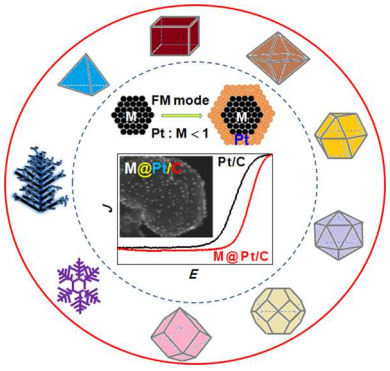

CONTENTS

1. INTRODUCTION

Global energy demands are projected to grow 36% over the current level by the year 2030.[1] Polymer electrolyte membrane fuel cells (PEMFCs) are among the most promising candidates for the reliable and efficient conversion of hydrogen, produced from fossil or renewable sources, into electric power in automotive, distributed power generation, and portable electronic applications on a large scale.[2−11] However, the large-scale implementation of fuel cell technology for use in commercial residential or transportation applications is hindered largely by the high cost associated with platinum-based electrocatalysts,[12,13] which account for over 55% of the total cost.[14] At the current stage of technology, Pt-based

Received: September 15, 2014
Published: April 14, 2015

DOI: 10.1021/cr500519c
Chem. Rev. 2015, 115, 3433−3467

nanoparticles,[15] which are usually supported on porous carbon particles, are the only electrocatalysts presently used in applied PEMFCs, since among all pure metals, platinum supported on carbon has the highest catalytic activity for the oxygen reduction reaction (ORR).[15−22] Therefore, intense research has been undertaken to improve the intrinsic activity of Pt-based electrocatalysts for the ORR to reduce the Pt loading of the electrodes without compromising fuel cell performance.

Alloying has become an attractive strategy to develop advanced Pt-based electrocatalysts,[23−29] in which the addition of another metal can form a Pt alloy[30] and thus alter the availability of active surface sites (the ensemble effect) or the binding strength of reactants, intermediates, products, and spectator species (the electronic and/or strain effect).[31] Research on advanced Pt-based alloy electrocatalysts has recently flourished, and a large number of research papers, as well as some review papers,[32−36] have been dedicated to the strategic improvement and development of high-performance carbon-supported Pt-alloy electrocatalysts, rather than traditional carbon-supported Pt electrocatalysts. It has been reported in the literature[37−46] that when bifunctional Pt-alloys were used as cathode catalysts, the best performance was achieved by alloying Pt with first-row transition metals;[37−40] adding a third element to the respective binary catalysts for both anode and cathode materials has been attempted to attain higher catalytic performance.[37,40−46] The enhanced catalytic activity resulted from the changes of physiochemical properties of Pt such as the change in Pt−Pt interatomic distance, the number of Pt nearest neighbors, the Pt 5d band vacancy, and the Pt-metal content on the particle surface.[40]

In the synthesis process, catalyst particle size, shape/morphology/nanostructure, and composition are critical factors for improving catalytic activity and stability.[33−35,47−49] In the past several decades, diverse experimental methods have been proposed to synthesize size-dependent, carbon-supported, Pt-based alloy nanoparticle catalysts in a variety of shapes, such as rod, wire, polyhedron, dendrite, dimmer, belt, star, and cage.[11] These experimental strategies have included (1) controlling the size of Pt-based nanocatalysts within a small range of 3−5 nm to yield a high electrochemical active area and catalytic activity, (2) controlling the shape of Pt-based catalysts to give more complex morphologies (e.g., a dendritic morphology), (3) obtaining high-index facets in nanocatalysts favoring high activity and stability for fuel cell applications, (4) designing controlled architectures (e.g., textured structure, such as core−shell, Pt skin, or Pt monolayer) for Pt-based catalysts, (5) developing new support materials with high conductivity, chemical stability, and surface area,[50,51] and (6) achieving a uniform distribution of Pt or Pt-alloy nanoparticles on advanced support materials with high conductivity.

This review addresses the current development of size-dependent, shape-selected, and composition-controlled carbon-supported Pt-alloy electrocatalysts for enhancing electrochemical catalytic performance in PEMFCs. It starts with an overview of carbon support in carbon-supported Pt-alloy electrocatalysts and then proceeds to the theoretical studies on the impact of Pt-alloy particle size, shape, and composition, and the experimental research on the particle size, shape, and composition of Pt-alloy catalysts, particularly strategies to control particle size, shape, and composition, and their impacts on catalyst activity toward the ORR. This review, by examining the most recent progress and research trends in both theoretical and experimental studies of carbon-supported Pt-based alloy electrocatalysts with uniform sizes, desirable shapes, and controlled compositions, provides a systematic and comprehensive survey of material selection, synthesis methods, structural characterization, and catalytic performance, with an emphasis on their relation to the size, shape, and composition of catalyst particles.

2. CARBON SUPPORT IN CARBON-SUPPORTED PT-ALLOY ELECTROCATALYSTS

To improve the catalytic activity, stability, and utilization of Pt-alloy catalysts, high surface area carbon black particles have been considered to be the best choice as the electrocatalyst support due to their large specific surface area favoring the dispersion of an active component, good electric conductivity, porous structure, and low cost.[3,21,52−55] The commonly used carbon support materials, along with some physical properties, are listed in Table 1.[56,57]

Table 1. Commonly Used Carbon Materials in PEMFC Electrocatalyst[a]

sample	suppplier	type of carbon	BET surface area ($m^2 g^{-1}$)[b]	DBP adsorption (units)[c]
Vulcan XC 72	Cabot Corp.	Furnace black	250	190
Black Pearls 2000	Cabot Corp.	Furnace black	1500	330
Ketjen EC300J	Ketjen Black International	Furnace black	800	360
Ketjen EC 600JD	Ketjen Black International	Furnace black	1270	495
Shawinigan	Chevron	Acetylene black	80	
Denka black	Denka	Acetylene black	65	165

[a]Reprinted with permission from ref 57. Copyright 2010 Elsevier B.V. [b]BET: Brunauer−Emmett−Teller method. [c]DBP: dibutyl phthalate number (measure of carbon void volume).

2.1. Interaction of Pt-Alloy with Carbon Support

Generally, Pt-alloy catalysts are deposited on nanostructured carbon support in order to increase the specific surface area, which is the prerequisite to obtain an acceptable catalytic performance.[58−60] The surface physicochemical properties and the structure of carbon materials play an important role on the activity and the stability of the resultant carbon supported Pt-alloy catalysts because the interaction between carbon and Pt-alloy can modify the physicochemical and electronic structure of Pt-alloy which in turn influences the catalytic activity and durability.[61−65]

In the research on carbon-supported Pt-alloy catalysts, more and more attention has been paid to the interaction between Pt-alloy and carbon support which affects the growth, the structure, and the dispersion of Pt-alloy nanoparticles on the carbon support[57,66−68] and is closely related to the size, shape, and composition of Pt-alloy nanoparticles. These effects and mechanism of interaction, vis-a-vis overall performance, need to be clearly understood to obtain highly catalytic electrocatalysts for PEMFCs. It is well-known that carbon support is not a mere inert material[69] and it can alter the system's Galvani potential, raise the electronic density in the catalysts, and lower the Fermi level, which favor the electron transfer at the electrode−electrolyte interface and thus accelerate the electrode processes.[57,70] In the carbon-supported Pt-alloy system, the

DOI: 10.1021/cr500519c
Chem. Rev. 2015, 115, 3433−3467

interaction generally results from the electronic effect of Pt-alloy clusters and carbon through electron transfer from Pt-alloy clusters to oxygen atoms adsorbed on carbon surface since the electron was found transferred from Pt microdeposits to carbon.[71,72] In many cases, chemical bonds can be formed due to the charge transfer between the contacting phases.

So far varous physical, spectroscopic, and electrochemical methods have been utilized to investigate the electron interaction effect of Pt-alloy nanoparticles with carbon support. Electron-spin-resonance (ESR) studies, for instance, clearly demonstrated electron donation by Pt to the carbon support.[73] This was further supported by X-ray photoelectron spectroscopy (XPS) studies that showed Pt as an electron donor to carbon and their interaction was dependent on the Fermi-level of electrons in both Pt and carbon.[74] Specifically in the XPS studies, the Pt $4f_{7/2}$ in the carbon-supported Pt system, in particular with the Pt size in the 1−2 nm range, tended to shift to higher binding energies with respect to that of unsupported Pt due to the Pt-carbon electronic effect.[75−78] Compared to the carbon-supported Pt, the carbon-supported PtRu was also studied by Antolini et al.[79] using XPS. They found a further shift to higher energy values for the Pt $4f_{7/2}$ of PtRu/C by 0.2−0.3 eV with respect to pure Pt/C because of an enhanced Pt-carbon interaction or smaller Pt particle size. They explained that the presence of Ru precursors and their decomposition could result in the acid−base properties of the carbon support, and then enhanced metal−support interaction with a change of electronic nature of the Pt sites. After the observation by using a combination of XPS, extended X-ray absorption fine structure (EXAFS), and ESR measurements on a carbon-supported PtRu system, Goodenough and Manoharan[80] concluded that the synergistic catalytic effect could be attributed to an intra-alloy electron transfer from Ru to Pt. McBreen and Mukerjee[81] performed Pt X-ray absorption near-edge structure (XANES) at 0.0, 0.24, and 0.54 V at the respective Pt L3 and L2 edge of Pt/C and PtRu/C catalysts. They found that alloying with Ru can cause electronic effects on the Pt such as an increase in the number of Pt d band vacancies and a decrease in the Pt−Pt distance. To understand and investigate the interaction between Pt-alloy and carbon support at atomic resolution structural level, electron microscopy studies such as field emission transmission electron microscopy (FETEM)[82] and probe corrected scanning transmission electron microscopy (pcSTEM)[83] were also performed on PtRu/C and Pd_3Pt_2/C, respectively. The result in the former evidenced that the carbon support may affect the geometry and electronic structure of Pt-alloy nanoparticles while the data in the latter showed that some disordered surface atoms, which can form a disordered shell over a corrugated crystalline core, are susceptible to atomic rearrangement at the carbon interface, and along with strong electronic binding of Pd to the 20−50 nm carbon particles, facilitate strong wetting on the carbon as evidenced by the acute contact angle (58−76°) formed at the particle−support interface. The strong wetting interaction for the alloy can modify the morphology of the particles at the metal−carbon interface, likely altering the alloy electronic structure and contributing to the 1.8 fold enhanced ORR activity over pure Pt.

It can be concluded from the discussion above that the electrons in a carbon supported Pt-alloy system have been proved to transfer not only within Pt-alloy, but also from Pt-alloy to carbon.[71−78] According to Bogotski and Snudkin,[84] however, the rise in electron density on Pt-alloy could be attributed to carbon support synergism on the basis of changes in the electronic state of Pt after its deposition, thus enhancing the electrocatalytic activity. Also, it should be noted that during supported Pt-alloy catalyst formation, Park et al.[85] evidenced the presence of the interaction between metal precursor and carbon support in the carbon supported Pt−Ru system. They found that the deposition and dispersion of Pt and Pt−Ru nanoparticles were largely dependent on the surface chemistry of carbon support, which was closely related to the anchorage of metal precursor ions (i.e., precursor−support interaction[86−90]) and nanoparticles.[88,89] At the same time, the solvent polarity can impose a significant influence on the deposition and dispersion of Pt−Ru nanoparticles on carbon support.[90]

2.2. Loading Methods of Pt-Alloy on Carbon Support

Carbon supported Pt-alloy catalysts in PEMFCs are highly sophisticated products made from chemicals by various preparation procedures. To some extent, the loading method of Pt-alloy on carbon support, coupled with the quality of the raw materials, can determine the catalytic properties of the final product.[91] The choice of loading method to prepare carbon supported Pt-alloy catalysts indeed depends on the physical and chemical characteristics desired in the final composition. It is reasonably understood that the loading method of Pt-alloy on carbon is also dependent on the choice of the base materials and experience shows that several ways of Pt loading can be considered in the preparation of carbon supported Pt-alloy catalysts, even for a given selection of the base material.[92,93]

In recent years, a number of approaches have been developed to synthesize nanoparticle based electrocatalysts. Accordingly, some useful loading methods have also been developed to load Pt-alloy catalysts onto carbon support.[94] Special emphasis has been placed on the high degree of control over shape, size, and dispersion of Pt-alloy particles on the carbon support. Of equal importance is to develop a reproducible low cost loading method that can be used for the production scale-up. What is more, the technical target in practical catalyst preparation is that the production of stable and robust catalysts can preserve their initial morphologies under fuel cell operation over long periods, in particular maintaining their narrow Pt-alloy particle size distribution, regardless of the technology used to load the Pt-alloy catalysts onto the carbon support. In fact, one established loading method in the procedures can provide a strategy which may be advantageous over others, depending on the end application of the catalyst and the instrumentation available.[93,94]

Currently, there have been some loading methods to prepare Pt-alloy supported on carbon for the PEMFC electrocatalyst application such as chemical precipitation, sol−gel, impregnation, colloidal, microemulsion, polyol method, microwave assisted polyol, electrodeposition, pulse electrodeposition, vapor phase method, sputter deposition technique, cationic exchange, sonochemistry and sonoelectrochemistry, ultrasonic spray pyrolysis, supercritical fluids, high energy ball milling, etc.[93,94] Typically, colloidal method is a simple Pt-alloy loading method similar to the chemical precipitation method in which with the addition of reducing agent such as $NaBH_4$ or hydrazine, PtM bimetallic alloyed nanoparticles can be directly reduced and coprecipitated on the carbon support.[95] In a typical colloid experimental procedure of carbon supported Pt-alloy, some starting materials such as the metal salt, a reducing agent, and a capping agent have to be mixed while carbon support is added before or after the formation of the Pt-alloy

DOI: 10.1021/cr500519c
Chem. Rev. 2015, 115, 3433−3467

particles. The capping agent can be used to control the size of Pt-alloy particles and thus prevent agglomeration of the particles. The production of Pt-alloy nanoparticles depends on reducing agents and experimental conditions (e.g., pH, reaction temperature, solvent, etc.). For example in the preparation of carbon supported PtRu/C catalyst, Watanabe et al.[96] clearly evidenced a formation of colloidal "PtO_2" from chloroplatinic acid (H_2PtCl_6) with the reduction of $NaHSO_3$ and oxidative decomposition with H_2O_2 at pH 5 in the first step. Then, a brown-colored colloid "RuO_2" was formed after $RuCl_3$ was added into the solution. Finally, H_2 was used to realize a complete reduction and the carbon-supported PtRu alloy was formed after the addition of carbon. Compared to the colloidal method, ultrasonic spray pyrolysis (USP)[3,97] is a novel way for loading Pt-alloy on carbon support. As seen in Figure 1,

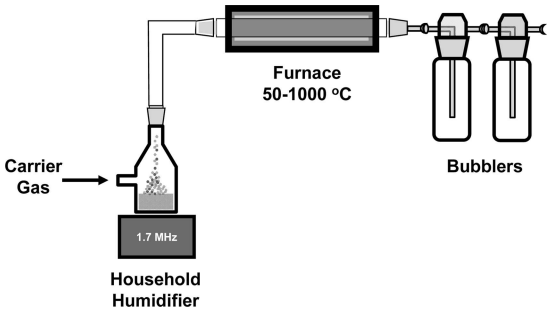

Figure 1. Ultrasonic spray pyrolysis (USP) experimental apparatus. Reprinted with permission from ref 97. Copyright 2007 American Chemical Society.

an aqueous solution with Pt precursor is atomized into a carrier gas that is passed through a furnace and then deposited onto a substrate, where it reacts and forms the final product.[97,98] There are many advantages in this process: (1) easy formation of alloys by manipulating the spray solution; (2) facile vacuum/high-purity target setup; (3) controlled deposition rates; (4) moderate operation temperatures; (5) low environmental impact on the process, and (6) favorable scale-up. It is noted that ultrasonic nebulizers[99] can be utilized to provide micrometer- and submicrometer-sized droplets, benefiting nanoscaled size and size distributions in the carbon supported Pt-alloy catalysts.

2.3. Impact of Carbon Support on ORR Activity

In current carbon-supported Pt (Pt-alloy) catalysts for PEMFC application, carbon support is well-known to play a key role in improving Pt utilization, ORR activity, and stability.[15] According to the requirements for electrocatalyst support,[3,100] the basic properties of carbon support are (1) high electrical conductivity, (2) high specific surface area and high porosity, (3) good interaction of support with Pt (Pt-alloy), and (4) easy Pt recycling in the used electrocatalyst.[101] Among various carbon supports, the correct selection of carbon material is one of primary importance to realize electrocatalyst application for the real commercialization of PEMFCs. The carbon support may not only modify the electronic character of the Pt-alloy[52] but also influence the shape and distribution of the deposited Pt-alloy particles.[102,103] It has been found that the specific surface area, pore size distribution, and surface properties of carbon material strongly influence the size, size distribution of Pt-alloy particles, surface structure and morphology, and alloying degree and therefore the structure and morphology of the catalyst, affecting the number of the active sites on the catalyst surface and thus ORR activity in PEMFCs.[94]

Much of the literature has reported the impact of carbon support on the electrocatalytic activity of the carbon supported Pt-alloy catalysts.[39,104−109] Limpattayanate and Hunsom[107] studied the effect of three carbon materials such as domestic Hicon Black (HB), multiwalled carbon nanotubes (MWCNT), and commercial Vulcan XC-72 on catalytic performance of carbon-supported Pt−Pd catalyst. HB, MWCNT, and Vulcan XC-72 had the BET surface area of 87, 117, and 217 $m^2\ g^{-1}$, respectively, while the oxygen surface groups followed the order of Vulcan X-72 (4.74 mEg g^{-1}) < HB (4.95 mEg g^{-1}) < MWCNT (5.03 mEg g^{-1}). With all three carbon-supported Pt−Pd catalysts being prepared by a seeding and impregnation method, the Pt−Pd/Vulcan XC-72 showed a better catalyst dispersion, smaller particle size (~6.78 nm), a higher Pt:Pd ratio (49.6:50.4), and the highest ORR activity under the PEM fuel cell testing condition. They concluded that the specific surface area of the support as well as the oxygen surface groups affected the particle size and dispersion and catalytic performance. Gamez et al. also studied the effect of Vulcan XC-72R as a support in comparison with graphite material (e.g., HSAG 300 Lonza) for Pt−Pd nanoparticles.[109] It was concluded that Vulcan carbon provided significantly higher active surface area probably due to a good interaction of Pt−Pd with Vulcan than with HSAG even though the later had a higher surface area than the former.

2.4. Impact of Carbon Support on Catalyst Stability

Inspite of the positive impact of carbon on the catalytic activity, the reported oxidation of carbon support may cause a severe sintering/agglomeration of Pt-alloy nanoparticles under long-term fuel cell operation[110,111] and thus the decrease of electrocatalytic surface area, resulting in the degradation of catalyst and the decrease of catalytic activity and fuel cell performance.[3,112−115] The detailed degradation mechanisms[116,117] revealed the transportation of Pt ions through liquid and/or ionomer and the transportation of electrons through carbon support, respectively. Pt supported carbon particles are prone to degradation during fuel starvation due to the reaction ($C + 2H_2O \rightarrow CO_2 + 4H^+ + 4e^-$) while the oxidation of carbon is catalyzed by the presence of Pt.[118] The carbon support can be converted to CO_2 and Pt may be lost from the electrode, leading to loss of fuel cell performance. Also, catalyst sintering or agglomeration is another problem for the reduction of fuel cell durability because the catalyst sintering could reduce the electroactive surface area of the Pt catalyst, lower the Pt utilization, and degrade its catalytic activity.[115] It has been the durability issue of the PEMFC electrocatalyst with a carbon support that has been one of the most important challenges hindering PEMFC commercialization. Therefore, there have been some research efforts in developing novel supports that are more durable than carbon by using composite support or ceramic support.[51] However, this review only focuses on the assessment of carbon-supported Pt-based alloy electrocatalysts.

3. THEORETICAL STUDIES

Catalysts used for theoretical studies are dominated by spherical Pt or Pt-alloy nanoparticles supported on standard or graphitized carbon black, including conventional homogeneous Pt and Pt transition-metal alloy nanoparticles[13,116,117,119,120] and designer nanoparticles with controlled

DOI: 10.1021/cr500519c
Chem. Rev. 2015, 115, 3433−3467

particle size, shape, composition, and spatial distribution to increase activity and reduce Pt loading.[121,122] It has been reported that carbon-supported Pt alloy can achieve at least two to four times greater ORR activity compared to Pt/C catalysts, due to a positive shift in the onset potential for OH_{ads} formation on the alloy catalyst.[13,123−126] Theoretical studies revealed that size, shape, and composition of the Pt-alloy catalytst particles are three critical factors that contribute to the improvement of ORR activity.

3.1. Impact of Pt-Alloy Particle Size on ORR Activity

Carbon-supported Pt-alloy catalysts, in the form of nanoparticles, can provide much higher surface area for the reacting molecules in an electrochemical reaction. Moreover, the Pt-alloy nanoparticle is often in a crystalline form, with the metal atoms located in a variety of configurations, such as steps, kinks, edges, and corners.[127−130] Using density functional theory (DFT) as a research approach, Nørskov et al.[131,132] demonstrated theoretically that electrocatalytic activity was significantly affected by nanoparticle size. They found that, with increasing particle size, the catalytic rate per surface site of Au particles sharply increased, whereas a decrease was observed for Pt particles as the particle size decreased. This difference resulted from a volcano-shaped relationship between electrocatalytic activity and the electronic state of the atoms. In Pt alloys, Pt tends to congregate in the first layer and then be induced to form a surface strain, which strongly influences its reactivity, depending on the type of transition metal(s) in the alloy.[133]

To improve catalytic performance and consequent enhancement of ORR activity, Jacob and Goddard III[134] used highly dispersed particles rather than extended surfaces, because those particles provided, overall, a larger reactive surface area for simultaneous catalytic reactions. The improved reactivity of nanoparticles was believed to be closely related to particle properties such as the quantum size effect for small particle sizes or polymorphic particle shapes.[135,136] The catalyst surface was related to different surface faces connected via step edges or kinks, probably resulting in different catalytic reactivities. Using DFT as a research tool to handle rather small system sizes (around <100 atoms) in the modeling, they found a more structured potential energy surface for binding on the alloy surface than on pure Pt, which could lead to higher localization of the adsorbents. Also, a strong overlap was examined on the preferred surface sites for O_2 and H_2 as representatives of charge-donating and charge-accepting adsorbents, respectively. Both aspects might play a role in enhancing the overall ORR activity. They thought that the highly dispersed catalysts including Pt-alloy catalysts were more useful in practical industrial applications than the semi-infinite surfaces because the catalysts can provide a larger surface area in which the catalytic reaction can run simultaneously with higher activities. The size of these catalyst particles might range from <1 to 5 nm in diameter, which is strongly dependent on the catalytic effect of extended surfaces on those nanoparticles.[134]

3.2. Impact of Pt-Alloy Particle Shape on ORR Activity

Since the majority of electrocatalytic reactions are structure-sensitive or site-demanding, it is imperative to fundamentally understand the relationship between the structure or shape of nanomaterials and their electrocatalytic properties.[137−140] However, in contrast to the growing number of studies on the correlation between the size of spherical nanoparticles and their catalytic activity, very little theoretical work has been conducted to evaluate the effects of nanoparticle shape on ORR activity since these structures are not easily accessible.

Mophology control plays a key role in developing high-performance catalysts with unique physical and chemical properties as reported in the literature.[141−146] These nanostructures often correspond to a precise particle shape and controlled particle size, with different surface areas and crystallographic facets. The catalytic performance of Pt-based catalysts was found to be dependent on their crystal facets.[147] Well-defined shapes of Pt-based nanocatalysts can mimic the catalytic property of the bulk metal but exhibit superior catalytic activity due to the manipulation of crystal facet[147,148] that allow the fine-tuning of both the selectivity and the reactivity for many major catalytic reactions, so as to achieve high catalytic performance.[149−152] According to proposed mechanisms such as the uniform sphere model[153] and the hydrocarbon catalysis model,[154] shape as one of the most important surface properties is strongly related to designed crystal facets which can provide a large number of active sites located at the edges or corners of a rough Pt surface and enhance the material's catalytic activity, Wang et al.[155] reported the 5- and 9-fold enhancement of ORR activity for the Pt monolayer on Pd and Pd_3Co cores. Their density functional theory calculations (DFT) using a nanoparticle model revealed the effect of nanosize-induced surface contraction on facet-dependent oxygen binding energy. The moderately compressed {111} facets were most conducive to ORR on small nanoparticles, which could result in the compressive strain effect and thus enhance the ORR activity. In addition, it is suggested that a nanostructure with high-index facets exhibits higher catalytic activity than common nanostructures with low-index facets because more atoms are added at the former's steps, edges, and kinks.[148,156−158]

As mentioned earlier, there have not been enough theoretical studies to clearly disclose the ORR enhancement mechanism for the shape-controlled and/or facet-dependent Pt-alloy catalysts. In fact, shape-controlled Pt-alloy catalysts are much more complicated and challenging than Pt catalysts for the theoretical studies and the experimental preparation and characterization. In the experimental sections of this review, some typical shapes such as core−shell, Pt monolayer/skin, and crystal facet will be discussed on the enhancement of ORR activity for carbon-supported Pt-alloy catalysts. However, there is a lack of theoretical studies with regard to these shapes.

3.3. Impact of Pt-Alloy Composition on ORR Activity

To date, many carbon-supported Pt-alloy catalysts (PtM/C, M = Co,[159,160] Ni,[161] Cu,[159] Fe,[162−164] Cr,[165] Au,[166] Pd,[167,168] W,[169] etc.) have been successfully synthesized. With the addition of a metal (M), the Pt content in the catalyst decreases, as does the cost of materials. The formation of Pt-alloying can result in two key changes favorable to the enhancement of Pt-alloy catalysts. One is that the alloying of Pt might change the electronic properties of Pt while the other is that the adsorption properties of Pt may be altered by alloying Pt, which is closely related to ORR.[133] However, the relationship between electrocatalytic activity and alloy composition in Pt-alloy catalysts does not follow a simple monotonic trend, since the concentration of different alloying elements can substantially affect the catalytic performance due to the resulting changes in intrinsic properties (e.g., electronic structure and surface segregation).[147,170]

DOI: 10.1021/cr500519c
Chem. Rev. 2015, 115, 3433−3467

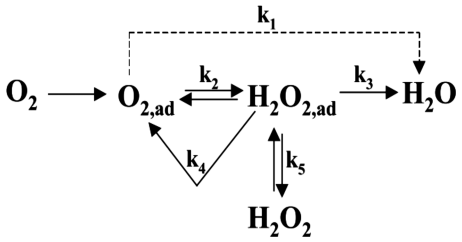

Figure 2. Reaction schemes proposed for the ORR by Wroblowa et al. O_2 can be electrochemically reduced either directly to water with a rate constant of k_1 without the formation of intermediate $H_2O_{2,ad}$ (so-called "direct" $4e^-$ reduction) or with a rate constant k_2 ("series" $2e^-$ reduction). The adsorbed peroxide can be electrochemically reduced to water, with a rate constant k_3 ("series" $4e^-$ pathway), catalytically (chemically) decomposed on the electrode surface (k_4), or desorbed into the bulk of the solution (k_5). Reprinted with permission from ref 245. Copyright 2001 Wiley Interscience.

To understand theoretically the effect of Pt-alloy composition on ORR activity, Paulus et al.[171] calculated theoretical atomic densities for two selected carbon-supported PtM alloy catalysts (M = Ni, Co) with fixed atomic ratios of Pt to M (3:1 and 1:3, respectively) and a total metal content of 20 wt %. After the comparison of theoretical atomic densities and the experimentally determined active surface areas, they found that the difference in alloy composition and the corresponding hydrogen adsorption pseudocapacitance indeed influenced the number of Pt surface atoms and the surface composition. Using the analysis of temperature-dependent oxygen reduction Tafel plot, they obtained the activation energies for the ORR on carbon-supported Pt-alloy catalysts in 0.1 M $HClO_4$, as presented in Table 2,[171,172] and revealed the following order

Table 2. Activation Energies for the ORR on Carbon-Supported Pt-Alloy Catalysts in 0.1 M $HClO_4$[a]

		activation energy	
catalyst	potential (V)	kJ/mol	eV
Pt/C	0.93	21	0.22
Pt_3Ni/C	0.93	24	0.25
PtCo/C	0.93	24	0.25
Pt_3Co/C	0.93	25	0.26
Pt/C	0.88	20	0.21
Pt_3Ni/C	0.88	22	0.23
PtCo/C	0.88	28	0.29
Pt_3Co/C	0.88	28	0.29
Pt/C	0.83	23	0.24
Pt_3Ni/C	0.83	26	0.27
PtCo/C	0.83	24	0.25
Pt_3Co/C	0.83	26	0.27

[a]From the work of Paulus et al.[171] Reprinted with permission from ref 172. Copyright 2005 American Chemical Society.

of increasing catalytic activity: Pt/C < Pt_3Ni_1/C < Pt_3Co_1/C < Pt_1Co_1/C. This clearly suggested that the Pt alloy's composition substantially affected its ORR activity.

To further examine the correlation between Pt-alloy composition and electrocatalytic activity, Wang et al.[170,173] followed the materials' compositional evolution and the formation of Pt-skeleton nanostructures, using atomic-level microscopic analysis of the compositional profiles and modeling of the nanoparticle structures. Differences in the Pt-alloy composition affected the structure and thus resulted in different properties, as the researchers revealed through studying Pt_xNi_{1-x}/C alloy catalysts. Using Monte Carlo simulations, they monitored structural changes in simulated 5 nm PtNi particles during Ni dissolution on the surface (see Figure 3).

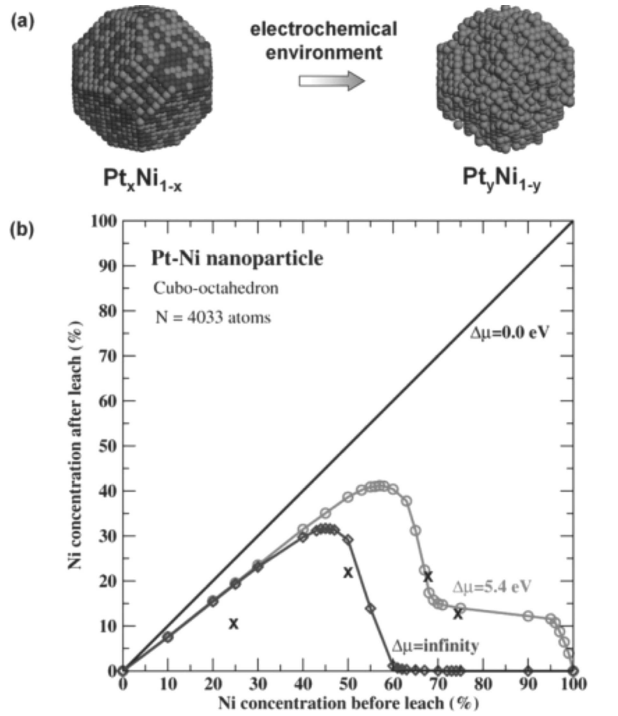

Figure 3. Monte Carlo simulation of the nanostructure evolution of PtNi NPs in an electrochemical environment. (a) Initial and final cofigurations of the PtNi NP. The simulated NP has a cuboctahedral shape and contains 4033 atoms (~5 nm) in the initial configuration. In the final configuration, the Ni atoms exposed to the electrochemical environment have been dissolved, forming a Pt_yNi_{1-y} ($y > 0.5$ here) NP. (b) Calculated Ni concentration in the final configuration of the Pt–Ni NP, under the assumption that the dissolution of Ni atoms is driven by a chemical potential of $\Delta\mu$ at $T = 300$ K. The symbol "x" in the figure marks the results from experiments. Reprinted with permission from ref 173. Copyright 2011 Wiley Interscience.

They found that the catalytic properties were determined by the thickness of the Pt skeleton layer, which depended on the initial composition of the Pt-bimetallic alloy catalysts.[173] The intermediate composition with a Pt:Ni ratio of 1:1 exhibited the highest ORR activity (see Figure 4).[170] Matanović et al.[174] also selected three different Pt–Ni alloys—Pt_3Ni_1, Pt_1Ni_1, and Pt_1Ni_3—to study the correlation between structure, reactivity, and stability using periodic DFT calculation. They found that the catalytic activity for Pt–Ni alloys increased in the order of Pt < Pt_3Ni_1 < Pt_1Ni_3 < Pt_1Ni_1, and they also confirmed that the Pt–Ni alloy catalyst with an atomic ratio of 1:1 had the maximum ORR activity. They assumed that the improved catalytic activity of this Pt–Ni alloy catalyst was due to the modification of the electronic structure of the platinum atoms on the surface, induced by a specific distribution of nickel atoms in the layers directly below.

It should be noted that, in many cases, some mismatches exist between the theoretical and experimental studies on the ORR activity of carbon-supported Pt-alloy electrocatalysts. For instance, the theoretical studies conducted by Paulus et al.[171] with the atomic ratio of Pt:Co from 3:1 to 1:1 showed that the catalytic activity increased in the order of Pt_3Co_1/C < Pt_1Co_1/

DOI: 10.1021/cr500519c
Chem. Rev. 2015, 115, 3433–3467

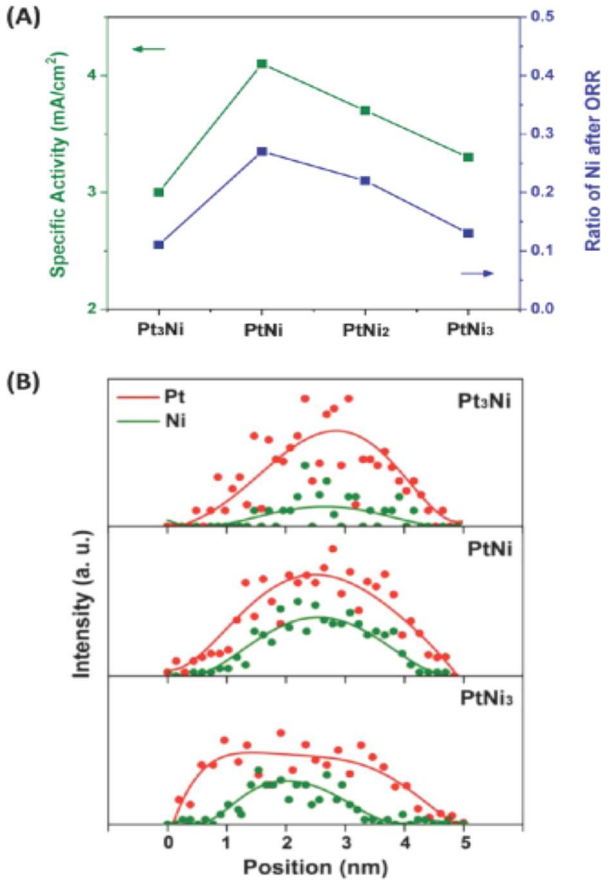

Figure 4. Composition dependence of Pt alloy electrocatalysts. (A) The dependence of ORR catalytic activity and the ratio of Ni preserved after electrochemical measurements on the initial alloy composition for Pt_xNi_{1-x}/C nanocatalysts. (B) Composition line profiles for Pt_xNi_{1-x}/C nanocatalysts after ORR measurements. Reprinted with permission from ref 170. Copyright 2012 American Chemical Society.

C while the experimental results[175] in Strasser's group exhibited the reverse activity order: Pt_1Co_1/C < Pt_3Co_1/C. Another example was the carbon-supported Pt−Ni electrocatalyst. The theoretical results from Matanović et al.[170,174] showed higher ORR activity for the Pt:Ni ratio of 1:1 than the Pt:Ni ratio of 3:1 but the experimental results from Sung's group[176] revealed that the ORR activity order was Pt_3Ni_1/C > Pt_1Ni_1/C. These mismatches basically resulted from the differences in research conditions between the theoretical and experimental studies. Therefore, it is important to check the experimental conditions while comparing theoretical with experimental studies. The detailed discussion on the experimental studies of carbon-supported Pt-alloy electrocatalysts will be presented below.

4. EXPERIMENTAL STUDIES ON THE CONTROL OF CARBON-SUPPORTED PT-ALLOY PARTICLE SIZE

4.1. Importance of Particle Size and Distribution

Some of the most important challenges in synthesizing carbon-supported Pt-alloy nanoparticles are the diverse nucleation and growth rates of different elements, which are directly related to the formed nanoparticle size and size distribution, and thus to ORR activity.[177,178] Typically, the reduction of the Pt precursor (e.g., platinum acetylacetonate, $Pt(acac)_2$) occurs faster than that of some 3d transition metals such as Mn, Fe, Ni, Co, and Cu, in the synthesis of carbon-supported Pt-alloy particles because Pt has a much higher reduction potential ($Pt^{2+} + 2e^- \leftrightarrow Pt$, $E^0 = +1.2$ V) than 3d transition metals ($E^0 = -0.2 \sim -0.4$ V).[170] As a result, the precious metal is prone to nucleate first and grow into separate nanoparticles or form Pt-rich regions in the product.[179,180]

In fact, multiple factors can affect the size of Pt-alloy nanoparticles formed in solution during the crystal nucleation and growth process. In the synthesis of carbon-supported Pt-alloy nanoparticles, nucleation can be induced by increasing temperature, adding a precursor, and adding a secondary metal precursor.[177,181−184] According to Lamer's plot,[181] both a fast nucleation step and gradual growth on formed nuclei can result in a monodispersed and homogeneous alloy nanomaterial, which is particularly advantageous for the synthesis of Pt-alloy nanoparticles with high catalytic activity.[180,185−190]

In a conventional nucleation and growth process, some metal atoms, which form through either the reduction of metal precursors or bond breakage in compounds, collide to produce small, thermodynamically unstable clusters and then dissolve before they reach a critical radius or form thermodynamically stable nuclei by overcoming a critical free energy barrier. These latter nuclei grow into nanoparticles by consuming free atoms in solution or in unstable small clusters.[191−193] According to classical nucleation theory, three key variables control the rate of nucleation: temperature, surface free energy, and degree of supersaturation.[12] High surface free energy results in large critical radius and high critical free energy, which creates serious difficulty for the formation of clusters and nuclei in nucleation. High reaction temperature and a high degree of solute supersaturation (i.e., the ratio of saturation solute concentrations to equilibrium solute concentration) can accelerate nucleation.[194−196] For colloidal synthesis, the degree of supersaturation varies throughout the nucleation and growth stages and can be described as a function of reaction time.[181] Separation of the nucleation and growth steps is critical to prepare homogeneous nanoparticles. "Burst nucleation", i.e., forced nucleation occurring in a very short period of time, is the most effective strategy for the synthesis of highly uniform nanoparticles using a colloidal chemical approach.[181,193,197,198]

4.2. Approaches to Control Particle Size

A broad size distribution and relatively large particle size will lead to nonuniform chemical composition among alloy nanoparticles and thus decrease the catalyst's ORR activity.[199] Therefore, an appropriate particle size, especially 2−5 nm, is of key importance for Pt-alloy catalysts to achieve high ORR activity in PEMFCs.[121,200] However, it is not easy to control particle size and size distribution, since very small particles (<2 nm) are significantly prone to agglomeration or corrosion under practical synthesis conditions. Recently, much research has been devoted to developing various new methods to reduce Pt-alloy size and narrow down particle size distribution to enhance catalytic performance, including thermal evaporation in a vacuum, electron-beam lithography and pulsed laser deposition, buffer-layer assisted growth, chemical vapor deposition, gas condensation, ionized cluster beam deposition, electrochemical deposition, sol−gel or colloidal techniques, deposition−precipitation and impregnation, and the use of molecular cluster precursors.[201] In these methods, protective agents, heat treatment temperature, reactant composition, and pH are the critical factors in controlling the size and morphology of synthesized nanoparticles.[4,21,25]

DOI: 10.1021/cr500519c
Chem. Rev. 2015, 115, 3433−3467

4.2.1. Protective Agents. In general, protective agents are used to stabilize nanostructured colloidal metal and prevent agglomeration.[202−204] The two main mechanisms for stabilization against aggregation[205,206] are shown in Figure 5.

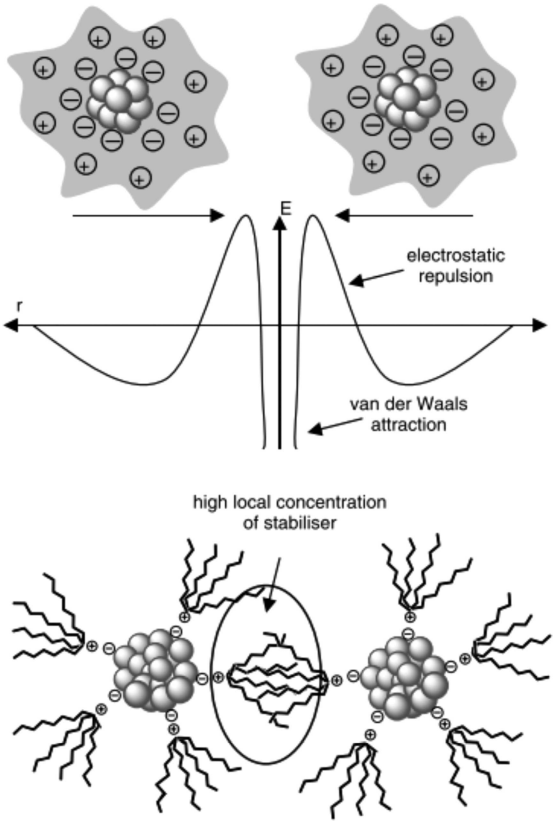

Figure 5. (A) Electrostatic stabilization of nanostructured metal colloids, (B) steric stabilization of nanostructured metal colloids. Reprinted with permission from ref 205. Copyright 2008 Wiley Interscience.

Electrostatic stabilization is one of the mechanisms: the attraction of van der Waals forces is counterbalanced by the repulsion of the Coulomb forces acting between the negatively charged colloidal particles (see Figure 5A).[206] Some typical ionic protective agents include sodium acetate (SA), citric acid (CA), citrate, tetraoctylammonium bromide (TOAB), adecyltrimethylammonium bromide (CTAB), dodecyldimethyl (3-sulfo-propyl) ammonium hydroxide (SB12), sodium bis(2-ethylhexyl) sulfosuccinate (AOT), sodium dodecyl sulfate (SDS),[21] triton X-100, oleic acid, and oleylamine (OAM). Steric stabilization is the other mechanism (Figure 5B),[205] which can be achieved by the coordination of sterically demanding nonionic surfactants or polymers that produce strong repulsion between particles and droplets as protective shields on a metallic surface. The main types of protective agents for steric stabilization are polymers (e.g., poly(*N*-vinyl-2-pyrrolidone); poly(vinyl alcohol); *N*-dodecil-*N*,*N*-dimethyl-3-amino-1-propan sulfonate; Pluronic F127); P, N, and S donors (e.g., phosphanes, amines, thioethers); solvents such as THF, THF/MeOH, and propylene carbonate; long-chain alcohols; surfactants; and organometallics.

Jeon et al.[207] investigated the effect of SA on the particle size of 40 wt % Pt_1Ni_1/C catalyst. They prepared the catalyst using a borohydride reduction method in anhydrous ethanol solvent, with a molar ratio of SA to total metal of 22:1. Figure 6 shows TEM images of the catalyst before and after heat treatment at

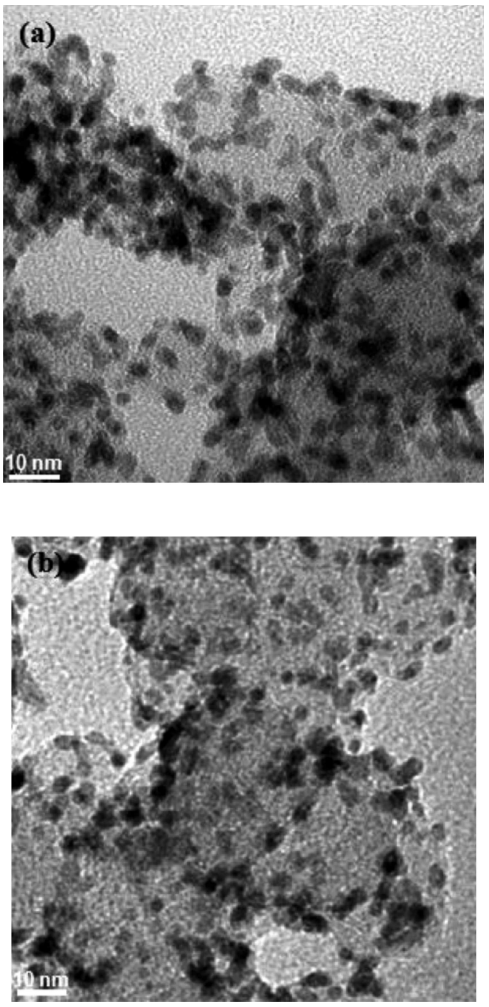

Figure 6. TEM images of 40 wt % Pt_1Ni_1/C catalyst (A) as-prepared sample and (B) sample heated for 3 h in Ar atmosphere. Reprinted with permission from ref 207. Copyright 2009 American Chemical Society.

300 °C for 3 h under Ar atmosphere. The average size of the obtained Pt−Ni particles was approximately 3.4 nm, regardless of heat treatment, since 300 °C was not sufficient to sinter carbon-supported Pt−Ni alloy nanoparticles and thus resulted in incomplete alloying (~35%). It should be mentioned that as a stabilizer, SA was helpful in protecting the formed nanoparticles, which had a controlled size and shape, as no marked changes in their shape or size were observed during the TEM analysis after heat treatment.

Compared to SA, CA is well-known for its dual functions as a reducing and stabilizing agent in nanocolloidal chemistry.[208−210] In particular, the three carboxyl anions of CA can be adsorbed onto the surface of metal particles and exert either hydrophobic or Coulombic effects on the particles, thereby stabilizing nanoparticles.[211] So far, various carbon-supported Pt-alloy catalysts have been successfully synthesized with CA as a stabilizer, including PtCo, PtCu, and PtAu.[212−216] Rao et al.[212] utilized CA as a stabilizer to investigate its effect on the size of 40 wt % Pt_xCo_y/C catalysts with different Pt:Co atomic ratios of 1:1, 2:1, 3:1, and 4:1. In the presence of citric acid, a

DOI: 10.1021/cr500519c
Chem. Rev. 2015, 115, 3433−3467

series of Pt_xCo_y/C catalysts were prepared by borohydride reduction method. Based on the Debye−Scherrer equation,[217] all catalysts showed an average size of 6.0 nm. No size difference was found for various catalysts due to the identical conditions maintained during the preparation procedure.

To understand the effects of different stabilizers on Pt-alloy size, Kim et al.[218] employed SA, OAM, TOAB, and CTAB as stabilizing agents to synthesize 40 wt % Pt_3Co_x/C electrocatalysts via a borohydride reduction method in an argon atmosphere at room temperature. They found that the particle sizes of 40 wt % Pt_3Co_x/C were smaller than those of commercial 40 wt %Pt/C; when the amount of stabilizer was 15 times the total moles of Pt and Co, the order of sizes was commercial (3.3 nm) > SA-15 (2.7 nm) > TOAB-15 (2.5 nm) > OAM-15 (2.2 nm). In the case of CTAB, the amount of stabilizer was 25 times the total moles of Pt and Co (designated CTAB-25) and yielded a synthesized particle size of 2.2 nm. In addition to the effects of stabilizing agents, Kim et al.[218] also studied the effect of heat treatment temperature on particle size. The optimum heat treatment temperature for each stabilizer was determined by temperature-programmed reduction from 30 to 1000 °C at a heating rate of 5 °C/min. After the heat treatment, XRD spectra (see Figure 8A,B) indicated that the sizes of most of the particles had grown substantially, from 2.7 to 10.6 nm (SA-15), 2.2 to 7.6 nm (OAM-15), and 2.5 to 5.0 nm (TOAB-15). However, the size of the CTAB-mediated Pt_3Co_x/C catalyst increased only slightly from 2.2 to 2.8 nm, because it had a lower annealing temperature of 250 °C, at which agglomeration was not induced. The TEM results in Figure 7C show that the CTAB-mediated Pt_3Co_x/C catalyst has a narrower size distribution, with maximum counts at 2.5 nm, compared to commercial Pt/C, whose particle size ranges from 1 to more than 5 nm, with maximum counts at 2.5−3.5 nm. It was thus concluded that CTAB is the most appropriate stabilizer for the fabrication of the Pt_3Co_x/C catalyst because the dispersion of Pt−Co particles on the carbon support is much more uniform than in a commercial Pt/C catalyst.

Poly(*N*-vinyl-2-pyrrolidone) (PVP) is a linear polymer that has been used as a typical protecting agent, via steric stabilization, against the agglomeration of metal colloids by forming a complex with metal ions before the reduction reaction occurs.[219] For example, Wu et al.[220] employed PVP as a stabilizer in combination with different additives (benzoic acid, aniline, or potassium bromide) to prepare a series of water-soluble carbon-supported Pt−Ni nanocrystals with different shapes, e.g., octahedron, truncated octahedron, and cube corresponding to the use of benzoic acid, aniline, and potassium bromide, respectively. They found that the Pt−Ni nanocrystals with three different shapes showed different average particle size of 11.8, 12.5, and 16.1 nm, respectively. Generally, particle size can be well controlled by tuning the concentration of the polymer stabilizer:[221,222] the better the stabilization effect (i.e., the higher the PVP concentration), the smaller the metal particles. However, some polymers, including PVP, bind too strongly bound to the nanoparticle surface to be removed, which can result in decreased catalytic performance.[222] Therefore, it is necessary to completely get rid of the polymer (stabilizer) in practical fabrication.

4.2.2. pH Control. In addition to the use of protecting agents, pH control is another strategy that can help to control particle size in the synthesis of Pt-based nanoparticle catalysts.[223,224] Fang et al.[4] developed a homogeneous deposition (HD) strategy for the synthesis of carbon-supported

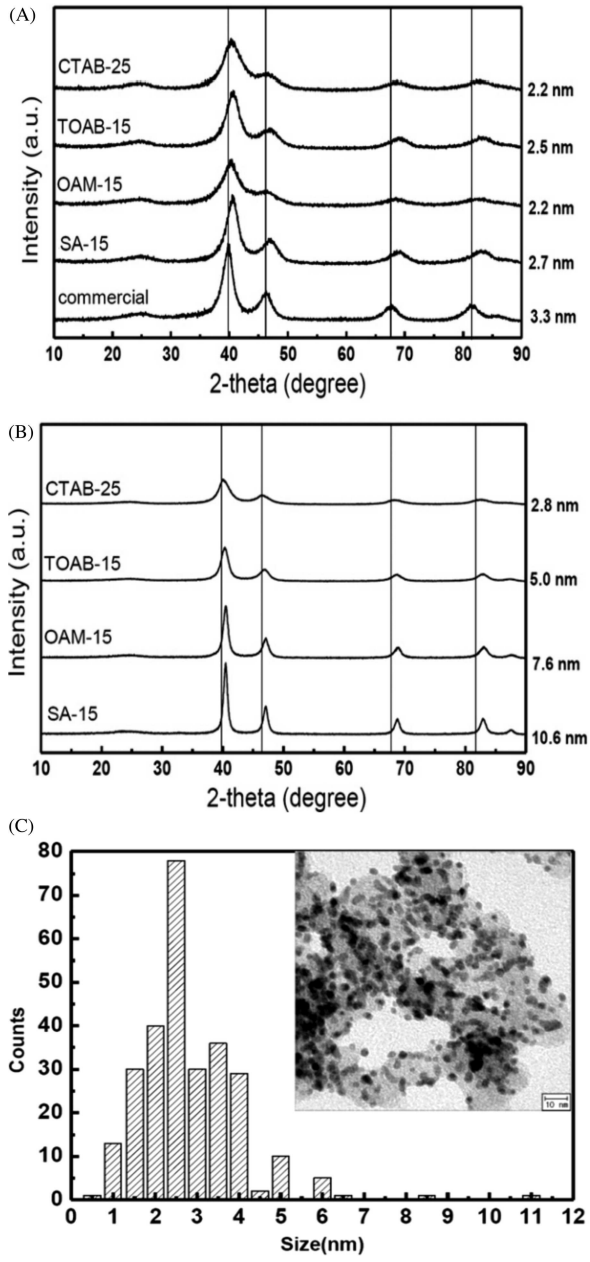

Figure 7. (A) XRD spectra for as-prepared Pt_3Co_x/C catalysts, (B) XRD spectra for heat-treated Pt_3Co_x/C catalysts, (C) particle size and TEM images for heat-treated CTAB-mediated Pt_3Co_x/C catalysts. Reprinted with permission from ref 218. Copyright 2011 Elsevier B.V.

Pt nanoparticles, in which a gradual increase in pH was realized by in situ hydrolysis of urea. As a result, a Pt complex species with small particle sizes was uniformly deposited onto the carbon support. A subsequent uniform reduction of the deposited Pt complex species by ethylene glycol (EG) in a polyol process gave further control over the size and dispersion of Pt nanoparticles. It was found that when the amount of urea in the starting Pt-salt aqueous solution was increased the size of the Pt complex species decreased, as did that of the metallic Pt nanoparticles, as shown in Figure 8. The decrease in the size of the Pt complex species was attributed to two factors: the steric contraction effect, resulting from the substitution of H_2O and/or Cl^- by OH^-, which reduced the ionic radius of the Pt complex species; and the electrostatic charge repulsion effect, which limited the growth of the Pt complex species with more

DOI: 10.1021/cr500519c
Chem. Rev. 2015, 115, 3433−3467

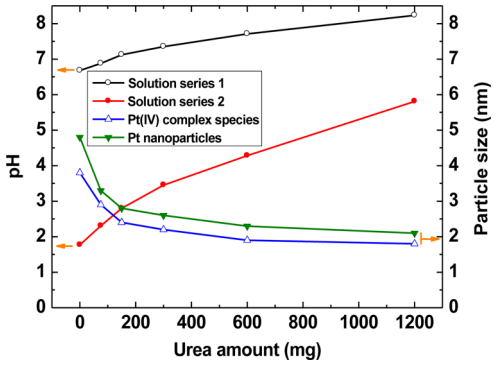

Figure 8. pH values and sizes of Pt(IV) complex species and metal nanoparticles versus amount of urea added. Solution series 1: urea-carbon solutions. Solution series 2: Pt(IV)-urea-carbon solutions. Reprinted with permission from ref 4. Copyright 2009 American Chemical Society.

negative charges. Kim et al.[25] employed an HD strategy to synthesize carbon-supported 40 wt % Pt−Ru catalysts under various initial pH conditions. They reported that the initial pH value in the starting solution had a significant influence on the Pt−Ru alloy particle size. With an initial pH of 9−10, the supported Pt−Ru catalyst had the smallest particle size.

Rusnaeni et al.[225] employed 1, 5, 10, and 25 mL of NaOH to adjust the pH of a metal precursor reduction solution to 7, 10, 12, and 13, respectively, in an EG-assisted polyol approach to prepare 30 wt % PtNi/C catalyst. Figure 9 shows the effect of

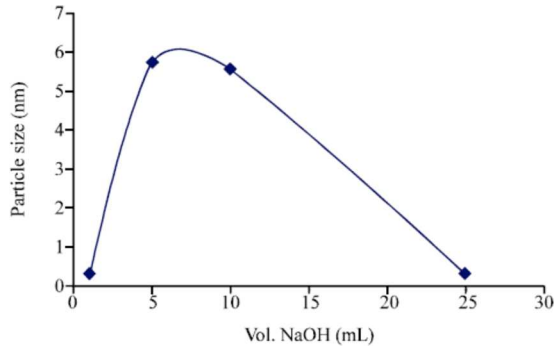

Figure 9. Effect of pH on particle size of prepared 30 wt % PtNi/C catalysts. Reprinted with permission from ref 225. Copyright 2010 Asian Network for Scientific Information.

pH variation on particle size. The largest improvement in particle size reduction was observed in a pH range of 7−10. It was concluded that the glycolate anion concentration determined the process of nucleation and growth.[225,226] The formation step of nucleation was too slow to match the growth step because the glycolate anion concentration was too low at a pH of around 7. A consistent nanoparticle size was achieved in a pH range of 10−12 due to the good balance between the formation and growth steps. However, at a pH of around 13, the nanocrystal growth stopped. In comparison with carbon-supported Pt−Ni alloy nanoparticle catalysts made by the polyol approach, a carbon-supported core−shell Pt−Co alloy catalyst that had been prepared via reduction reaction and subsequent electrolysis deposition was also found to be sensitive to pH. Table 3 compares the properties of various PtCo/C catalysts (prepared in pH 4.0, 2.5, and 1.5, respectively) and those of Pt/C.[227] It is evident that, with a decrease in pH, the size of the Pt−Co alloy particles increased from 2.5 to 3.1 nm. It has thus been proven that pH is a key factor influencing the particle size of synthesized Pt-based nanoparticle catalysts.

4.2.3. Composition. Composition is one of the most important factors affecting the size of as-synthesized Pt-alloy particles.[208,226−230] The size of binary Pt alloys is closely related to the type of the second metal.[231] It was observed that the addition of Fe (at atomic ratios of Pt to Fe from 3:1 to 1:6) could effectively prevent Pt particles from agglomerating and decrease the particle size of Pt−Fe/C from 4.4 to 3.2 nm, based on the Pt (220) diffraction peak in XRD spectra. In particular, Pt−Fe nanoparticles made with a Pt to Fe atomic ratio of 1:6 had a size distribution in the range of 2−6 nm, even after heat treatment at 900 °C under H_2/Ar atmosphere. Recently, Strasser et al.[175] synthesized a series of PtCo/C nanoparticle catalysts with 28.2 wt % Pt loading through a freeze-drying method, followed by annealing at 250 °C for 2 h and at 800 °C for 7 h under a 4 vol % H_2/96 vol % Ar atmosphere. When a high surface area carbon (HSAC) was used as the support, they found that the particle size of the PtCo/C alloy increased from 3.6 to 4.0 nm as the Co to Pt ratio decreased from 3:1 to 1:3 (see Figure 10). However, for a group of dealloyed Pt_xNi_{1-x}/C (D-Pt_xNi_{1-x}/C) nanoparticle catalysts,[232] it was discovered that the D-Pt_xNi_{1-x}/C catalyst displayed the smallest particle size (~4.7 ± 0.7 nm) among three Ni-rich dealloyed core−shell catalysts (D-PtNi/C, D-$PtNi_3$/C, and D-$PtNi_5$/C), as shown in Figure 11. These results suggest that Ni content has a strong influence on Pt−Ni alloy particle size. Notably, increasing the proportion of the second metal does not monotonically reduce the size of Pt-alloy nanoparticles; their size also often depends on the reaction conditions (e.g., the synthesis method and heat treatment), in addition to the type of second metal and its content.

4.2.4. Heat Treatment. Heat treatment has been extensively studied as a means of controlling particle size in the synthesis of various carbon-supported PtM (M = V, Co, Fe, Ni, Cu, Ti, Pd, and Cr) alloy catalysts.[233] The role of heat treatment is mainly to assist alloy formation by increasing the mobility of the supported Pt. However, high-temperature heat

Table 3. Comparison of the Properties of Various PtCo/C (Nominal Ratio 1:3) and Pt/Catalysts[a]

catalyst	pH	particle size[b] (nm)	lattice parameter (Å)	Pt−Pt interatomic distance (Å)	metal loading[c] (%)	Pt:Co (real atomic ratio)[d]	specific activity, j_k (mA/cm^2_{Pt})
PtCo/C	4.0	2.5	3.881	2.744	17.4	1:2.8	0.555
PtCo/C	2.5	2.6	3.849	2.722	16.3	1:2.2	0.894
PtCo/C	1.5	3.1	3.920	2.770	11.2	9:1	0.497
Pt/C		2.5	3.931	2.780	22.1		0.230

[a]Reprinted with permission from ref 227. Copyright 2010 Elsevier B.V. [b]Estimate from XRD data using Scherrer formula. [c]Determined by TGA analysis without any correction. [d]Based on EDX analysis.

DOI: 10.1021/cr500519c
Chem. Rev. 2015, 115, 3433−3467

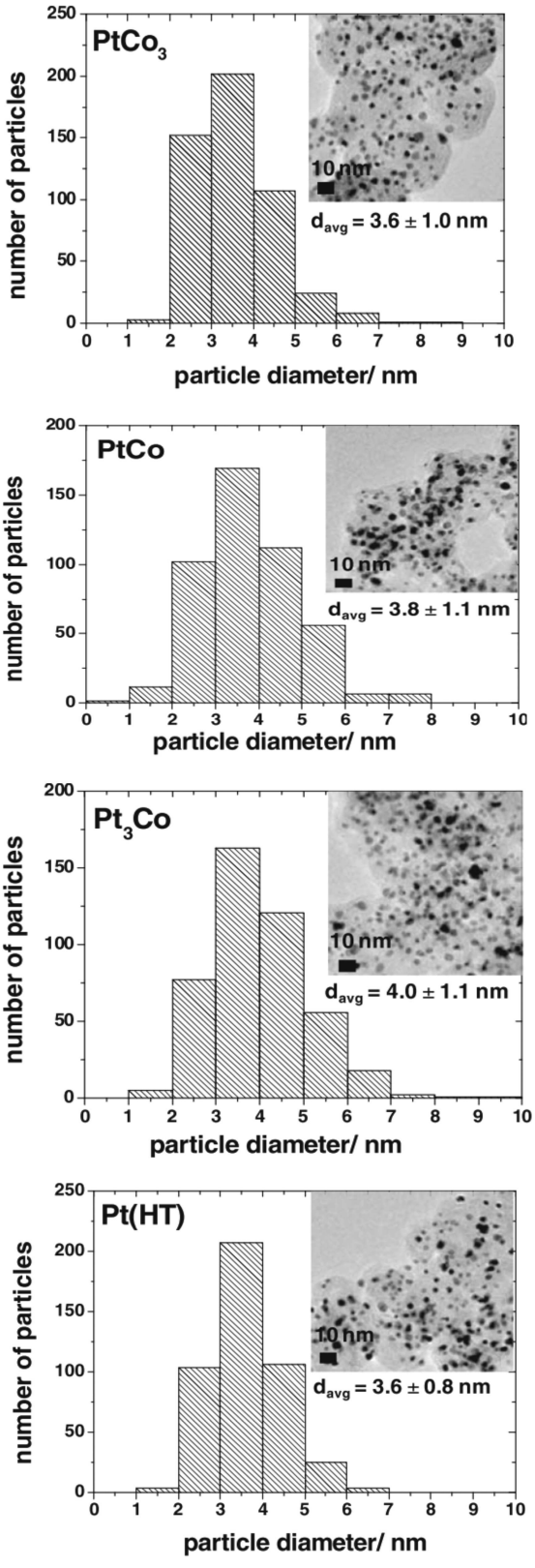

Figure 10. Histograms of particle size distribution and corresponding TEM images for as-synthesized $PtCo_3$, PtCo, and Pt_3Co alloy nanoparticles. The average particle size (d_{avg}) was determined from TEM images by counting more than 400 particles. Reprinted with permission from ref 175. Copyright 2012 The Electrochemical Society.

treatment can cause agglomeration of particles, reduction of specific surface area, and broadening of particle size

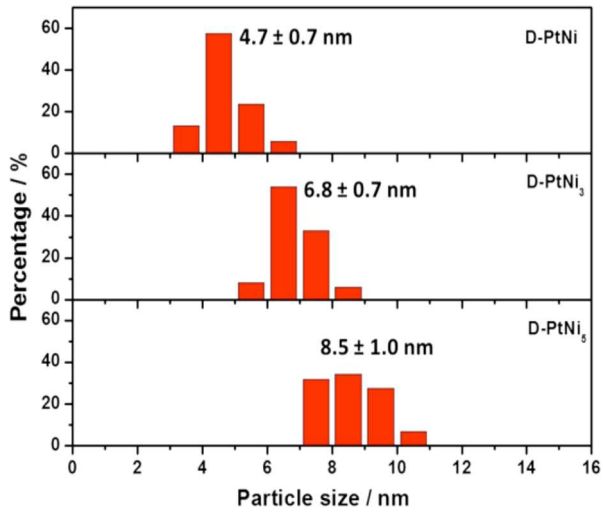

Figure 11. Particle size distribution for D-Pt_xNi_{1-x} nanoparticles supported on carbon. Reprinted with permission from ref 232. Copyright 2012 American Chemical Society.

distribution.[234−236] Table 4 summarizes the effect of heat treatment on the particle size, lattice constant, and alloying degree of various reported carbon-supported PtM alloy catalysts.[39,55,159,237−243] Obviously, the particle size considerably increases with the heat treatment temperature. The degree of alloying is found to be dependent on the lattice constant and is also a function of the treatment temperature, while the lattice constant decreases with increasing temperature. Therefore, the degree of alloying can be controlled by adjusting the heat treatment temperature, even though high temperature may increase the particle size. It should be noted that the effect of heat treatment temperature on lattice constant and particle size is often intertwined with the synthesis methods and conditions. For example, heat-treated PtCo/C alloys prepared at a pH of around 2 exhibited bigger particles sizes, more ordered structure, and greater alloying degree than those prepared at a pH of around 11 using a physicochemical method.[238]

4.3. Effect of Particle Size on ORR Activity

It is well-known that the mass activity of a catalyst for the ORR is inversely proportional to the particle size, while the specific activity is assumed to be independent of the particle size.[244] To establish a fundamental connection between the ORR activity and the particle size of Pt-based alloys, Marković et al.[245] started with two model electrode systems, Pt single crystal and Pt-based bimetallic surfaces, in which particle size was coupled with the corresponding particle shape. According to their proposed ORR mechanism (see Figure 2),[246] the significant improvement in the ORR within Pt-based alloy systems primarily resulted from the inhibition of Pt−OH formation on Pt surrounded by "oxide"-covered Ni and Co atoms beyond 0.8 V. The intrinsic activity of Pt for the ORR of supported Pt-alloy catalysts depended on both particle size and shape.[247,248] In addition, the effect of particle size on the ORR kinetics was related to the specific adsorption of Nafion polymer electrolyte in the catalyst electrode. Ultimately, they reported that, compared to the PtNi alloy, the PtCo alloy was a promising catalyst for the ORR due to two reasons: (i) the amount of Pt may substantially be reduced (by ca. 25−50%) and (ii) the activity can be significantly improved after alloying. Pt modified with pseudomorphic Pd metal film was the best catalyst for O_2 reduction in alkaline solution.[116,171]

DOI: 10.1021/cr500519c
Chem. Rev. 2015, 115, 3433−3467

Table 4. Effect of Heat Treatment on Structural Parameters of Reported PtM/C Catalysts[a]

no.	second metal (M) in Pt-M/C (Pt:M)	heat-treatment conditions	treatment temperature/time period (T (°C)/t (h))	particle size[b] (nm)	lattice constant (Å)	crystal structure	alloying	year, refs
1	V (1:1)	as-prepared furnace (Ar/H_2)		3.4	3.8834		22	2002, 237
			500/2	3.9	3.8800		25	
			800/2	5.4	3.8686	fcc, Pt_2V	33	
2	Co (3:1)	furnace (N_2/10% H_2)	600/2.5	3.83	3.855	fcc, Pt_3M		2000, 55
			700/2.5	2.95	3.876		61[c]	
			900/2.5	6.60	3.866		79[c]	
			1100/2.5	8.63	3.868		75[c]	
3	Cr (3:1)		700/2.5	4.23	3.903		39[c]	
			900/2.5	6.23	3.884		78[c]	
			1100/2.5	10.4	3.883		81[c]	
4	Ni (3:1)		700/2.5	4.62	3.858		53[c]	
			900/2.5	6.35	3.841		70[c]	
			1100/2.5	10.2	3.836		75[c]	
5	Co[d] (3:1)	as-prepared furnace		3.4	3.925			1990, 238
			700/2	8.4	3.870	fcc, Pt_3Co		
			900/2	8.0	3.867			
			1200/2	12.0	3.864	Fcc, Pt_3Co		
6	Co[e] (3:1)	as-prepared furnace		<2.5	3.927			
			700/2	2.5	3.894			
			900/2	4.1	3.907			
			1200/2	10.4	3.910			
7	Co (3:1)	furnace (H_2)	550/3	3.9	3.911		7	2004, 239
			900/3	6.8	3.897		35	
8	Co (3:1)	as-prepared		1.8	3.501		79	2007, 240
		furnace (H_2)	400/2	9.6	3.90			
		furnace (air/H_2)	200/1 (air)+300/1 (H_2)	8.3	3.90			
9	Co (5:1)	as-prepared furnace ($Ar/10\%H_2$)		3.6				2002, 241
			200/1	4.9				
			900/1	6.6				
10	Cu (3:1)	as-prepared furnace ($Ar/10\%H_2$)		4.7	3.86	fcc, Pt_3Cu		2006, 242
			300/1	6.9	3.86			
			600/1	17.1	3.88			
			900/1	29.6	3.85			
11	Fe (1:1)	as-prepared furnace ($Ar/10\%H_2$)		6.2	3.848(1)	Tetragonal		2005, 159
			500/1	6.3	3.847(1)			
			600/1	6.5	3.845(2)			
			800/1	6.8	3.848(1)			
12	Co (1:1)	as-prepared furnace ($Ar/10\%H_2$)		5.5	3.782(1)			
			650/1	5.8	3.780(2)			
13	Ti[f]	as-prepared furnace (He)		4.8	3.926			1986, 243
			700/2	11.0	3.916			
			900/2	12.5	3.907	Pt_3Ti		
			1200/2	14.4	3.906	Pt_3Ti		
14	Ti[f]	as-prepared furnace (He)		<4.0	3.927			
			700/2	5.0	3.922			
			900/2	7.0	3.922			
			1200/2	28.0	3.908	Pt_3Ti		

[a]Surface area measured by CO chemisorption. [b]Measured by XRD. [c]According to ref 39. [d]Acidic route: $Co(OH)_2$ + HCl (pH 2). [e]Alkaline route: $Co(NO_3)_2$ + NH_4OH (pH 11). [f]Methanol: water solution (1:1) [f]Methanol: water solution (1:1), pH 10.

Carbon-supported PtM bimetallic catalysts alloyed with various transition metals, such as Co, Ni, Cu, Fe, V, Cr, Zr, Mn, Ag, W, etc., have been extensively studied, and it has been found that the ORR activity of PtM is at least twice that of pure Pt.[13,171,249−254] Jayasayee et al.[254] prepared a series of PtM/C (M = Co, Ni, and Cu, 10 wt % Pt) alloy catalysts using an annealing treatment under a H_2/Ar atmosphere at 350 and 900 °C, respectively. They found that the annealing temperature significantly influenced the alloying phase and the particle size, thus improving the electrocatalytic activity (see Table 5). They also found that a dealloying process during electrochemical measurement with 0.5 M $HClO_4$ led to decreased particle sizes close to 3 nm, and as a result, the PtM/C catalysts exhibited 3−4.5 times higher mass activity than pure Pt/C. They concluded

DOI: 10.1021/cr500519c
Chem. Rev. 2015, 115, 3433−3467

Table 5. Compositional, Structural, and Morphological Analyses of Carbon Supported PtM (M = Co, Ni, and Cu) Catalysts[a]

catalyst (EDS based composition	anneal. temp. (°C)	Pt:M composition, XRD	lattice constant, a (Å)	crystallite size, d_{XRD} (nm)	particle size fresh, d_{TEM} (nm)	particle size aged, d_{TEM} (nm)
Pt/C	350	100:0	3.92	2	2.3 ± 0.8	6 ± 3
Pt/C	600	100:0	3.92	6	4 ± 1	7 ± 2
Pt/C	950	100:0	3.92	13.8	9 ± 2	11 ± 3
$Pt_{75}Co_{25}/C$	350	81:19	3.85	4.3	3 ± 1	7 ± 2
$Pt_{75}Co_{25}/C$	950	81:19	3.85	7.2	6 ± 2	7 ± 2
$Pt_{20}Co_{80}/C$	350				4 ± 2	9 ± 2
$Pt_{20}Co_{80}/C$	950	15:85/-	3.58/3.54	9.2	9 ± 2	10 ± 2
$Pt_{75}Ni_{25}/C$	350	100:0/60:40	3.92/3.75	3.5/5.4	3 ± 1	
$Pt_{75}Ni_{25}/C$	950	80:20	3.84	8.3	10 ± 1	11 ± 3
$Pt_{50}Ni_{50}/C$	350	100:0/60:40	3.91/3.75			
$Pt_{20}Ni_{80}/C$	350	50:50/0:100	3.72/3.52	5.7/13		
$Pt_{20}Ni_{80}/C$	950	12:88/-	3.57/3.53	13	8 ± 3	9 ± 3
$Pt_{75}Cu_{25}/C$	350	81:19	3.86	3	3 ± 1	8 ± 2
$Pt_{75}Cu_{25}/C$	950	77.5:22.5	3.85	9.2	10 ± 3	10 ± 3
$Pt_{15}Cu_{85}/C$	350	$Fm\bar{3}m$ 23:77	$Fm\bar{3}m$ 3.68	5.4/6	6 ± 1	7 ± 2
		Pm-3m 10:90	Pm-3m 3.64			
$Pt_{15}Cu_{85}/C$	950	Pm-3m 10:90	Pm-3m 3.64	11.7	8 ± 1	8 ± 3

[a]Reprinted with permission from ref 254. Copyright 2012 Elsevier B.V. d_{XRD} of HiSPEC 4000 (40%Pt on Vulcan XC-72R) = 4.5 nm.

Table 6. Particle Size, Mass Activity, Coulombic Charges (Qw, Qs), and Pt Surface Area (Scv) for Pure Pt and PtM Catalysts[a]

				Coulombic charge (C/g Pt)			
no.	catalysts	particle size (Å)	mass activity (A/g Pt)	Qw[b]	Qs[b]	Qs/Qw	Pt surface area (Scv)[c] (m^2/g Pt)
1	PtV	36	40.9	73.0	38.4	0.520	53.5
2	PtCr	38	61.0	92.0	55.0	0.598	70.0
3	PtMn	48	37.1	74.3	38.6	0.520	53.8
4	PtFe	45	56.2	93.0	55.0	0.591	70.5
5	PtCo	39	44.0	95.1	44.7	0.470	66.6
6	PtNi	37	51.0	85.4	47.0	0.550	63.0
7	PtCu	43	31.2	70.4	31.1	0.442	48.3
8	PtZr	38	42.8	88.6	41.8	0.472	62.1
9	PtAg	60	34.0	93.9	38.4	0.409	63.0
10	PtW	63	33.9	84.2	35.5	0.422	57.0
11	Pt	31	29.1	83.8	36.1	0.431	57.1

[a]Calculated from the current measured at 0.8 V after the oxygen reduction test for 140 min. [b]Qw; 80−180 mV, Qs; 180−400 mV, CV conditions; scan rate = 30 mV/s, scan from 50 mV to 1000 mV in 2.5 M H_2SO_4 at 25 °C. [c]Calculated from the sum of Qw and Qs with 210 $\mu C/cm^2$.

that the catalyst with a particle size less than 3.5 nm displayed the lowest mass activity among the synthesized catalysts, showing about 1.5 times higher mass activity than Pt. In addition to evaluating the catalyst activity of these PtM/C catalysts in relation to particle size, they also examined their durability through a scan test of 1000 cyclic voltammograms (CVs) and analyzed particle sizes before and after. It was observed that for both Pt and Pt alloys particle size was significantly greater after the durability tests.

Watanabe's group[255] synthesized a series of carbon-supported PtM (M = V, Ni, Cr, Co, and Fe) catalysts with a Pt:M atomic ratio of 50:50 using a nanocapsule approach. Specifically, the catalysts were prepared by the simultaneous reduction of platinum acetylacetonate and the second metal acetylacetonate within nanocapsules formed in diphenyl ether in the presence of carbon black. The PtM alloy particles were found to be highly dispersed on carbon black and had a narrow particle size distribution (2.0−2.5 nm), regardless of the catalyst loading (which ranged from 10 to 55 wt % on carbon black). The area-specific ORR activities of Nafion-coated PtM/C catalysts in O_2-saturated 0.1 M $HClO_4$ solution were found to be 1.3 to 1.8 times higher than that of Pt/C, with the ORR activity increasing in the order of Pt/C < PtNi/C < PtFe/C < PtCo/C < PtV/C < PtCr/C.

Sung et al.[253] prepared a series of Pt_3M/C (M = V, Cr, Mn, Fe, Co, Ni, Cu, Zr, Ag, and W) catalysts with a relatively large particle size (ranging from 3.8−6.3 nm) via an impregnation method with subsequent heat treatment at 900 °C for 2 h. In contrast to Pt/C catalyst, whose maximum mass activity was normally obtained with particle sizes around 3.5 nm,[256] all the PtM/C catalysts Sung's group synthesized exhibited higher mass activity than Pt/C, as shown in Table 6. They speculated that the amount of the Coulombic charge of strongly adsorbed hydrogen (Qs) was affected by the particle size as well as by the amount of an certain active plane (i.e., the (100) plane);[55] the catalytic activity of Pt bimetal alloys for the ORR was correlated with the Pt site that was responsible for the strongly adsorbed hydrogen in the cyclic voltammogram.[257]

To reduce the Pt loading without compromising the catalyst's performance, some noble metals, such as Pd and Ru, have been applied to synthesize Pt-noble metal alloys instead of Pt-transition metal alloys. The use of Pd is of interest since, first, it is at least 50 times more abundant on the earth than Pt and, second, it is in the same family as Pt in the periodic

DOI: 10.1021/cr500519c
Chem. Rev. 2015, 115, 3433−3467

Table 7. Typical Shapes of Pt Alloy Nanoparticles Supported on Carbon[a]

no.	metal precursor	reducing agent	surfactant	additive	synthesis condition	Pt alloy	shape	year, refs
1	K_2PtCl_4, $CoCl_2$	$NaBH_4$	TOAB	pH	RT	Pt_1Co_1	C/S	2010, 227
2	$PtCl_4$, $CuCl_2$	hydrazine, H_2			800 °C/6 h under 7%H_2	Pt_1Cu_1	C/S	2010, 281
3	$H_2PtCl_6{\cdot}6H_2O$, $CoCl_2{\cdot}6H_2O$	$NaBH_4$, EG	PVA, PVP	NaOH	reflux, 1 h	Pt_3Co	C/S	2013, 282
4	H_2PtCl_6, nickel(II) acetate	1,2 PDO, $NaBH_4$	oleic acid, PVP	NaOH	reflux, 2 h	$PtNi_2$	C/S	2012, 283
5	H_2PtCl_6, $HAuCl_4$	$NaBH_4$	decanethiol oleylamine		280 °C, 300−800 °C	$Pt_{100-n}Au_n$	C/S	2010, 284
6	$H_2PtCl_6{\cdot}2H_2O$, $AgNO_3$	$NaBH_4$, EG	sodium citrate	KOH	90 °C/4h	Pt_1Ag_1	C/S	2012, 285
7	$Pt(acac)_2$, $Ni(acac)_2$	oleylamine	oleylamine, oleic acid	$W(CO)_6$	130 °C, 230 °C	Pt_3Ni_1	C and O	2010, 286
8	$Pt(acac)_2$, $Ni(acac)_2$, $Fe(acac)_3$, $Co(acac)_2$, $Pd(acac)_2$,	CO	oleylamine, oleic acid	1-adamantan, acetic acid,	210 °C under CO	Pt_xM_y (M=Ni, Co, Fe, Pd)	C and O	2011, 287
9	$Pt(acac)_2$, $Ni(acac)_2$	TBAB, hexadecanediol	amines	ACA	190 °C/1 h	Pt_3Ni_1	TO	2010, 288
10	$Pt(acac)_2$, $Ni(acac)_2$	DMF			200 °C/24 h	Pt_3Ni_1, Pt_1Ni_1	C, CT; O, TO	2012, 289
11	$Pt(acac)_2$, $Ni(acac)_2$	CO, H_2			200 °C	$Pt_{1.5}Ni_1$	O	2014, 290
12	$Pt(acac)_2$, $Ni(acac)_2$, $HAuCl_4$, $Pd(acac)_2$,	CO	oleylamin (OAm), oleic acid (OA)		210 °C	Pt_3Ni_1, Pt_3Pd_1, Pt_1Au_1	ICO	2012, 291
13	K_2PtCl_6, palladium nitrate	$NaBH_4$	octadecylamine, dodecyltrimethylammonium bromide	H_2SO_4	RT	Pt-monolayer/Pd	NW, C/S	2011, 292
14	H_2PtCl_6, $NiCl_2$	oleylamine			240 °C, 280 °C	Pt_xNi_{1-x}	C, concave T	2014, 293
15	$Pt(acac)_6$, $CoCl_2$, $Cr(NO_3)_3$, $FeCl_2$	$NaBH_4$	Sodium dioctyl sulfosuccinate (AOT), 1-butanol		RT	PtM (M=Co, Cr, Fe)	SP	2008, 294
16	H_2PtC_6, $Ni(NO_3)_3$	oleylamine			160 °C, 270 °C	PtNi	NF	2014, 295
17	K_2PtCl_4, Na_2PdCl_4	ascorbic acid (AA)	Pluronic F127		RT, potential cycling treatment	PtPd	NC	2013, 296
18	$Pt(acac)_2$, $Cu(acac)_2$	oleylamine			180 °C, 220 °C	PtCu	NF	2014, 297
19	H_2PtCl_6, $CuCl_2$	H_2			60 °C, 300 °C, 1000 °C	PtCu	HOL	2012, 298

[a]C/S = core/shell structure; C = cubic; O = octahedral; *T* = tetrahedral; CT = cuboctahedral; ICO = icosahedral; NW = nanowire; TO = truncated octahedral; SP = spherical particle; NF = nanoframe; NC = nanocage; HOL = hollow structure. EG = ethylene glycol; PDO = propanediol; TOAB = tetraoctylammonium bromide; TBAB = borane-*tert*-butylamine complex; ACA = adamantanecarboxylic acid; PDDA = poly(diallyldimethylammonium chloride); NP5 = poly(oxyethylene)5nonylphenol ether; NP9 = poly(oxyethylene)9nonyl phenol ether. RT = room temperature.

table and thus may offer some advantages over other metals. Maghsodi et al.[258] used $NaBH_4$ as a reducing agent to obtain carbon-supported 40 wt % Pt−Pd catalysts. Although the calculated crystallite size of Pt−Pd alloy in PtPd/C was around 7.8 nm, which was bigger than the Pt in 20 wt % Pt/C prepared by the same method (around 6.3 nm), the 40 wt % PtPd/C catalyst showed better ORR activity, as a result of the weakened O−O bond on the Pd-modified Pt nanoparticles, the synergistic effect between Pt and Pd nanoparticles, and the uniform dispersion of Pd and Pt on the carbon support. Interestingly, using Pd as the second metal in PtM/C catalyst was found not only to enhance the ORR activity but also to increase the catalyst's methanol tolerance.[259,260]

Among various carbon-supported PtM nanoparticle alloy catalysts, core−shell structured alloy catalysts with M or PtM alloy as the core and Pt as the shell have been found to exhibit considerably higher performance for the ORR than pure Pt/C. Strasser's group[261,262] has synthesized a series of core−shell structured PtM/C (M = Co, Cu) catalysts with PtM alloy as the core and Pt as the shell through a dealloying process. They first deposited Co onto 28.2 wt % Pt/C (Carbon, TEC10E30E) to obtain $PtCo_3$/C alloy via an impregnation method with an annealing step in a reductive atmosphere (4 vol % H_2/96 vol % Ar) at 650 °C, 800 and 900 °C, respectively.[262] An electrochemical leaching (dealloying) process was then employed to leach out the non-noble element and produce the core−shell structure with its Pt-rich shell and stable intermetallic $PtCo_3$ core. It was found that when the annealing temperature was increased, the particle sizes of the core−shell structured Pt−Co alloy catalysts and their catalytic activities toward the ORR increased due to the formation of a mixture of alloy phases (i.e., ordered and disordered) in the Pt−Co alloy core.[263,264] For example, after heat treatment at 800 °C for 7 h, the dealloyed PtCo/C catalyst showed a particle size of only 2.2 nm, favoring the balance between mass and specific ORR activity. It was also reported that the catalyst was three times more active on the basis of equivalent Pt mass activity (~380 mA mg_{Pt}^{-1}) and four to five times more active in terms of electrochemical active surface area (ECSA)-based specific activity (~804 μA cm_{Pt}^{-2}) than 28.2 wt % pure Pt/C, due to

DOI: 10.1021/cr500519c
Chem. Rev. 2015, 115, 3433−3467

geometric strain effects. Later, their group used this electrochemical dealloying method to prepare the core−shell structured PtNi/C catalysts and ternary Pt-based electrocatalysts; they obtained high ORR activities (>500 mA mg_{Pt}^{-1} at 0.9 V under single-cell test)[261,265,266] and stable catalytic activity by keeping the particle size in the range of 5−10 nm.[266]

5. EXPERIMENTAL STUDIES ON THE CONTROL OF CARBON-SUPPORTED PT-ALLOY PARTICLE SHAPE

Electrocatalytic activity is shape-dependent, since the electrocatalytic reaction is sensitive to catalyst structure and the reaction rate varies significantly with catalyst shape and/or crystallographic facets.[267−269] It has been proven that the Pt-alloy nanostructure in Pt alloy supported on carbon exhibits different electrocatalytic activities in its various facets.[147]

5.1. Importance of Particle Shape

Among recent research efforts to design and synthesize high-performance carbon-supported Pt-alloy nanoparticle electrocatalysts for the ORR, controlling particle shape has been one of the most important strategies.[12,34] Generally, the shape of nanoparticles in carbon-supported Pt-alloy catalysts is determined by thermodynamics and kinetics during the synthesis process: it is also dependent on the intrinsic structural properties of the Pt alloy and the reactants, such as the solvent, capping agent, and reducing agent, used in the synthesis process.[12,270−272] During the formation of Pt-alloy nanoparticles, some facets similar to the three basal low-index planes in the formation of platinum (i.e., (100), (110), and (111)) often form to minimize surface energy and total excess free energy. Plane (111) has the lowest surface energy while plane (110) has the highest.[273,274] Interestingly, Stamenkovic et al.[147] found that the different planes of a Pt alloy exhibited different ORR activities.

It is well-known that synthesis conditions, such as reactant type and concentration, reaction time and temperature, are also very important in controlling particle shape. In particular, there are a variety of choices when selecting Pt precursors, solvents (e.g., water or organic solvents), reducing agents, surfactants, and additives.[274−276] For platinum precursors, the choices include chloroplatinic acid hexahydrate ($H_2PtCl_6{\cdot}6H_2O$), potassium hexachloroplatinate (K_2PtCl_6), potassium tetrachloroplatinate (K_2PtCl_4), platinum acetylacetonate ($Pt(acac)_2$), and tetraammineplatinum(II) chloride hydrate ($Pt(NH_3)_4Cl_2{\cdot}xH_2O$). A broad range of reducing agents can be utilized in the synthesis of shape-dependent Pt-alloy nanoparticles,[11,12,277−279] such as borohydride, hydrazine, hydrogen, citrate, and ascorbic acid; polyols, diols, or amines also can be used as reducing agents in special organic systems.[221,280] In addition to Pt precursors and reducing agents, some chemicals, including polymers, surfactants, inorganic and organic molecules, as well as ions, can be used as protecting agents that not only are able to restrict particle aggregation and particle size growth but also can contribute to the formation of unique anisotropic shapes by altering the natural growth of the Pt-alloy.

The ideal predetermined shapes of Pt-alloy nanoparticles may have certain low-index planes for high performance. Table 7 presents some typical shapes of carbon-supported Pt-alloy nanoparticle electrocatalysts, gathered from selected reports.[227,281−298] In contrast to the shapes of the Pt nanoparticles shown in Figure 12,[12] the shapes of the Pt alloys seem to lack variety, probably because, on the one hand, it is not easy

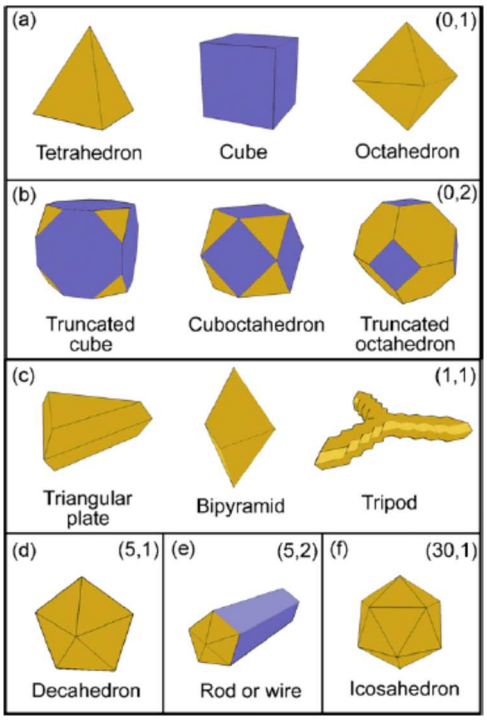

Figure 12. Possible shapes of platinum nanoparticles. Reprinted with permission from ref 12. Copyright 2009 Elsevier B.V.

to control particle shape in the synthesis of Pt alloys supported on carbon, and on the other hand, only a few of the expected shapes of Pt alloys can achieve high catalytic activity. Furthermore, those predetermined shapes must be stable in the physicochemical circumstances of fuel cell operating conditions. Zhang et al.[286] developed a simple wet-chemical approach to prepare monodispersed Pt_3Ni nanoctahedra and nanocubes terminated with {111} and {100} facets, respectively. Table 7 shows the synthesis conditions and shapes of their catalysts together with catalysts made by other groups, and Figure 13 shows SEM and TEM images of their Pt_3Ni nanoctahedra and nanocubes.[286] The Pt_3Ni nanoctahedra could be assembled into a multilayered superlattice with characteristic dimensions on the order of micrometers. Arrays of rhombus projection images clearly indicated that all of the octahedral nanocrystals were patterned on the grid (and on the SEM substrate) in {110} projected orientation with an average side length of ∼10.6 ± 0.3 nm.[299] Using a projection along a direction of ⟨110⟩, high-resolution TEM (HRTEM) images showed a {111}-*d*-spacing of ∼2.23 Å, which corresponded well with the lattice spacing of Pt_3Ni ⟨110⟩. No structural defects in the crystal cores, such as dislocations or lattice distortions, were observable in the HRTEM images. Therefore, they believed that the nanocrystals were dominated by {111}-terminated faces. In these same images they also observed a highly crystalline cube that had clearly resolved lattice fringes with a {200}-*d*-spacing of ∼1.94 Å. The extended Pt_3Ni (111) surfaces possessed enhanced ORR catalytic activity compared to state-of-the-art carbon-supported Pt nanoparticle catalysts. Hence, the design and synthesis of advanced Pt alloys with well-controlled shapes is very important for improving ORR activity.

5.2. Approaches to Control Particle Shape

5.2.1. Organic Capping Agents. It is well-known that organic capping agents play a significant role in the synthesis of

DOI: 10.1021/cr500519c
Chem. Rev. 2015, 115, 3433−3467

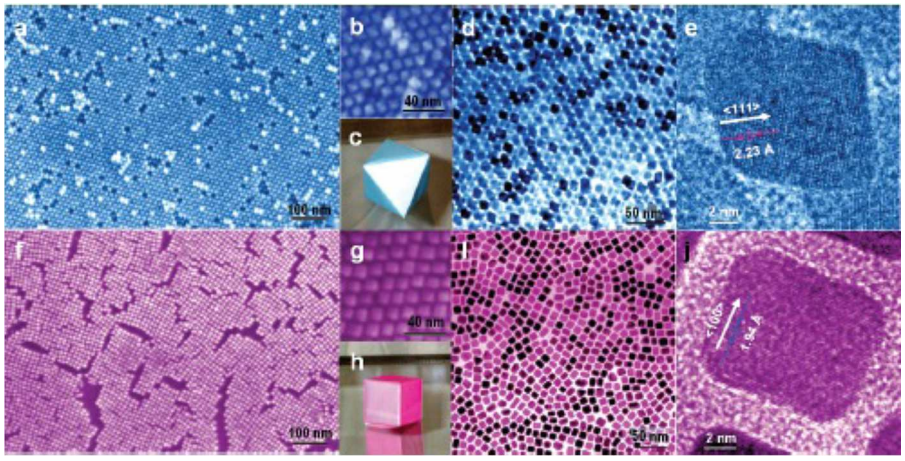

Figure 13. (a–e) Images of Pt_3Ni nanoctahedra. (f–j) Images of Pt_3Ni nanocubes. (a, f) Field-emission SEM images. (b, g) High-resolution SEM images. (c) 3D image of an octahedron. (d, (i) TEM images. (e, j) High-resolution TEM images of single nanocrystals. (h) 3D image of a cube. Reprinted with permission from ref 286. Copyright 2010 American Chemical Society.

shape-controlled colloidal metal nanoparticles.[272] Binary Pt-based nanocrystals have been extensively investigated since they are highly tunable and are superior to their monometallic counterparts.[300−302] In general, long hydrophobic carbon chains of organic capping agents can provide a steric barrier to prevent direct contact between relatively high energy metallic surfaces and therefore stabilize the metal nanoparticles. Because the capping agent is adsorbed, the total excess free energy decreases, thus preventing the metal nanoparticles from further growth and aggregation. In other words, the morphology of the nanocrystals can be well controlled once a capping agent is selectively adsorbed onto the surface of the metal nanoparticles.[272] A capping agent can be selectively adsorbed onto a specific type of facet, since different crystal facets have different atomic arrangement and electronic structures, which bring about the relative growth rates along particular crystallographic directions. However, the solute atoms are more likely to attach to less protected metal surfaces, resulting in anisotropic growth. Therefore, it is very important to select the proper capping agent for shape-controlled synthesis to ensure proper interaction between the guest molecules and the various metal facets during the adsorption/desorption process.[142,303]

Given the effect of organic capping agents on the shapes of particles during synthesis, some efforts have been made to prepare Pt-alloy nanocrystals with special shapes. To improve ORR activity in PEMFCs, Wu et al.[288] successfully prepared carbon-supported truncated-octahedral Pt_3Ni (*t,o*-Pt_3Ni) nanoparticle catalysts with a dominant exposure of {111} facets by a facile colloidal approach. To control the shape of the synthesized nanocrystals, long-alkane-chain amines were used as the main capping agent, while adamantanecarboxylic acid (ACA) or adamantaneacetic acid (AAA) was employed to control the reaction kinetics.[304,305] Figure 14 shows TEM images of cubic and truncated-octahedral nanocrystals.[288] The population of the truncated-octahedral shape depended on the types and amounts of reducing and capping agents used. Wu et al.[288] believed that the two types of long-alkane-chain amines resulted in different portions of truncated octahedral: when hexadecylamine was used as a capping agent, a small portion of cubes was observed (Figure 15a,b) while the use of dodecylamine led to 100% truncated-octahedral nanocrystals of Pt_3Ni, as shown in Figure 14c. In addition to the use of

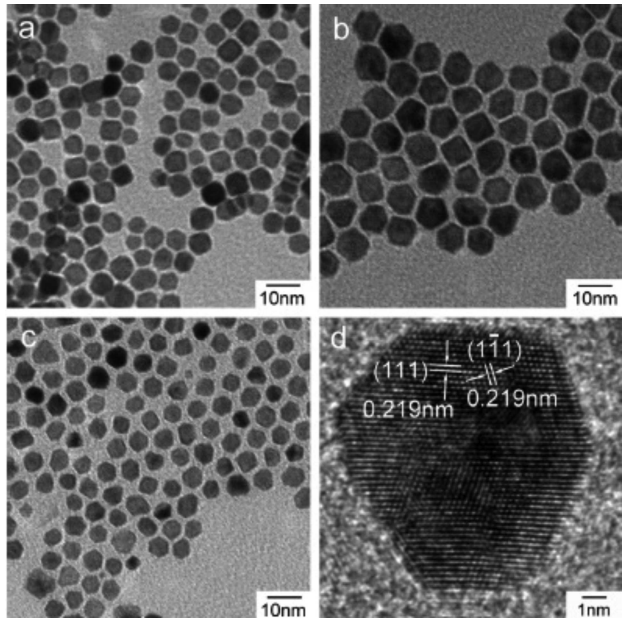

Figure 14. TEM images of Pt_3Ni nanocrystals with truncated octahedron populations of (a) 70%, (b) 90%, and (c) 100%. (d) High-resolution TEM image of a truncated octahedron showing the (111) lattice. Reprinted with permission from ref 288. Copyright 2010 American Chemical Society.

different alkane chain lengths, a combination of strong (borane-*tert*-butylamine complex, TBAB) and mild (hexadecanediol) reducing agents was used to effectively adjust the nucleation and growth rate.

In contrast to the nonhydrolytic system mentioned above, an aqueous solution was used by Shao's group[306] to prepare a sub-10 nm bimetallic core–shell Pd@Pt nanocrystal. In this method, nontoxic poly(ethylene oxide)-poly(propylene oxide)-poly(ethylene oxide) [Pluronic F127 ($PEO_{100}PPO_{65}PEO_{106}$)] amphiphilic triblock copolymer was used as the reducing agent, stabilizer, and capping agent to fabricate a dendritic core–shell structure.[307−310] The composition of the Pd@Pt nanocrystals determined the growth mode of the Pt shell and the corresponding morphology. Using HRTEM and high-angle annular dark-field scanning TEM with

DOI: 10.1021/cr500519c
Chem. Rev. 2015, 115, 3433−3467

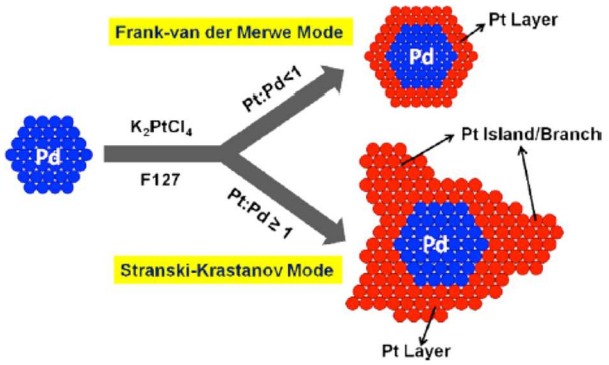

Figure 15. Two Pd−Pt bimetallic nanocrystals consisting of a Pd core and a Pt shell with different Pt:Pd molar ratios. Reprinted with permission from ref 306. Copyright 2013 American Chemical Society.

an energy-dispersive X-ray (EDX) spectra (HAADF-STEM-EDX), two Pd−Pt bimetallic nanocrystals consisting of a Pd core and a Pt shell with different Pt/Pd molar ratios were identified (see Figure 15). Notably, this was the first time that PEO−PPO−PEO copolymer had been utilized as a reductant to prepare core−shell nanocrystals. Shao's group believed that PEO segments in the PEO−PPO−PEO triblock copolymer were able to reduce metal ions, thus forming cavities (pseudocrown ethers) binding $PdCl_4^{2-}$ from the starting precursors: the bound $PdCl_4^{2-}$ ions might then be reduced via oxidation of the oxyethylene segments by the metal center.[311,312] Spherical Pd nanocrystals with an average particle size of 4.96 nm were observed in TEM images. These Pd nanocrystals were used as seeds for the overgrowth of Pt by injecting a given amount of K_2PtCl_4 aqueous solution into the Pd colloid solution. Pt atoms were then reduced from $PtCl_4^{2-}$ ions by F127 deposited on the surface of the Pd monocrystals to form the core−shell structure of Pd core and Pt shell.

5.2.2. Inorganic Ions and Molecules. Similar to organic capping agents, inorganic ions and other small molecules can also prevent metal nanoparticle size from increasing and affect the shape of formed metal nanoparticles.[313−320] However, after they are adsorbed onto specific facets of metal nanoparticles, inorganic species cannot afford the counterpart in the interaction to promote or inhibit further growth along given directions.[295,314,315] Typically, inorganic ions such as Br^- and I^- in a solution of KBr and KI have proven to be as the adsorption/protective agents on the surface of Pt−Pd alloy nanoparticles, favoring the stabilization of the (100) facet and thus the formation of monodispersed sub-10 nm Pt−Pd tetrahedrons and cubes.[320] Moreover, PVP was found to be suitable only as an alternative reducing agent, while formaldehyde was found to have a negative effect on the formation of regularly shaped PtPd nanocrystals due to the possible strong adsorption of several intermediate chemical species, decomposed from formaldehyde, on the (111) surface.[321,322]

5.2.3. Templating Approaches. Template assisted-synthesis approaches have been considered effective ways to prepare shape-controlled Pt-based alloys, evidenced by the successful synthesis of various Pt nanostructures, typically in polycrystalline form, using a template.[323−326] Both chemical and physical templates can offer confined spaces and/or functionalized structures for the formation and growth of a Pt alloy.[327−330] The templates are often classified into two basic categories: hard and soft.[331−333] The hard templates (e.g., anodic aluminum oxide (AAO), mesoporous silica, and lithographically patterned templates) consist of spatially well-defined physical structures, while the soft templates include self-assembled and self-organized structures in solution, such as micelle, reverse micelle, microemulsion, and liposome. Compared to hard templates, soft templates are more common in actual synthesis because they, especially surfactant molecules, can often provide hydrophilic heads and lipophilic long carbon tails favoring the formation of shape-controlled Pt alloys.

Sui et al.[334] successfully synthesized PtFe nanotubes using AAO membrane as a hard template. Specifically, they first employed electrodeposition to deposit PtFe inside the AAO, then carried out a wet etching process using NaOH aqueous solution to remove the AAO template. However, this method was relatively complex, allowing no further electrochemical investigation to evaluate the catalyst's structure and performance. Cheng et al.[335] prepared nest-like $Ni_{1-x}Pt_x$ spheres of submicrometer sizes through a template-replacement route in which poly(styrene-*co*-methacrylic acid) (PSA) was employed as a soft template. The replacement reaction between K_2PtCl_6 and Ni led to the formation of $Ni_{1-x}Pt_x$, which was directly deposited onto the surface of the PSA. After the formation of a $Ni_{1-x}Pt_x$-PSA core−shell structure, the final $Ni_{1-x}Pt_x$ alloy hollow spheres were obtained by completely dissolving the PSA core template in toluene.

5.3. Effect of Particle Shape on ORR Activity

In recent years, precise shape-controlled Pt-based alloy electrocatalysts have exhibited great potential to deliver superior ORR activity in PEMFCs and thus have become a leading focus of research. Novel-shaped nanoparticles often exhibit unique physical and chemical properties. In addition, shaped Pt-based alloy nanostructures often present unusually high catalytic activity.

5.3.1. Crystal Facet. It has been well evidenced that the catalytic activity of Pt-based nanocatalysts strongly depends on their crystal facets.[147] The obtained shape of a Pt or Pt-alloy nanocrystals is a competition in surface energies among different facets because nanocrystal growth may occur by adatom incorporation perpendicular to high-energy crystal planes with a low stability.[34,336] For a specific synthetic method, the specific facets in crystal growth dominantly determine the final shape of nanocrystals.[181,337−340] On the basis of the relationship between shape and facet in Pt-alloy nanocrystals, well-controlled shapes of Pt-based nanocatalysts can not only retain the catalytic property of the bulk metal but also greatly enhance the catalytic activity because the facet can increase the number of Pt active sites.[34,148,341−345] Wang et al. reported that a nanocube Pt catalyst was four times more active for the ORR than a Pt nanoparticle, since Pt{111} facets can provide optimal binding energy between platinum atoms and the adsorbed species for ORR.[248,341]

Wu et al.[288] reported truncated-octahedral Pt_3Ni (*t,o*-Pt_3Ni) catalysts with a particle size of 5−7 nm that had a dominant exposure of {111} facets. Three sets of Pt_3Ni nanocrystals were generated with various mixtures of truncated octahedral (exposing both {111} and {100} facets) and cubes (exposing only {100} facets). They have developed a correlation of the area-specific and mass activities with the fraction of {111} surfaces of these Pt_3Ni catalysts and concluded that the observed differences in the mass and area-specific ORR activities increased almost proportionally with the increase in the fraction of {111} surfaces over the entire surface areas of the carbon-supported Pt_3Ni catalysts. Also, the ORR mass

DOI: 10.1021/cr500519c
Chem. Rev. 2015, 115, 3433−3467

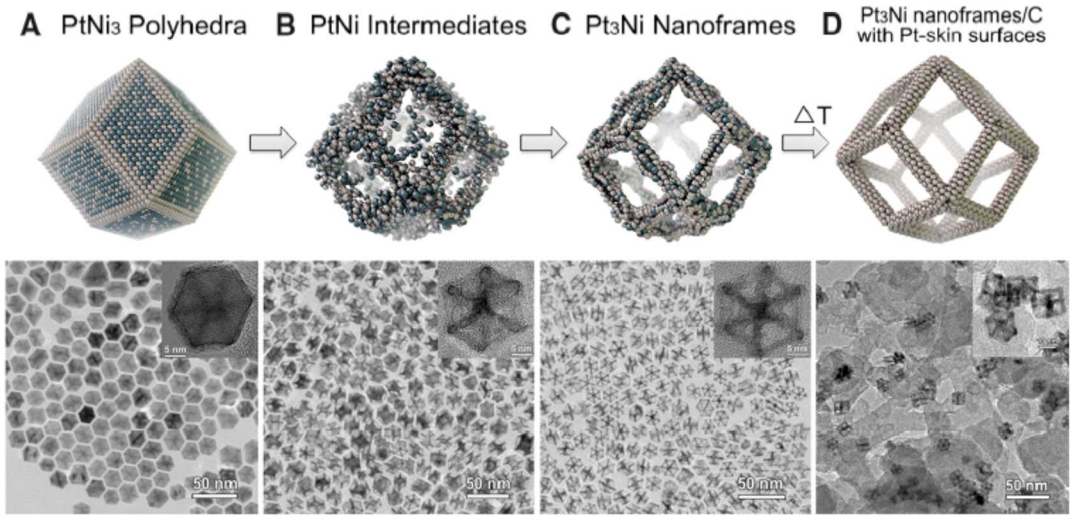

Figure 16. Schematic illustrations and corresponding TEM images of the samples obtained at four representative stages during the evolution process from polyhedral to nanoframes: (A) initial solid $PtNi_3$ polyhedra. (B) PtNi intermediates. (C) Final hollow Pt_3Ni nanoframes. (D) Annealed Pt_3Ni nanoframes with Pt(111)-skin like surfaces dispersed on high surface area carbon. Reprinted with permission from ref 295. Copyright 2007 American Association for the Advancement of Science (AAAS).

activity (~530 mA mg^{-1}_{Pt}) of carbon-supported Pt_3Ni catalyst showed values that were 4 times higher than that of the standard Pt/C catalyst (~140 mA mg^{-1}_{Pt}). Since {111} facet has the lowest surface energy among the low-index facets, face-centered cubic (fcc) of crystals always tends to grow along the ⟨100⟩ direction into an octahedron-like shape. It is a real challenge to obtain the desired shapes of single-facet surface. To solve this problem, Zhang et al.[286] used tungsten carbonyl ($W(CO)_6$) as the decelerator to develop the Pt_3Ni nano-octahedra and nanocube with {111} facets and {100} facets exposed, respectively. At a similar size, a comparison of ORR activity between Pt_3Ni nano-octahedra and nanocubes revealed that the former was ~5-fold higher than the latter. Importantly, the specific and mass activities of carbon-supported Pt_3Ni nano-octahedra were found to be ~7 and ~4 times, respectively, higher than those of the commercial Pt/C catalysts. Considering that an over 7-fold improvement in area-specific activity for ORR was successfully achieved by changing the morphology from the (100) to (111) Pt_3Ni single crystal surfaces,[147] Wu et al.[287] utilized CO as a gas reducing agent and made two Pt_3Ni nanocrystals with octahedral and cubic morphologies. According to their results of XRD and HRTEM, the cubic shape was bound by the {100} facets, while the octahedral shape was bound by {111} facets. The adsorption of CO on {100} facets was found to be stronger than on {111} facets, which favors the formation of the octahedral shape in the synthsis process. They showed that the ORR activity increased with the change of shapes from cube to octahedron and the ORR specific activity of the octahedral Pt_3Ni achieved a five-time improvement over that of the commonly used Pt/C (~0.20 mA cm^{-2}_{Pt}). The ORR activity of this octahedral Pt_3Ni catalyst (~440 mA mg^{-1}_{Pt}) is about three times that of the reference Pt/C (~140 mA mg^{-1}_{Pt}). However, the absolute values of the specific activities of the nanocrystals were still in the same range as that observed on extended Pt-alloy single crystal surfaces[147] due to several probable factors such as facet size effect, impurities and defects in the nanocrystal surface, incomplete formation of smooth and segregated Pt layers on the facet surfaces although the {111} facets of thenanocrystals showed much higher specific activity than the {100} facets.

Recently, Chen et al.[295] obtained a nanoframed Pt_3Ni/C catalyst by the control of structure at the atomic level. In the first step, solid $PtNi_3$ polyhedral nanoparticles were prepared and then a chemical evolution was used to form the open-cell three-dimensional (3D) nanoframe structure. Finally, carbon and $PtNi_3$ were combined for the preparation of Pt_3Ni/C catalysts. The shape polyhedral $PtNi_3$ should have a single crystalline face-centered cubic atomic structure, which could be enclosed by the {111} planes offering a large active area because Pt_3Ni {111} crystal surface with only the active {111} facets being reported to exhibit an exceptionally high ORR activity of 18 mA cm^{-2}_{Pt}.[121] After a selective corrosion, the formed 3D Pt_3Ni nanoframes were composed of eight facets in each frame while the surface of each edge was rich in single-crystalline Pt, favoring oxygen reduction and hydrogen evolution reactions. The corrosion process hollowed out the nanoparticles spontaneously in air and resulted in a desired Pt-skin, Pt−Ni core−shell surface structrure (see Figure 16). The final carbon supported Pt_3Ni nanoframes showed more than 22 times the catalytic activity (5.7 A mg^{-1}_{Pt}) of conventional Pt/C catalyst at 0.9 V.

Beside the effect of facets on the ORR activity of Pt−Ni alloy supported on carbon, Wang et al.[155] also systematically investigated the effects of Pt shell thickness, facets, and particle size on the specific and mass activities via stepwise deposition of a Pt monolayer on Pd and Pd_3Co cores. Their results showed that the specific activity of the Pt-monolayer catalysts on 4 nm Pd and 4.6 nm Pd_3Co cores was about 5- and 9-fold enhanced, respectively, over that of 3 nm Pt nanoparticles while only the 2- and 3-fold enhancements in specific activity can be attributed to the nanosize- and lattice mismatch-induced contraction in {111} facets. The ORR effect of facet was also studied in other PtM (M = Cu, Mn) alloy nanocrystals supported on carbon. For example, using an interior erosion method, Han et al.[297] obtained polyhedral Cu_3Pt nanoframes with a core−shell structure, which was also a single crystalline face-centered cubic atomic structure enclosed by the {111} planes. After incorporation of carbon, carbon supported Cu_3Pt

DOI: 10.1021/cr500519c
Chem. Rev. 2015, 115, 3433−3467

catalyst exhibited a superior ORR activity. Kang and Murray[346] showed that the cubic Mn−Pt nanocrystals gave a higher ORR activity than the spherical MnPt nanocrystals in H_2SO_4 while the spherical nanocrystals were more active in $HClO_4$. This indicated that the ORR activity of Mn−Pt nanocrystals was higher on {111} facet than on {100} facet in $HClO_4$, whereas the ORR activity was higher on {100} facet than on {111} facet in H_2SO_4. This also suggested that the catalytic evaluation of facet-dependent Pt-alloy nanocrystals also depended on the reaction medium, which was in agreement with the results on the catalytic activity of single Pt nanocrystals.[347,348] These results for unsupported PtM alloy with different facets are very interesting, but these two research groups did not provide any activities of carbon-supported PtM alloy in their studies.

5.3.2. Pt Monolayer/Skin. To reduce Pt content and enhance catalytic activity, Adzic et al.[349] reported a series of Pt-monolayer fuel cell electrocatalysts, in which a Pt monolayer deposited on carbon-supported metal or metal-alloy nanoparticles resulted in the highest Pt utilization because almost every Pt atom on the surface participated in the electrocatalytic reactions. The Pt monolayer deposition process involved the galvanic displacement of a Cu monolayer by Pt,[349] as shown in Figure 17. Some Pt monolayer (Pt_{ML}) electrocatalysts have

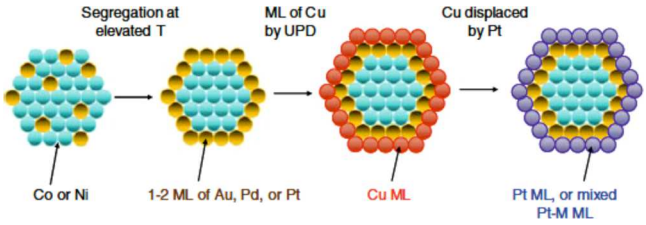

Figure 17. Synthesis mode for Pt monolayer catalyst on non-noble metal−noble metal substrate. Reprinted with permission from ref 349. Copyright 2007 Springer.

exhibited excellent activities because the interaction between the Pt monolayer and the substrate material induced a synergistic effect on the ORR kinetics.[350−352] When Pt atoms deposit onto a foreign metal or alloy, the Pt surface undergoes compression or extension due to the difference in their atomic radii, inducing a D-band center shift and thus affecting the catalyst's activity.[353] Moreover, the electronic (ligand) effect from the electronic coupling between the Pt_{ML} and its supporting substrate also plays a role in determining the catalytic activity.[349,354] Based on density function theory (DFT) calculations, it was proven that the binding energies and reactivity of small adsorbates are strongly correlated with the position of the d-band center on strained surfaces and metal overlayers.[355−357] Adzic et al.[349] synthesized Pt/Pd/C and Pt/Pd_3Fe/C catalysts with a Pt monolayer. According to the ORR polarization curves of these two catalysts obtained in 0.1 M $HClO_4$ solution at 1600 rpm, as presented in Figure 18a, the total noble mass-specific activity of Pt/Pd_3Fe/C was about five times larger than that of Pt/C at 0.8 V, as depicted in Figure 18b, while Pt/Pd/C had an enhancement factor of 3. In addition, they also synthesized and tested similar core−shell structured catalysts with a Pt monolayer on top of either Ir or Pd_3Co/C. When normalized in terms of Pt content, the mass activities of these two catalysts were 1.01 and 0.57 A mg^{-1}, respectively.

Among Pt_{ML} electrocatalysts, those using Pd as the substrate were found to be the most active and durable,[358] exhibiting the

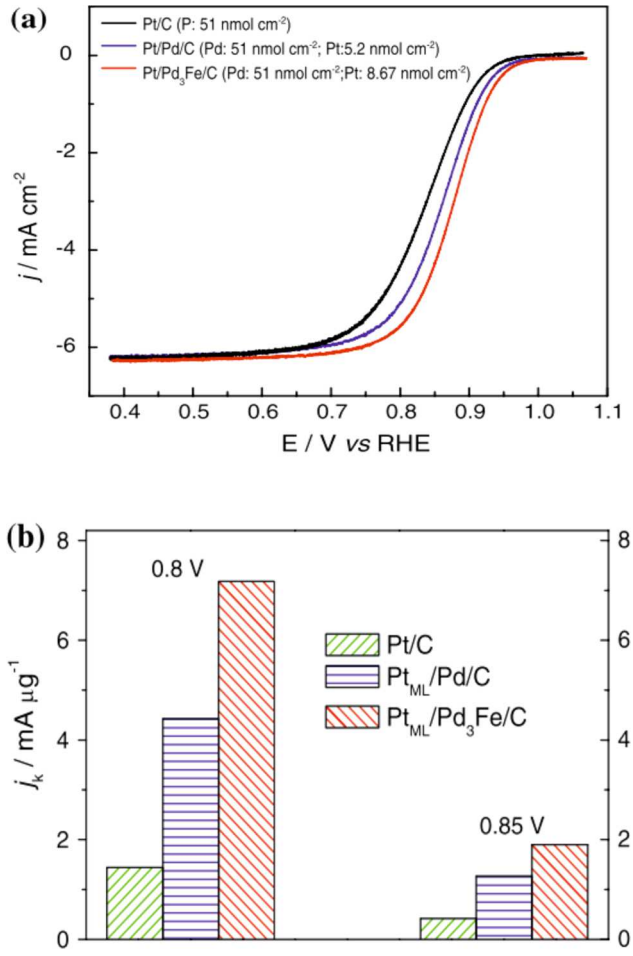

Figure 18. (a) Polarization curves for the ORR on Pt/Pd/C, Pt/Pd_3Fe/C, and Pt/C electrocatalysts, and (b) the total noble-metal mass-specific activities of these electrocatalysts at 0.8 and 0.85 V in 0.1 M $HClO_4$. It should be noted that, for all polarization curves, their top baselines around or above 1 V showed an irregularity, indicating an improper preparation of sample under RDE test. Reprinted with permission from ref 349. Copyright 2007 Springer.

highest activity, even higher than Pt (111).[351,358] To further enhance the ORR activity and durability, Adzic's group[359] introduced bromide ions as an agent to effectively reduce the number of low-coordination sites on Pd and Pd-alloy nanoparticles and to obtain a smooth Pd nanoparticle surface with an increased number of (111)-oriented facets, since a low number of coordination sites and high percentage of atoms on faceted surfaces were found to play decisive roles in improving the activity and durability of ORR electrocatalysts with nanoparticle sizes below 10 nm.[256] After post-treatment with Br^-, Pt_{ML}/Br-treated Pd/C showed a 1.5-fold enhancement in specific and Pt mass activities for the ORR compared with Pt_{ML}/Pd/C. Adzic et al.[360] also deposited amorphous Au clusters onto carbon-supported Pt nanoparticles through galvanic replacement reactions to mitigate the dissolution of Pt electrocatalysts; after potential cycling between 0.6 and 1.1 V for over 30 000 cycles, no loss in ORR activity was observed. In addition, they also selected a series of single metal elements such as Au, Pd, Rh, Ir, Os, or Re, as the alternative M component in the deposition of mixed Pt-M monolayers (six couples) on Pd(111) and carbon-supported Pd nanoparticles for rotating disk tests. It was found that the total noble-metal

DOI: 10.1021/cr500519c
Chem. Rev. 2015, 115, 3433−3467

mass activity of $(Pt_{0.8}Re_{0.2})_{ML}/Pd_{20}/C$ was 4−4.5 times higher than Pt/C commercial catalyst.[249,349]

In addition to Pt_{ML} electrocatalysts, Pt-skin electrocatalysts with multiple layers (at least two) of Pt on top of a carbon-supported metal or metal-alloy have become other attractive possibilities for electrocatalyst systems.[361] By comparing the surface properties of well-defined bulk PtNi (Pt-skeleton surface) and PtCo alloys (Pt-skin surface), Stamenkovic et al.[147] found that the ORR kinetics was dependent on the arrangement of Pt on the surface region. The catalytic activity at different surfaces was in the order of Pt_{bulk} < Pt-skeleton < Pt-skin. Also, the bulky 30 nm $Pt_3Ni\{111\}$ catalyst showed a 10-fold improvement in ORR activity compared to Pt{111} catalyst and was 90 times more active than current state-of-the-art Pt/C catalysts for PEMFCs. This catalyst has been studied as the most active cathode catalyst to date.[147] Villullas's group evaluated the nanoscale Pt-skin effects on the ORR activity of carbon-supported PtFe nanocatalysts, in which a ratio of Pt to Fe ratio of 3:1 was used and a thermal treatment[362−364] was conducted to promote Pt surface segregation and thus to form a Pt-skin. They observed an almost 2-fold enhancement of intrinsic ORR activity due to Pt-skin effects, resulting in lattice contractions,[353,365] electronic effects,[366] changes in the Pt−Pt distance, and increased Pt d-electron vacancy.[367−369] Okaya et al.[370] developed a two-step method to form a two-monolayer Pt-skin layer ($Pt_{2\ ML}$) on Pt_xCo core particles supported on graphitized carbon black (GCB; see Figure 19). Based on the

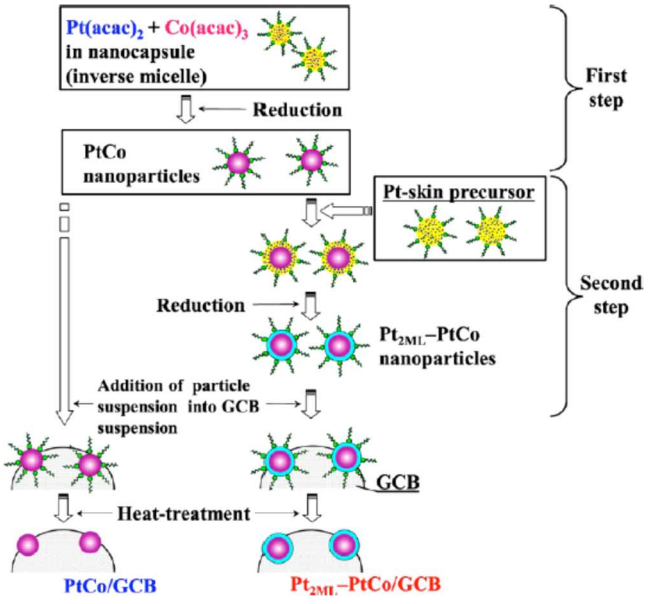

Figure 19. Preparation protocol of $Pt_{2\ ML}$-PtCo/GCB and PtCo/GCB catalysts. Reprinted with permission from ref 370. Copyright 2012 American Chemical Society.

nanocapsules formed by the surfactants oleic acid and oleylamine,[255,371] the average diameter of the synthesized PtCo core was 2 and 3 nm, respectively. The Pt skin was then formed on the surface of the PtCo core in the second step.[371] Electrochemical evaluation showed that, on the one hand, Co dissolution from the PtCo particles during the ORR was considerably suppressed by the stabilized Pt-skin structure (as per the nature of a core−shell structured Pt alloy), and on the other hand, the kinetically controlled mass activity (MA_k) for the ORR of $Pt_{2\ ML}$-PtCo/GCB (PtCo core size of 2 nm) at E = 0.85 V versus reversible hydrogen electrode (RHE) was about two times larger than that for a standard commercial Pt/CB catalyst at 80−90 °C.

5.3.3. Core−Shell Structure. To obtain a typical core−shell structure for PtM alloy nanoparticles, one basic strategy is to introduce large amounts of M core particles into reaction mixtures in the presence of mild reducing agents or small amounts of Pt metal precursors.[12] In this way, Pt should be preferentially deposited onto the metal particle core M in a layer-by-layer fashion or Frank-van der Merwe (FM) model (see Figure 20), since the lattice mismatch between Pt and M is

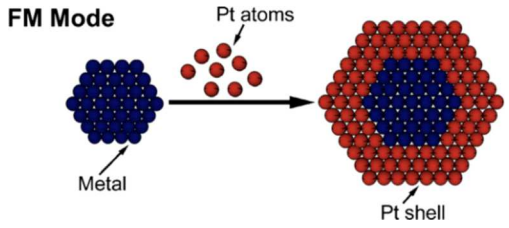

Figure 20. Layer-by-layer model for PtM core−shell structure. Reprinted with permission from ref 12. Copyright 2009 Elsevier B.V.

small, and the sum of the surface energy of the depositing metal and the interfacial energy is less than the surface energy of the M substrate metal.[12,372−375]

Wang et al.[376] synthesized a Pt_3Co/C nanoparticle catalyst with a core−shell structure by a one-step impregnation reduction method[377−381] at different temperatures under a flowing H_2/N_2 mixed gas atmosphere. After heat treatment at 700 °C, the mean particle size of the synthesized Pt_3Co/C was 5 nm, which was slightly smaller than the value calculated from XRD results. This core−shell structure was composed of Pt_3Co ordered intermetallic cores with two to three atomic-layer Pt shells (Pt_3Co@Pt). They believed that the L12 ordered intermetallic cores along the [001] zone axis (see Figure 21) directly resulted in the material's high catalytic performance. Testing yielded a mass activity of 520 mA mg^{-1}_{Pt} at 0.9 V in O_2-saturated 0.1 M $HClO_4$ at room temperature, with a rotation rate of 1600 rpm and a sweep rate of 5 mV s^{-1}; this was the highest activity among carbon-supported Pt−Co systems reported in the literature for similar testing conditions. These Pt_3Co/C catalysts exhibited over 200% increase in mass activity and over 300% increase in specfic activity when compared with disordered Pt_3Co alloy nanoparticles as well as Pt/C particles. In addition to Co, other metals, such as Au,[284] Ag,[285] Cu,[214] Ni,[382] and Pd,[383,384] have also been used as the core inside a Pt shell.

Choi et al.[383] employed 6 nm Pd nanoparticles as seed cores to prepare a series of Ketjenblack carbon-supported Pd@Pt_x (x = 1.0, 1.5, and 2.0) nanoparticles with various Pt shell thicknesses by adjusting the amount of Pt precursor. These Pd@Pt/C nanoparticles exhibited enhanced electrochemical activity and superior stability toward the ORR compared to Pt/C catalyst, due to the former's lower OH_{ad} bonding strength. Based on ORR measurements in O_2-saturated 0.1 M $HClO_4$ at a scan rate of 20 mV·s^{-1} and a rotation rate of 1600 rpm, Pd@$Pt_{0.5}/C$ showed the highest mass activity among the various catalysts prepared, whereas Pd@$Pt_{1.5}/C$ demonstrated the highest enhancement in specific activity. Interestingly, Liu et al.[384] prepared PdPt-alloy/C, Pd(core)-Pt(shell)/C, and Pt-(core)-Pd(shell)/C nanoparticles, by a coreduction and sequential approach using PVP as a protective stabilizer and

DOI: 10.1021/cr500519c
Chem. Rev. 2015, 115, 3433−3467

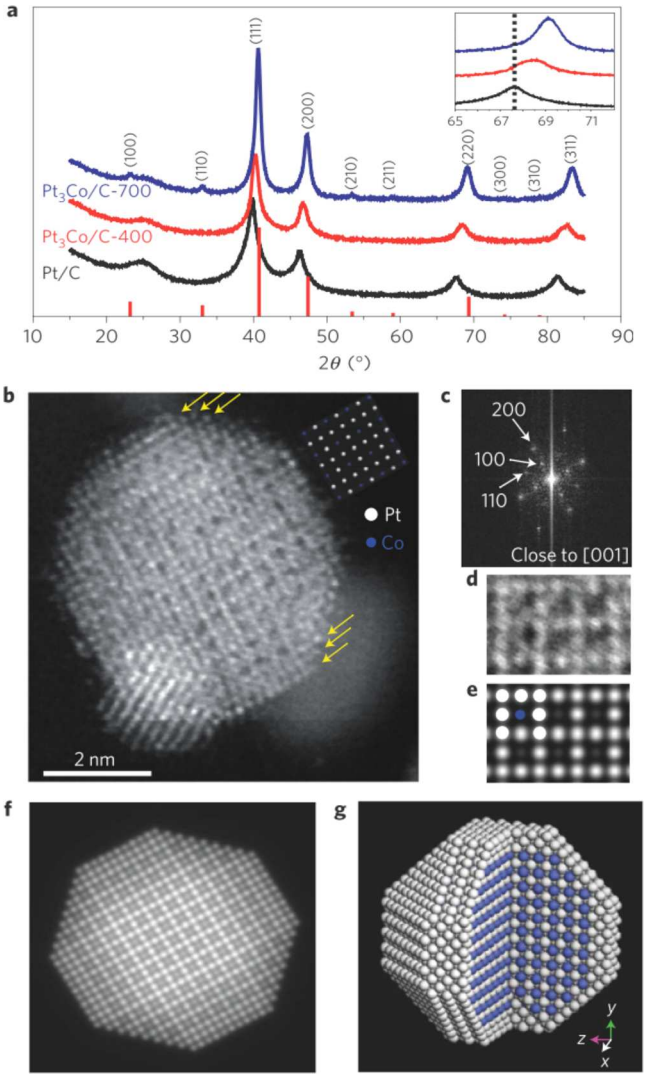

Figure 21. (a) XRD patterns of Pt/C, Pt3Co/C-400, and Pt3Co/C-700. The inset shows the enlarged region of the Pt(220) diffraction peaks, with the black dotted line corresponding to the peak position of pure Pt. The red vertical lines indicate the peak positions of the intermetallic Pt3Co reflections (PDF card # 04-004-5243). (b) Atomic-resolution ADF-STEM image of Pt_3Co/C after Richardson-Lucy deconvolution, with yellow arrows indicating the Pt-rich shell. A smaller particle (lower left) overlaps the larger particle in projection. The inset shows the projected unit cell along the [001] axis. (c) Diffractogram of the center particle in (b), (d). A crop of the super lattice feature from (b), (e). A simulated ADF-STEM image of $L1_2$ ordered Pt_3Co along [001] using a simple incoherent linear imaging model. (f) Multislice simulated ADF-STEM (100 kV, probe-forming angle = 27.8 mrad, ADF collection angles = 98−295 mrad) image of the idealized nanoparticle shown in (b). (g) Idealized atomic structure of the Pt_3Co core−shell nanoparticle. The white and blue spheres in (e) and (g) represent Pt and Co atoms, respectively. Reprinted with permission from ref 376. Copyright 2013 Nature Publishing Group.

EG as a reducing reagent, then compared their ORR activity with that of Pt/C, Pd/C, and PdPt bialloy/C in fuel cells. Figure 22 illustrates the proposed structures of the three bimetallic nanoparticles. The average particle sizes for the as-synthesized PdPt-alloy, Pd(core)-Pt(shell), Pt(core)-Pd(shell), and Pd and Pt samples were 11.2, 8.1, 7.6, 6.5, and 7.2 nm, respectively. The bimetallic nanoparticles, irrespective of alloys or core−shell assemblies, had larger sizes than monometallic Pd

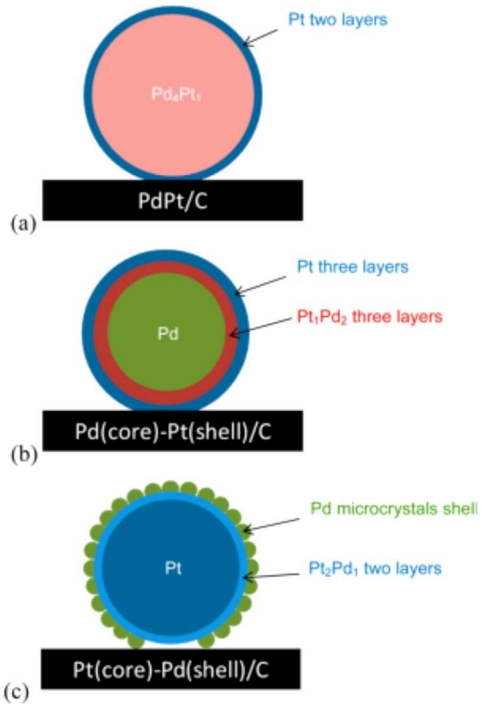

Figure 22. Proposed structures of the bimetallic nanoparticles in (a) PdPt alloy/C, (b) Pd(core)-Pt(shell)/C, and (c) Pt(core)-Pd(shell)/C catalysts. Reprinted with permission from ref 384. Copyright 2012 American Chemical Society.

and Pt nanoparticles. The Pt surface-enriched catalysts, such as PdPt-alloy/C and Pd(core)-Pt(shell)/C, exhibited a higher Pt-based mass activity than the other Pt catalysts, as shown in Figure 23. However, neither the electronic (ligand) effect nor the compressive strain effect was significantly observed in their characterizations. The establishment of reliable design and characterization methods is highly necessary for the development of low Pt-loading, robust electrocatalysts to be utilized in next-generation fuel cell cathode catalysts.

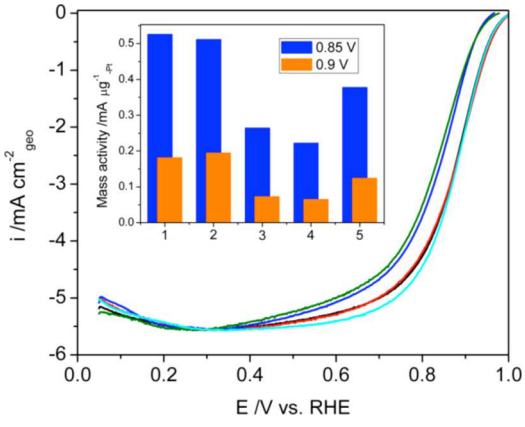

Figure 23. Linear scan voltammograms with anodic sweep of 10 mV s^{-1} at 1600 rpm, and Koutecky−Levich plots (inset) of the catalysts: (1) PdPt alloy/C (black), (2) Pd(core)-Pt(shell)/C (red), (3) Pt(core)-Pd(shell)/C (blue), (4) Pd/C (olive), and (5) Pt/C (cyan). It should be noted that, for all polarization curves, their top baselines around or above 1 V showed an irregularity, indicating an improper preparation of sample under RDE test. Reprinted with permission from ref 384. Copyright 2012 American Chemical Society.

DOI: 10.1021/cr500519c
Chem. Rev. 2015, 115, 3433−3467

In addition to the sequential reduction method, a chemical or electrochemical dealloying method has also been developed to prepare core−shell structured PtM/C (M = Co, Ni, Cu, Cr, Fe, etc.) nanoparticle catalysts.[261−265,385,386] Aricò's group developed a two-step synthetic route to prepare 50 wt % Pt_3Co/C nanoparticle catalysts.[387−389] In the first step, Ketjenblack EC (KB) carbon black (BET area of 850 $m^2\ g^{-1}$) and self-prepared $Na_6Pt(SO_3)_4$ were used to prepare amorphous PtO_x/C via a sulfite complex route,[390] while in the second step, carbon-supported Pt−Co alloy was formed by cobalt impregnation and carbon thermal reduction at 600 °C in an Ar atmosphere. Then, a subsequent preleaching of the final PtCo/C catalyst at 80 °C in 0.5 M $HClO_4$[119] was carried out to promote Pt enrichment in the outermost layers, which is similar to a dealloying process for obtaining a core−shell structured PtCo alloy. It was found that after the preleaching step the alloy size of 50 wt % PtCo/C decreased from 3.1 to 2.9 nm, a finding verified through their TEM images.[388] However, the alloy size of the preleached 50 wt % PtCo/C sample slightly increased from 2.9 to 4.2 nm when the thermal reduction temperature was changed from 600 to 800 °C.[387] When evaluated in a 5 cm^2 single-cell test at 80 °C under H_2/O_2 and 100% relative humidity, the preleached 50 wt % PtCo/C sample was found to have a mass activity of 360 mA mg^{-1} at 0.9 V.

Electroless deposition is another method that has been employed to synthesize core−shell structured PtCo/C nanoparticle catalysts.[227,391−395] Cobalt nanoparticles were first loaded onto a carbon support, then electroless deposition was performed simply by mixing the resulting Co/C with Pt precursor. The Co atoms on the surface of the Co nanoparticles were replaced by Pt atoms to form an outermost Pt shell following the replacement reaction ($Co + PtCl_4^{2-} \rightarrow Co^{2+} + Pt + 4Cl^-$), which occurred spontaneously because the standard reduction potential of $PtCl_4^{2-}$/Pt (0.67 V vs SHE) is higher than that of Co^{2+}/Co (−0.277 V vs SHE). In this method, the pH value of the synthesis solution determined the Pt to Co ratio and the thickness of the Pt layer outside of the Co core. As the pH value decreased from 4 to 1.5, the crystal size of the Pt−Co alloy changed from 2.5 to 3.1 nm with a Pt to Co nominal molar ratio of 1:3. It was found that the core−shell structured PtCo/C catalyst made using the above method had a similar crystallite size (~2.5 nm) as that of Pt/C catalyst, based on XRD analysis, and its intrinsic activity for the ORR was found to be two to four times higher than that of Pt/C.[227]

6. EXPERIMENTAL STUDIES ON THE CONTROL OF CARBON-SUPPORTED PT-ALLOY COMPOSITION

6.1. Composition and Formation of Pt Alloys

Carbon-supported Pt-alloy systems are known as solid solutions of Pt and other metal(s), among which carbon-supported Pt-based bimetallic alloys are popular electrocatalysts in PEMFCs.[13,57,396,397] To obtain low-cost, high-performance ORR electrocatalysts, suitable metal combinations and optimum compositions of Pt-based alloys have been extensively studied. Pt alloys can be generally divided into three forms, according to their crystalline order: random, clustered, and ordered, as shown in Figure 24.[12] With the long-range atomic orders, the alloy can be defined as an intermetallic compound (or simply "intermetallic").[191,398] It is very important to control the composition of Pt alloys and their corresponding structures, as doing so can essentially determine the intrinsic electrochemical catalytic properties of a carbon-supported Pt-alloy system in a PEMFC electrocatalyst.

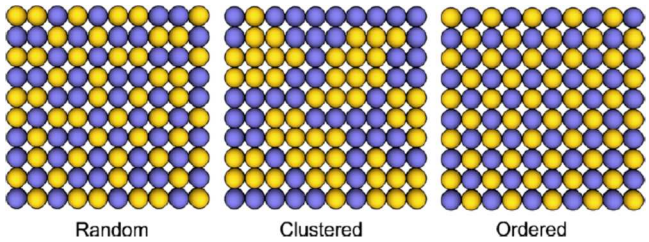

Figure 24. Schematic representation of three types of Pt alloys: random, clustered, and ordered forms. Reprinted with permission from ref 12. Copyright 2009 Elsevier B.V.

The formation of Pt alloys during the synthesis process is closely controlled by temperature.[191,192,399] According to the theory of excess Gibbs free energy,[194−196] high temperatures can result in entropy making more of a contribution than enthalpy to the change in internal energy; consequently, the excess free energy becomes negative, leading to the formation of alloys. Conversely, alloys will not form in a system that has a positive excess Gibbs free energy at a low synthesis temperature. When both metals are immiscible, a miscibility gap forms in the area of nonalloy in the two metals' bulk phase diagram. Generally, the formation of a nonalloy in the synthesis of carbon-supported Pt-based nanoparticle catalysts is not often expected to improve catalytic performance. In terms of the behavioral relationship between excess Gibbs free energy and entropy/enthalpy, the random atomic arrangement in a bimetallic Pt-alloy system should correspond to the lowest excess Gibbs free energy. In addition, the size difference between Pt and other metals can result in strain formation in Pt alloys, which is one of the most important factors affecting their catalytic activity toward oxygen reduction.[24,252,400] Furthermore, the areas of ordered arrangement or/and disordered arrangement in the composition of a Pt alloy play an important role in determining the catalytic activity of fuel cell electrocatalysts.[263,376,401,402] Synthesis conditions, including temperature, time, the size of the other metal atom, and the ratio of starting materials, determine the local atomic arrangement in the Pt alloy. In particular, the initial ratio of the starting materials dictates the Pt alloy's composition.

One of the major factors limiting PEMFC commercialization is the high cost of Pt catalysts used in the electrodes, as this represents about 30−40% of the total cost of the fuel cell. To reduce the Pt content and, at the same time, substantially alter the surface electronic properties and boost catalytic performance, non-Pt metals, especially non-noble metals, have often been employed.[403] Therefore, composition control is an important subject for obtaining designed Pt-alloy nanoparticles with high catalytic activity for the ORR in PEMFCs.

6.2. Approaches to Control Pt-Alloy Composition

6.2.1. Colloidal Pt Alloys. The colloidal chemical synthesis method is the most popular approach for producing carbon-supported PtM (M = Co, Cu, Fe, Ni, Pd, Ru, etc.) nanoparticle catalysts;[404−409] the solute atoms of Pt and another metal can be reduced simultaneously in solution at both nucleation and growth stages and at designed concentrations to obtain nanoalloys. Usually, thermally decomposable metal precursors are considered good candidates for preparing of Pt alloys by the colloidal method, since they can be reduced to the corresponding metals. Pt ion is reduced more easily than

DOI: 10.1021/cr500519c
Chem. Rev. 2015, 115, 3433−3467

Table 8. Composition of Carbon-Supported Binary PtM_3 (M = Co, Ni, and Cu) Nanoparticle Fuel Cell Cathode Electrocatalysts after Electrochemical Dealloying[a]

nominal composition	EDS composition (as prepared) (at. %)	XPS composition (as prepared) (at. %)	ICP composition (after dealloying) (at. %)	XPS composition (after dealloying) (at. %)	$ECSA_{Pt}$ ($m^2\ g^{-1}_{Pt}$)	mass activity@ 0.9 V (A mg^{-1}_{Pt})	specific acitivty@0.9 V ($\mu A\ cm^{-2}_{Pt}$)
Pt					63	0.104	166
$Pt_{25}Co_{75}$	$Pt_{26}Co_{74}$	$Pt_{42}Co_{58}$	$Pt_{83}Co_{17}$	$Pt_{86}Co_{14}$	70	0.346	491
$Pt_{25}Ni_{75}$	$Pt_{18}Ni_{82}$	$Pt_{38}Ni_{62}$	$Pt_{82}Ni_{18}$	$Pt_{77}Ni_{23}$	111	0.275	248
$Pt_{25}Cu_{75}$	$Pt_{35}Cu_{65}$		$Pt_{87}Cu_{13}$	$Pt_{98}Cu_2$	72	0.340	472

[a]Reprinted with permission from ref 261. Copyright 2011 Elsevier B.V.

other metal ions due to its higher standard reduction potential.[300] To make Pt-alloy nanoparticles with predetermined compositions, a strong reducing agent—such as sodium borohydride, hydrazine, or hydrogen—is often introduced to reduce all the metal precursors simultaneously at the proper rates (i.e., coreduction).[406,410−414] The disadvantage of the coreduction colloidal approach is that it is difficult to synthesize monodispersed alloy nanoparticles of controlled size and composition without using special agents (e.g., a template). Interestingly, counterions and solvents can change the redox potentials and thus the reduction reaction rates of given metal ions. This kind of tuning of the reaction kinetics favors the formation of Pt-alloy nanostructures with designed compositions, resulting to some extent in their high catalytic performance in PEMFCs. Therefore, selecting proper metal precursors, coupled with suitable reaction conditions, can lead to an appropriate reduction rate of metal ions in the synthesis of alloy nanoparticles.[415] Lee et al.[416] synthesized a monodispersed nanoparticle electrocatalyst of Pt−Ru supported on Vulcan carbon through the coreduction of platinum acetylacetonate ($Pt(acac)_2$) and ruthenium acetylacetonate ($Ru(acac)_3$) using 1,2-hexadecanediol as the reducing agent and oleic acid as the surfactants.[417] In their work, it was a typical long-chain diol, like 1,2-hexadecanediol, coupled with surfactants in organic solvents, that facilitated the control of the nucleation and growth processes.[185,189,416,418]

In the colloidal coreduction method, the selection of the anions in the metal precursors is important. For instance, carbonyl groups are often used in nonhydrolytic media because their decomposition products during thermal treatment are generally quite clean, which is favorable for controlling the reaction kinetics in colloid synthesis. For example, Santiago et al.[240] synthesized carbon-supported $Pt_{70}Co_{30}$ nanoparticles from platinum(II) acetylacetonate ($Pt(acac)_2$) and cobalt(II) acetylacetonate ($Co(acac)_2$) during thermal decomposition, achieving not only the desired composition but also a very small particle size of 1.9 ± 0.2 nm with a narrow distribution.

6.2.2. Platinum Intermetallic Compounds. A Pt intermetallic compound is a solid solution with a range of possible compositions, in which different metal elements, including Pt, are ordered into different sites in the structure, with distinct local environments and often a well-defined and fixed stoichiometry.[419] The ordered arrangement of an intermetallic compound can often destroy the original crystal structures of the corresponding pure metals, resulting in an asymmetrical arrangement. Although previous work reported low activities for ordered Pt-alloy catalysts such as Pt−Co catalysts, due to particle sintering during high-temperature annealing, attention has recently been given to the ordered alloy phase of Pt intermetallic compounds in an effort to explore more active carbon-supported Pt-alloy catalysts with superior catalytic performance.[264,420] It is believed that with a definite composition and structure ordered intermetallic phases could provide predictable control over structural, geometric, and electronic effects.[420−423] Usually, a sphere can be more easily controlled than other shapes in the case of Pt-alloy nanoparticles supported on carbon. Wang et al.[376] successfully synthesized an ordered Pt_3Co alloy with an intermetallic core, and a platinum shell two to three atoms thick, using a colloidal method with $H_2PtCl_6{\cdot}H_2O$ and $CoCl_2{\cdot}H_2O$ as the metal precursors. This ordered intermetallic phase was different from the disordered alloy phase, in which all columns have equal intensity and lack the (001) super period. Later, Botton's group developed a wet impregnation technique to synthesize a new structurally ordered intermetallic core−shell Pt_3Fe_2/C alloy catalysts, with an ordered Pt_3Fe_2 core encapsulated within a bilayer Pt-rich shell.[424] To obtain chemically ordered Pt−Fe alloy phases, an annealing step was required at 800 °C under 8 vol % H_2/Ar. So far, the sphere has remained as an easily controlled shape for the formation of intermetallic nanostructures.

6.3. Effect of Composition on ORR Activity

As with particle size and shape, alloy composition plays an important role in improving the catalytic performance of Pt-alloy catalysts supported on carbon. It was found that controlling the composition by fine-tuning the stoichiometric ratio of all the metal precursors (i.e., the ratio of Pt to other metals) had direct impacts on the ORR activity, the selectivity, and the durability of Pt-alloy catalysts.[147,425−430]

To examine the effects of atomic ratios on catalytic activity, certain metals, such as Co, Cr, Fe, Ni, and Mn, have been studied in Pt-based bimetallic alloy catalysts supported on carbon (i.e., PtM/C). It was found that PtM alloys with an atomic ratio of 3:1 exhibited 1.2−5.0 times higher specific activity and mass activity than Pt/C.[13,171,368,431,432] Paulus et al.[171] studied carbon-supported Pt−Ni (molar ratio of Pt:Ni = 1:1) and carbon-supported Pt−Co (molar ratio of Pt:Co = 3:1) alloy catalysts, respectively, and found that in comparison with pure Pt the activity (per Pt surface atom) was enhanced ca. 1.5 times for 25 at. % Ni or Co in Pt_3M/C (M = Ni or Co) catalysts with 20 wt % metal loading. Interestingly, Jeon et al.[176] found that thermal treatment induced dealloying of carbon-supported Pt−Ni alloy nanoparticles with various compositions of 3:1, 1:1, and 2:3. After heat treatment, the ORR activity of carbon-supported Pt−Ni alloy catalysts was enhanced due to phase separation between Pt and NiO, while the activity of as-prepared carbon-supported Pt−Ni alloy nanoparticles showed a monotonic dependence on Pt content. In particular, the mass-specfic activities (A g^{-1}_{PtNi}) at 0.85 V vs SHE followed a descending order of Pt/C (70.1) > Pt_3Ni_1/C (49.0) > Pt_1Ni_1/C (26.2) > Pt_2Ni_3/C (3.2), and in a heat-treated state, the order was Pt_1Ni_1/C (123.4) > Pt_3Ni_1/C (114.4) > Pt/C >

DOI: 10.1021/cr500519c
Chem. Rev. 2015, 115, 3433−3467

Table 9. Synthesis Method, Mass Activity, Cathode Loading, Fuel Cell Performance of Typical Carbon Supported Pt-Alloy Nanoparticle Catalysts[a]

no.	sample	synthesis method	ORR activity[b]	cathode loading[c]	fuel cell performance	year, refs
1	Pt_3Co_1/C, (50 wt % Pt)	chemical precipitation	260 (MEA, 80 °C, 3 bar)	0.3	(80 °C, 100% RH, H_2/O_2): (1) at 1, 1.5, 2, and 3 bar, current density of 0.9, 1.1, 1.2, and 1.4 A cm^{-2} at 0.6 V, respectively; (2) maximum power densities of 850 mW cm^{-2} at 3 bar.	2013, 389
2	Pd@$Pt_{1.5}$/C (40 wt % metal)	chemical precipitation	490−500 (RDE)	0.37	(80 °C, 100% RH, ambient pressure, H_2/O_2): (1) current density of 0.61 A cm^{-2} at 0.6 V; (2) maximum power density of 612 mW cm^{-2}; (3) at the same activation polarization, the current density of Pd@$Pt_{1.5}$/C is about 1.5 times higher than that of the Pt/C at 0.9 V versus RHE.	2013, 383
3	Pt_3Co_1/C (50 wt % Pt)	chemical precipitation	360 (MEA, 80 °C)	0.3, 0.3	(1) (80 °C, 100% RH, 3 bar <abs>, H_2/O_2): current density of 0.65−1.31 A cm^{-2} at 0.6 V and maximum power density of 885 mW cm^{-2}; (2) (80 °C, 33% RH, 3 bar <abs>, 1 M H_2SO_4, H_2/O_2): current density of 1.0−1.4 A cm^{-2} at 0.6 V and maximum power density of 840 mW cm^{-2}.	2012, 387
4	$PtCu_3$/C, $PtNi_3$/C, Pt/C	chemical precipitation	>440 (RDE), >440 (RDE)	0.1 0.1 0.4	(80 °C, 100% RH, 170 KPa, H_2/air): (1) initial performance of $PtNi_3$/C matched or exceeded that of Pt/C catalyst at all points of the polarization curve. For instance, the current density of $PtNi_3$/C was about 1 A cm^{-2} at 0.7 V (2) the $PtCu_3$/C showed very poor performance, particularly at high current density (1.05 A cm^{-2} at 0.6 V).	2012, 434
5	$Pt_{20}Cu_{20}Co_{60}$/C, $Pt_{25}Co_{75}$/C, $Pt_{20}Cu_{60}Co_{20}$/C, $Pt_{20}Cu_{40}Co_{40}$/C, (20−28 wt % Pt)	impregnation method	490 (RDE), 340 (RDE), 370 (RDE), 390 (RDE)	0.150, 0.146, 0.183, 0.150	(80 °C, 100% RH, H_2/O_2): at 1 A cm^{-2}, $Pt_{20}Cu_{20}Co_{60}$/C (0.815 V) > $Pt_{20}Cu_{40}Co_{40}$/C (0.808 V) > $Pt_{20}Cu_{60}Co_{20}$/C (0.802 V) > $Pt_{25}Co_{75}$/C (0.771 V)	2011, 265
6	Pt_3Co_1/C, (50 wt % Pt)	chemical precipitation		0.3	(1) (110 °C, 25% RH, 1.5 bar, H_2/O_2): current density of 0.5 A cm^{-2} at 0.6 V and maximum power densities of 700 mW cm^{-2}; (2) (110 °C, 50% RH, 1.5 bar, H_2/O_2): current density of 0.7 A cm^{-2} at 0.6 V and maximum power densities of 800 mW cm^{-2}; after 1500 cycles, the peak power density decreased by about 49%. (3) (130 °C, 100% RH, 3 bar, H_2/O_2): current density of 1.59 A cm^{-2} and maximum power density exceeding 1000 mW cm^{-2}. After 1500 cycles, the particle size of metal increased from 2.9 to 3.7 nm at 0.9−0.7 V/cell.	2010, 388
7	Pt_{ML}/Pd/C	underpotential method (UPD)	>360 (RDE)	(1) 0.077; (2) 0.099	(1) (0.6 A cm^{-2}, 80 °C, Pt/C anode): the cell voltage loss of about 120 mV after 1,000 h while the cell voltage loss of 140 mV after 2,900 h. (2) (0.417 A cm^{-2}, 80 °C, PtRu/C anode): catalyst performance of 0.47 kW g^{-1}_{Pt} after 450 h (the test was terminated when the membrane failed).	2007, 349
8	Pt_3M_1/C (M=Ni, Cr, Co) (15 wt % Pt)	unknown method from ETEK Inc.	>250 (RDE)	0.3	(95 °C, 100% RH, ambient pressure, H_2/O_2): current density order at 0.6 V is PtCr/C (2.1 A cm^{-2}) > PtCo/C (1.9 A cm^{-2}) > PtNi/C (1.85 A cm^{-2}) > Pt/C (1.4 A cm^{-2})	1993, 251

[a]RH = relative humidity. [b]In mA mg^{-1}_{Pt} at 0.9 V. [c]In mg_{Pt} cm^{-2}.

Chem. Rev. 2015, 115, 3433−3467 DOI: 10.1021/cr500519c

Pt_2Ni_3/C (24.5). To study the effect of composition on catalytic activity, Strasser's group used an impregnation method to prepare a series of high-surface-area carbon-supported Pt−Co alloy nanoparticle catalysts with atomic ratios of 1:3, 1:1, and 3:1.[175] After electrochemical treatment in 0.1 M $HClO_4$, the Pt-based mass activities increased 5-fold from Pt/C to Pt_1Co_3/C in the order of Pt/C < Pt_1Co_1/C < Pt_3Co_1/C < Pt_1Co_3/C, with similar particle sizes of 3−4 nm. Using electrochemical dealloying, Strasser's group also studied a series of PtM_3/C systems with different metals as the second alloy elements (M = Cu, Co, and Ni).[259] They examined the composition of PtM_3 using EDS (energy dispersive spectroscopy), XPS (X-ray photoelectron spectroscopy), and ICP-MS (inductively coupled plasma-mass spectroscopy; see Table 8) and found that the dissolution of 3d metals resulted in compositional changes. The degree of dealloying of Pt−Co and Pt−Ni binary systems was lower than that of Pt−Cu compounds, as evidenced by the presence of around 15−20 at. % non-noble metals near the surface and in the bulk of the dealloyed particles, whereas under the same dealloying conditions, Pt−Cu formed core−shell structures with a Pt-rich surface and a Pt−Cu core. The dealloyed binary PtM_3 catalysts showed a more than 3-fold improvement in the ORR activity for M = Co, Cu, and close to a 3-fold improvement for M = Ni in terms of the Pt-mass activity (~0.275 A mg^{-1}_{Pt}) in single fuel cell tests, in comparison with the performance of a 45 wt % Pt/C reference cathode catalyst. Improvement in the surface-area-normalized specific activity (~0.248 A cm^{-2}_{Pt}) was similar. To further improve electrocatalyst performance, Strasser's group developed a robust, facile, and surfactant-free solvothermal method to synthesize shape- and size-controlled octahedral Pt−Ni nanoparticles supported on Vulcan XC72.[433] They found that the reaction time was a critical parameter to tune the surface Pt:Ni composition and to optimize the ORR activity with a fixed molar ratio of Pt:Ni of 1:3. When the reaction time was increased to 42 h, the near-surface Pt at. % increased from 30 to 41 even though the size, shape, and bulk composition of the two Pt−Ni nanoparticles (Pt:Ni = 46:54) were identical. Moreover, the Pt−Ni/C nanoparticles (~9.5 nm) obtained after 42 h reached a 10-fold surface area-specific activity (~3.14 mA·cm_{Pt}^{-2}) as well as an unprecedented 10-fold Pt-based mass activity (1.45×10^3 mA mg^{-1}_{Pt}), approaching the theoretically predicted limits and outperforming a state-of-the-art Pt electrocatalyst. EDX analysis of the active ORR-tested Pt−Ni electrocatalyst revealed that the final bulk composition of the Pt−Ni alloy had changed to about $Pt_{75}Ni_{25}$ during the electrochemical dealloying process, similar to that of the ideal bulk composition of the highly active extended (111) surface.[433]

In addition to Stressor's group, other research groups have also made remarkable efforts to synthesize carbon-supported Pt-based nanoparticle catalysts and have investigated the relationship between the composition and ORR activity of electrocatalysts for PEMFC applications. For example, Carpenter's group developed a carbon-supported, dealloyed Pt−Cu nanoparticle catalyst[281] by a chemical dealloying method. They found that after dealloying the Pt:Cu molar ratio had changed from 0.3 to 1.8 due to the removal of copper in the dealloying process. The composition of Pt increased from 20 to 29 wt % while the Cu content decreased from 20 to 5.4 wt %. Dealloying resulted in an increase in mass activity from 0.21 to 0.29 A mg^{-1}_{Pt} at 0.90 V, and an increase in specific activity from 300 to 580 A cm^{-2}_{Pt}. Using fast Fourier transforms (FFT), they also revealed that most of the dealloyed Pt−Cu particles were disordered face-centered cubic (FCC) Pt-rich crystals with an *Fm*3*m* symmetry that was favorable for improving catalytic activity. General Motors Company[434] studied the effect of dealloying time on the activity of Pt_1Ni_3/C catalysts. It was found that the Pt content increased and the catalytic activity decreased when the catalyst dealloying time increased from 12 to 72 h. These research results suggest that there is a close set of relationships among catalyst composition, dealloying time, and ORR activity.

In addition to 3d transition metals, the noble metal Pd has also been utilized to make Pt−Pd alloy electrocatalysts supported on carbon for fuel cell applications. Zhang et al.[306] prepared sub-10 nm carbon-supported Pd(core)@Pt(shell) supported on carbon nanocatalysts by an aqueous-phase synthesis method and compared them with traditional Pt−Pd bulk alloys supported on carbon. They controlled the growth mode and morphology of the Pt shell on the Pd surface by simply adjusting the nominal Pt:Pd molar ratio. The RDE test results in 0.1 M $HClO_4$ for catalysts with Pt:Pd molar ratios of 1:3, 1:2, 2:3, 1:1, and 1:2 revealed dependence on the Pt shell morphology with $Pd_2@Pt_1/C$ (molar ratio of Pt:Pd = 1:2) having the highest mass activity and $Pd_1@Pt_2/C$ (molar ratio of Pt:Pd = 2:1) having the best area-specific activity; both values were significantly better than those of commercial Pt/C catalysts. Furthermore, the $Pd_2@Pt_1/C$ catalyst presented superior activity and durability in single H_2/O_2 fuel cell testing at very low Pt loadings (~0.15 mg_{Pd+Pt} cm^{-2}).

7. FUEL CELL PERFORMANCE OF CARBON SUPPORTED PT-ALLOY ELECTROCATALYSTS

The evaluation of carbon supported Pt-alloy nanocatalysts in an operating fuel cell is very important to validate the overall performance of the catalyst. In a PEMFC, the cathode ORR is known 6 or more orders of magnitude slower than the anode hydrogen oxidation reaction[121,279] and thus results in a limitation of the overall fuel cell performance. Hence, considerable research effort has been already put on the development and improvement of cathode catalysts and electrodes. According to the US DOE 2017 targets,[121,435,436] the power densities of MEAs should be able to reach a rated stack power of 8.0 kW g^{-1}_{Pt} at a total (anode and cathode) platinum group metals (PGM) loading of 0.125 mg cm^{-2}. The MEA is required to produce at least 0.6 V at 1.5−2 A cm^{-2}. Furthermore, the catalyst must maintain the catalytic activity over ~5000 h at 80 °C.

Although many scientists were able to obtain carbon supported Pt-alloy catalysts with a two or more fold higher ORR activity, measured by the rotating disk electrode (RDE) technique, than that of the commercial Pt/C, the performance of H_2/O_2 (or air)-PEMFCs with MEAs fabricated with these catalysts did not show direct correlation with the performance obtained through RDE tests, and as a result, these catalysts still need to be improved in order to meet the requirements of commercial PEMFCs in terms of cost, durability, power density, and Pt loading. It is widely expected that the fuel cell performance will be improved by applying the highly active carbon supported Pt-alloy catalysts in the fabrication of MEA. These alloy catalysts are often prepared by different size, shape, and/or composition-controlled synthesis routes for the achievement of high ORR activity. Table 9 lists the synthesis method, ORR activity through RDE tests, cathode loading, and fuel cell performance for some size, shape, and/or composition-

DOI: 10.1021/cr500519c
Chem. Rev. 2015, 115, 3433−3467

controlled carbon supported Pt-alloy catalysts surveyed in this review that were evaluated in both RDE tests and operating fuel cells. It can be seen that almost all PtM/C (M = Co, Pd, Cu, Ni, and Cr) catalyst samples in Table 9 exhibited an ORR activity above 250 mA mg^{-1}_{Pt}, along with a Pt loading of 15−50 wt % on the carbon support. At the cathode loading of 0.077−0.37 mg_{Pt} cm^{-2} in the MEA, the tested current density was found to be dependent on some factors such as temperature, pressure, and relative humidity (RH). It is also evidenced in the literature[387,388] that under fuel cell operation the particle size and lattice parameters in crystal increased to some extent over time during the degradation test, indicating a moderate dealloying for the Pt-alloy catalyst with nonprecious metals like Co. But this dissolution of nonprecious metal(s) is not beneficial to the stability of Pt-alloy and results in a deteriorating fuel cell performance, in particular under the long-term operation of fuel cells.

Therefore, for the preparation of carbon supported Pt-alloy catalysts by a size, shape, and composition-controlled route, the addition of a preleaching procedure can be beneficial for reducing the contamination during the fuel cell operation. The increase of particle size and the change of crystal parameters after the degradation suggest that the carbon supported Pt-alloy catalyst should not only be able to exhibit a high ORR activity but also have a physicochemical and electrochemical stability so that the catalyst can be utilized in the commercial PEMFC with a low PGM loading equal to or lower than 0.125 mg cm^{-2}.

8. CONCLUSIONS

The ORR at the cathode is the rate-determining step in the whole set of fuel cell reactions due to its sluggishness in comparison with the anode reaction. To date, Pt-based catalysts have been considered the most practical for the ORR. However, due to the high cost and limited supply of Pt, reducing Pt loading in the catalyst layer and thus the cost of the PEMFCs has become one of the key targets to achieve their widespread commercialization. The most common strategy in Pt load reduction is alloying Pt with other metal elements to form Pt-alloy catalysts. The use of metal alloys not only reduces the noble metal content but also increases the catalytic activity toward the ORR. To date, significant progress has been made in the preparation and evaluation of Pt-based nanostructured alloy electrocatalysts, and their catalytic activities toward the ORR have been revealed to be strongly dependent on the size and size distribution, shape, and composition of the alloy nanoparticles.

In an attempt to provide general observations on the current status of catalyst development as well as future research directions, this review broadly examined the most recent progress and research trends in the development of carbon-supported Pt-based alloy electrocatalysts with desirable shapes, uniform sizes, and controlled compositions, through both theoretical and experimental studies reported in the literature. Particularly in the review of experimental studies, systematic and comparative examinations have been carried out in terms of material selection, synthesis methods, structural characterization, and catalytic performance evaluation in relation to the size, shape, and composition of catalyst particles. It was concluded in this review refining the parameters of Pt-alloy nanoparticles (such as shape, size, and composition) could be used to precisely control their microstructure and properties and, consequently, to enhance the catalytic activity of electrocatalysts for the ORR. In general, the size and size distribution of Pt-alloy nanoparticles can be controlled at the molecular (nanometer) level. Particles with optimal size and uniform size distribution, coupled with desirable shape and composition, can yield a tremendous advantage over conventional Pt-alloy bulk catalysts in terms of ORR activity because of the former's much larger active surface area to volume ratio. Although the size, shape, and composition of Pt-alloy nanoparticles are all key parameters in the design and preparation of Pt-alloy nanocatalysts, a desirable particle shape (e.g., octahedral, tetrahedral, cubic, etc.) has been recognized to play a more dominant role in the improvement of ORR catalysis in PEMFCs. With more and more recent discoveries in the development of advanced Pt-based catalysts, the catalytic activity of monodispersed Pt-alloy nanoparticle catalysts supported on carbon is often found to depend on Pt-alloy shape, and optimal ORR activity can be achieved by controlling this shape. In particular, the core−shell structured Pt-alloy nanoparticles have been intensively studied. In the preparation of core−shell structured catalysts, Pt (or Pt alloy) is deposited on other MPt or non-Pt metal nanoparticle cores, followed by a dealloying process (or replacement reaction) to form the Pt or Pt-alloy shell. Core−shell structured Pt-alloy nanocatalysts have been proven capable of greatly enhancing not only the ORR activity but also the catalyst durability due to the electronic and strain effects that arise on the nanostructured surface, which can be adjusted by the selection of various materials and different synthesis routes.

Despite the exciting progress made in the past decade in terms of correlating the size, shape, and composition of carbon-supported Pt-based electrocatalysts with their electrocatalytic properties for the ORR, there is still a noticeable lack of mass production techniques for manufacturing high-quality, monodispersed Pt-alloy catalysts with optimized structural parameters, such as optimal size, desired shape, and controllable composition. Therefore, significant challenges still remain in developing facile and efficient methods for the synthesis of a designed Pt-alloy nanostructure with uniform particle size, desirable shape, and favorable composition. The requisite synthesis method needs not only to enable the precise tuning of catalyst parameters (e.g., size, shape, and composition) but also to be feasible for practical mass production. This review reveals that materials selection and synthesis methods both play a key role in the formation of desirable catalyst structures with enhanced ORR activity. In terms of synthesis methods, many approaches for preparing advanced Pt-based catalysts have been studied and reported, such as surfactant-free solvothermal methods, electrochemical dealloying methods, electrochemical deposition methods, freeze-drying methods, and wet chemical methods (e.g., aqueous-phase synthesis, colloid chemical methods, impregnation reduction methods, microemulsion methods, and coreduction methods). Among these approaches, wet chemical synthesis has been employed the most. In wet chemical synthesis, the chemistry of liquid−solid interfaces (e.g., the chemical reactivity of crystal planes) plays an essential role in the size- and direction-controlled growth of nanostrucures for catalysts, under a set of reaction conditions that include protective agent, reaction medium, pH value, pressure, and temperature. A number of issues are key for synthesizing a desirable catalyst with high ORR activity: (1) chemical compatibility among the different solid components; (2) structural (lattice) compatibility among the different solid phases in a designed nanocomposite; (3) the surface chemistry of adsorbed ligands and surfactants on the studied materials;

DOI: 10.1021/cr500519c
Chem. Rev. 2015, 115, 3433−3467

(4) the chemical stability of the resultant nanostructures in their synthesis environments; and (5) the stability of the prepared nanocatalyst product under ORR catalysis conditions. All these factors dictate what materials and synthetic strategy will be selected, so as to achieve technological breakthroughs in the microstructure and performance of ORR catalysts.

Based on the issues examined in this review, several important future research directions are proposed to understand the relationship between microstructure and ORR activity and to design highly active, carbon-supported Pt-based alloy electrocatalysts:

(1) Developing a fundamental understanding of the electronic and lattice structures of well-defined crystal surfaces or designed Pt-alloy nanocrystals and of their various properties, such as lattice shrinking, the skin effect, and d-band vacancy, to identify the correlations between ORR activity and catalyst features such as particle size, shape, and composition. Theoretical studies and modeling can play a guiding role in this effort.

(2) Developing new approaches to synthesize monodispersed and optimally sized nanostructured carbon-supported Pt-based alloy catalysts with desirable shape to obtain high activity and good durability. In particular, three major strategies can be considered. One is to obtain monodispersed, size-controlled Pt-alloy nanoparticle catalysts with rich, high-index facets; a second is to prepare Pt-alloy nanoparticle catalysts with diverse morphologies and compositions corresponding to high-index facets; and a third is to uniformly distribute and effectively connect Pt-alloy nanoparticles on the surface of carbon supports with the expected size, shape, and nanostructure. Carbon-supported Pt-alloy nanoparticle catalysts with well-defined morphologies can effectively enhance their performance in fuel cell applications. When preparing monodispersed and optimally sized Pt-alloy nanostructures, the experimental conditions should be carefully controlled.

(3) Optimizing the catalyst structure by tuning the size, shape, and composition of catalysts to achieve the best design. It is well-known that the composition of Pt alloys can play an important role in balancing high catalytic activity and stability. From an engineering perspective, nanoscale Pt-alloy phases and their corresponding structures (e.g., the core−shell structure) can be successfully controlled by a high-throughput, combinatorial screening method that can identify the combinations of alloy phases and compositions, thereby achieving an optimized balance between catalytic activity and stability.

AUTHOR INFORMATION

Corresponding Authors

*Tel: 1-604-221-3000 (Ext 5592). E-mail: Hui.Li@nrc-cnrc.gc.ca.
*Tel: 1-604-822-4408. E-mail: xbi@chbe.ubc.ca.
*Tel: 1-604-221-3038. E-mail: Haijiang.Wang@nrc-cnrc.gc.ca.

Notes

The authors declare no competing financial interest.

Biographies

Yan-Jie Wang obtained his M.S. and Ph.D. in Materials Science from North University of China in 2002 and Zhejiang University, China in 2005, respectively. Subsequently, he conducted two and a half years of postdoctoral research at Sungkyunkwan University, Korea, followed by two years as a research scholar at Pennsylvania State University, USA, studying advanced functional materials. In April of 2009, he was cohired by the University of British Columbia and the National Research Council of Canada to research fuel cell catalysts. From November of 2012, he worked solely as a senior research scientist for the University of British Columbia, under the supervision of Prof. Dr. Xiaotao T. Bi in the Department of Chemical and Biological Engineering, researching core−shell structured fuel cell electrocatalysts at Vancouver International Clean-Tech Research Institute Inc. (VICTRII). Dr. Wang has published 42 papers in peer-reviewed journals and conference proceedings. He is particularly interested in physicochemical synthesis and electrochemical technology in the field of energy conversion and storage.

Nana Zhao received her B.S. in Polymer Chemistry and Physics at Beijing Normal University, China, in 2000. She then joined Changchun University of Science and Technology as a teaching assistant for two years before commencing her Ph.D. program in Polymer Chemistry and Physics at the Changchun Institute of Applied Chemistry, Chinese Academy of Sciences, in 2002. After obtaining her Ph.D. in 2008, she joined Prof. Ting Xu's group as a postdoctoral fellow in Materials Science and Engineering at the University of California, Berkeley, USA. Upon completing one term of postdoctoral research, she took a position as a research associate at the National Research Council of Canada − Energy, Mining and Environment Portfolio (NRC-EME, formerly the NRC Institute for Fuel Cell Innovation) for two years. In 2013, she began working as a research scientist at Vancouver International Clean-Tech Research Institute Inc. (VICTRII). Her research interests include MEA design and

DOI: 10.1021/cr500519c
Chem. Rev. 2015, 115, 3433−3467

fabrication, catalyst layer/MEA evaluation, and the synthesis and characterization of inorganic nanocrystals.

Baizeng Fang earned his Ph.D. in Materials Science from the University of Science and Technology, Beijing, China, in 1997. He worked as a postdoctoral fellow (PDF) at the Energy Research Centre of The Netherlands (ECN) in 1998, as a Japan Society for the Promotion of Science (JSPS) research fellow and guest researcher from 2000 to 2004 at IRI, Japan, as a PDF from 2004 to 2005 at the National Institute of Advanced Industrial Science and Technology (AIST), Japan, and as a Lise Meitner Scientist at the Austrian Science Fund (FWF) from 2005 to 2006. He joined Prof. Jong-Sung Yu's group as a PDF at Hannam University, Korea, from 2006 to 2008 and as a research professor from March 2008 to March 2010 at Korea University. In July 2010, he joined Prof. David P. Wilkinson's research group as a senior research scientist at the University of British Columbia, Canada. Dr. Fang has published more than 80 research papers in peer-reviewed journals. His research interests include the development of novel nanostructured materials for applications in fuel cells, hydrogen storage, solar cells, electrochemical capacitors, secondary batteries (i.e., Li-ion batteries and redox flow batteries), metal–air fuel cells, photocatalysis, electrocatalysis, and electrochemistry.

Hui Li is a Research Council Officer and a Program Technical Lead under the Energy Storage program at the National Research Council of Canada – Energy, Mining and Environment Portfolio (NRC-EME, formerly the NRC Institute for Fuel Cell Innovation). Dr. Li received her B.S. and M.Sc. in Chemical Engineering from Tsinghua University, China, in 1987 and 1990, respectively. After completing her M.Sc., she joined Kunming Metallurgical Institute as a research engineer for four years and then took a position as an associate professor at Sunwen College, China, for eight years. In 2002, she started her Ph.D. program in Electrochemical Engineering at the University of British Columbia, Canada. After obtaining her Ph.D. in 2006, she carried out one term of postdoctoral research at the Clean Energy Research Centre (CERC) at the University of British Columbia with Prof. Colin Oloman and Prof. David Wilkinson. Since joining NRC in 2007, Dr. Li has been working on PEM fuel cell contamination and durability, PEM electrolysis, and zinc–air batteries. Dr. Li has years of research and development experience in theoretical and applied electrochemistry and in electrochemical engineering. Her research is based on PEM fuel cell contamination and durability testing, the preparation and development of electrochemical catalysts with long-term stability, catalyst layer/cathode structure, catalyst layer characterization and electrochemical evaluation, failure diagnosis and mitigation for PEM fuel cells and electrolyzers, and air-cathodes for zinc–air batteries. Dr. Li has coauthored more than 30 research papers published in refereed journals and coedited three books related to PEM fuel cells. She also has two granted patents and one technology licensed to the Mantra Energy Group.

Xiaotao T. Bi received BASc (1980–1985) and MASc (1985–1988) degrees from Tsinghua University, and a Ph.D. (1991–1994) degree from the University of British Columbia. He worked at the Ohio State University (1989–1991) as a research assistant, University of British Columbia (1994–1995) and Ecole Polytechnique de Montreal (1995–1996) as a postdoctoral fellow, and the Natural Gas Technologies Centre (1996–1997) as a research scientist before he joined UBC as a faculty member in 1997. He served as the associate chair of Chemical and Biological Engineering Department from 2006–2009 and currently as the associate director of the UBC Clean Energy Research Centre and manager of the Fluidization Research Centre. His current research has been focused on particle technology and multiphase reactor systems, spanning from electrostatics in particle systems, catalytic NOx reduction and biomass thermochemical conversion to water management in PEM fuel cells, life cycle analysis and integrated impact assessment of biomass energy systems. He has published more than 300 peer-reviewed papers. He also held patents on novel fluidized bed reactors for animal waste treatment, catalytic NOx reduction, and electrostatics monitoring. He was the recipient of a UBC Killam Senior Research Fellowship (2011) and the 2012 AIChE Particle Technology Forum Lectureship Award. He is a registered professional engineer at British Columbia (APEGBC) and a fellow of the Canadian Academy of Engineering.

DOI: 10.1021/cr500519c
Chem. Rev. 2015, 115, 3433–3467

Haijiang Wang received his Ph.D. degree in electrochemistry from the University of Copenhagen, Denmark, in 1993. He then joined Dr. Vernon Parker's research group at the Utah State University as a postdoctoral researcher to study electrochemically generated anion and cation radicals. In 1997 he began working with Natural Resources Canada as a research scientist to carry out research on fuel cell technology. In 1999 he joined Ballard Power Systems as a senior research scientist to continue his fuel cell investigation. After spending five years with Ballard Power Systems, in 2004, he joined the National Research Council Canada as a senior research officer, project manager of multiprojects, and team leader of the Unit Fuel Cell Team. He is also adjunct professor of the University of British Columbia and the University of Waterloo. Dr. Wang has made significant contribution to advancing the science and technology of proton exchange membrane fuel cell, direct alcohol fuel cell, metal−air battery, microbial fuel cell, and other electrochemical science and technology. To date, Dr. Wang has accumulated over 30 years professional research experience in electrochemistry and fuel cell technology. He has published 165 journal papers, three books, ten book chapters, 40 industrial reports, and 30 conference papers/presentations, and has been granted three patents. He was listed in the "The World's Most Influential Scientific Minds" published by Thomson-Reuters in 2014.

ACKNOWLEDGMENTS

This work was supported by the Vancouver International CleanTech Research Institute Inc. (VICTRII) and a matching Natural Sciences and Engineering Research Council of Canada Collaborative Research and Development (NSERC-CRD) Grant 452756-13. The authors would also like to acknowledge the contribution of Dr. Tim at VICTRII and of all members of Prof. Xiaotao Bi's catalyst group in the Department of Chemical and Biological Engineering at the University of British Columbia.

REFERENCES

(1) Tasbirul Islam, Md.; Shahir, S. A.; Iftakhar Uddin, T. M.; Saifullah, A. Z. A. *Renew. Sustain. Energy Rev.* **2014**, *39*, 1074.
(2) Bashyam, R.; Zelenay, P. *Nature* **2006**, *443*, 63.
(3) Wang, Y.-J.; Wilkinson, D. P.; Zhang, J. *Chem. Rev.* **2011**, *111*, 7625.
(4) Fang, B.; Chaudhari, N.; Kim, M.; Kim, J.; Yu, J. *J. Am. Chem. Soc.* **2009**, *131*, 15330.
(5) Fang, B.; Kim, J.; Kim, M.; Yu, J. *Chem. Mater.* **2009**, *21*, 789.
(6) Yoon, S.; Fang, B.; Kim, M.; Kim, J.; Yu, J. Chapter 4, Nano-structured Supported Catalysts for Low Temperature Fuel Cells. *Frontiers of Nanoscience* **2009**, *1*, 173.
(7) Fang, B.; Kim, J.; Kim, M.; Yu, J. *Acc. Chem. Res.* **2013**, *46*, 1397.
(8) Herring, A. M.; Zawodzinski, T. A., Jr.; Hamrock, S. J. *Fuel Cell Chemistry and Operation; ACS Symposium Series*; American Chemical Society: Washington, DC, 2010.
(9) Hoogers, G. *Fuel Cell Technology Handbook*; CRC Press: Boca Raton, FL, 2003.
(10) Li, Y. M.; Somorjai, G. A. *Nano Lett.* **2010**, *10*, 1078.
(11) Guo, S.; Wang, E. *Nano Today* **2011**, *6*, 240.
(12) Peng, Z.; Yang, H. *Nano Today* **2009**, *4*, 143.
(13) Gasteiger, H. A.; Kocha, S. S.; Sompalli, B.; Wagner, F. T. *Appl. Catal. B: Environ.* **2005**, *56*, 9.
(14) Lin, X.; Zheng, L.; Gao, G.; Chi, Y.; Chen, G. *Anal. Chem.* **2012**, *84*, 7700.
(15) Appleby, A. J. In *The Electrocatalysis of Fuel Cell Reactions*; Dudley, R., O'Grady, W., Srinivasan, S., Eds.; The Electrochemical Society Softbound Proceedings Series, PV 79−2, Princeton, NJ, 1979; p 23.
(16) Fang, B.; Kim, J.; Lee, C.; Yu, J. *J. Phys. Chem. C* **2008**, *112*, 639.
(17) Fang, B.; Kim, J.; Yu, J. *Electrochem. Commun.* **2008**, *10*, 659.
(18) Chai, G.; Fang, B.; Yu, J. *Electrochem. Commun.* **2008**, *10*, 1801.
(19) Fang, B.; Kim, J.; Kim, M.; Kim, M.; Yu, J. *Phys. Chem. Chem. Phys.* **2009**, *11*, 1380.
(20) Kim, J.; Fang, B.; Yoon, S.; Yu, J. *Appl. Catal. B: Environ.* **2009**, *88*, 368.
(21) Fang, B.; Kim, M.; Kim, J.; Song, M.; Wang, Y.; Wang, H.; Wilkinson, D.; Yu, J. *J. Mater. Chem.* **2011**, *21*, 8066.
(22) Kim, J.; Fang, B.; Song, M.; Yu, J. *Chem. Mater.* **2012**, *24*, 2256.
(23) Besenbacher, F.; Chorkendorff, I.; Clausen, B. S.; Hammer, B.; Molenbroek, A. M.; Norskov, J. K.; Stensgaard, I. *Science* **1998**, *279*, 1913.
(24) Strasser, P.; Koh, S.; Anniyev, T.; Greeley, J.; More, K.; Yu, C. F.; Liu, Z. C.; Kaya, S.; Nordlund, D.; Ogasawara, H.; Toney, M. F.; Nilsson, A. *Nat. Chem.* **2010**, *2*, 454.
(25) Kim, M.; Lim, S.; Chaudhari, N.; Fang, B.; Bae, T.; Yu, J. *Catal. Today* **2010**, *158*, 354.
(26) Kim, M.; Fang, B.; Chaudhari, N.; Song, M.; Bae, T.; Yu, J. *Electrochim. Acta* **2010**, *55*, 4543.
(27) Kim, J.; Fang, B.; Kim, M.; Yoon, S.; Bae, T.; Ranade, D.; Yu, J. *Electrochim. Acta* **2010**, *55*, 7628.
(28) Kim, J.; Fang, B.; Kim, M.; Tricoli, V.; Yu, J. *Catal. Today* **2009**, *146*, 25.
(29) Wang, Y.−J.; Wilkinson, D. P.; Guest, A.; Neburchilov, V.; Baker, R.; Nan, F.; Botton, G. A.; Zhang, J. *J. Power Sources* **2013**, *221*, 232.
(30) Maroun, F.; Ozanam, F.; Magnussen, O. M.; Behm, R. J. *Science* **2001**, *293*, 1811.
(31) Burch, R. *Acc. Chem. Res.* **1982**, *15*, 24.
(32) Watanabe, M.; Tryk, D. A.; Wakisaka, M.; Yano, H.; Uchida, H. *Electrochim. Acta* **2012**, *84*, 187.
(33) Wu, J. B.; Yang, H. *Acc. Chem. Res.* **2013**, *46*, 1848.
(34) Porter, N. S.; Wu, H.; Quan, Z. W.; Fang, J. Y. *Acc. Chem. Res.* **2013**, *46*, 1867.
(35) Liu, Z. M.; Ma, L. L.; Zhang, J.; Hongsirikarn, K.; Goodwin, J. G. *Catal. Rev. Sci. Eng.* **2013**, *55*, 255.
(36) Liu, M.; Zhang, R.; Chen, W. *Chem. Rev.* **2014**, *114*, 5117.
(37) Antolini, E. *Appl. Catal. B Environ.* **2007**, *74*, 337.
(38) Norskov, J. K.; Rossmeisl, J.; Logadottir, A.; Lindqvist, L.; Kitchin, J. R.; Bligaard, T.; Jonsson, H. *J. Phys. Chem. B* **2004**, *108*, 17886.
(39) Antolini, E. *Mater. Chem. Phys.* **2003**, *78*, 563.
(40) Antolini, E. *Appl. Catal. B Environ.* **2007**, *74*, 324.
(41) Luczak, F. J.; Landsman, D. A. U.S. Patent 4,447,506, 1984.
(42) Luczak, F. J.; Landsman, D. A. U.S. Patent 4,677,092, 1987.
(43) Luczak, F. J.; Landsman, D. A. U.S. Patent 4,711,829, 1987.
(44) Luczak, F. J.; Landsman, D. A. U.S. Patent 4,806,515, 1989.
(45) Luczak, F. J.; Landsman, D. A. U.S. Patent 4,880,711, 1990.
(46) Luczak, F. J. U.S. Patent 5,013,618, 1991.
(47) Loukrakpam, R.; Luo, J.; He, T.; Chen, Y.; Xu, Z.; Njoki, P. N.; Wanjala, B. N.; Fang, B.; Mott, D.; Yin, J. *J. Phys. Chem. C* **2011**, *115*, 1682.

DOI: 10.1021/cr500519c
Chem. Rev. 2015, 115, 3433−3467

(48) Long, N. V.; Thi, C. M.; Yong, Y.; Nogami, M.; Ohtaki, M. *J. Nanosci. Nanotechnol.* **2013**, *13*, 4799.
(49) Chen, C.; Kang, Y.; Huo, Z.; Zhu, Z.; Huang, W.; Xin, H.; Snyder, J. D.; Li, D.; Herron, J. A.; Mavrikakis, M.; Chi, M.; More, K. L.; Li, Y.; Markovic, N. M.; Somorjai, G. A.; Yang, P.; Stamenkovic, V. R. *Science* **2014**, *343*, 1339.
(50) Ignaszak, A.; Song, C.; Zhu, W.; Wang, Y.-J.; Zhang, J.; Bauer, A.; Baker, R.; Neburchilov, V.; Ye, S.; Campbell, S. *Electrochim. Acta* **2012**, *75*, 220.
(51) Wang, Y.-J.; Wilkinson, D. P.; Neburchilov, V.; Song, C.; Guest, A.; Zhang, J. *J. Mater. Chem. A* **2014**, *2*, 12681.
(52) Antolini, E. *Appl. Catal., B* **2009**, *88*, 1.
(53) Schmidt, T. J.; Gasteiger, H. A.; Stab, G. D.; Urban, P. M.; Kolb, D. M.; Behm, R. J. *J. Electrochem. Soc.* **1998**, *145*, 2354.
(54) Passalacqua, E.; Lufrano, F.; Squadrito, G.; Patti, A.; Giorgi, L. *Electrochim. Acta* **2001**, *46*, 799.
(55) Min, M.; Cho, J.; Cho, K.; Kim, H. *Electrochim. Acta* **2000**, *45*, 4211.
(56) Hoogers, G. *Fuel Cell Technology Handbook*; CRC Press, Boca Raton, FL, 2003; Chapter VI.
(57) Yu, X.; Ye, S. *J. Power Sources* **2007**, *172*, 133.
(58) Rodriguez-Reinoso, F. *Carbon* **1998**, *36*, 159.
(59) Pylypenko, S.; Borisevich, A.; More, K. L.; Corpuz, A. R.; Hlome, T.; Dameron, A. A.; Olson, T. S.; Dinh, H. N.; G, T.; O'Hayre, R. *Energy Environ. Sci.* **2013**, *6*, 2957.
(60) Shao, Y.; Sui, J.; Yin, G.; Gao, Y. *Appl. Catal. B Environ.* **2008**, *79*, 89.
(61) Hyun, K.; Lee, J. H.; Yoon, C. W.; Kwon, Y. *Int. J. Electrochem. Sci.* **2013**, *8*, 11752.
(62) Antolini, E.; Salgado, J. R. C.; Gonzalez, E. R. *J. Power Sources* **2006**, *160*, 957.
(63) Kim, C.; Kim, Y.-J.; Kim, Y.-A.; Yanagisawa, T.; Park, K.-C.; Endo, M.; Dresselhars, M. S. *J. Appl. Phys.* **2004**, *96*, 5903.
(64) Xu, J.; Zhao, T.; Yang, W.; Shen, S. *Int. J. Hydrogen Energy* **2010**, *35*, 8699.
(65) Shukla, A. K.; Neergat, M.; Bera, P.; Jayaram, V.; Hegde, M. S. *J. Electroanal. Chem.* **2001**, *504*, 111.
(66) Shao, Y.; Yin, G.; Gao, Y. *J. Power Sources* **2007**, *171*, 558.
(67) Aricò, A. S.; Shukla, A. K.; Kim, H.; Park, S.; Min, M.; Antonucci, V. *Appl. Surf. Sci.* **2001**, *172*, 33.
(68) Nilekar, A. U.; Xu, Y.; Zhang, J.; Vukmirovic, M. B.; Sasaki, K.; Adzic, R. R.; Mavrikakis, M. *Top. Catal.* **2007**, *46*, 276.
(69) Calderón, J. C.; Mahata, N.; Pereira, M. F. R.; Figueiredo, J. L.; Fernandes, V. R.; Rangel, C. M.; Calvillo, L.; Lázaro, M. J.; Pastor, E. *Int. J. Hydrogen Energy* **2012**, *37*, 7200.
(70) Zenyuk, I. V.; Litster, S. *J. Phys. Chem. C* **2012**, *116*, 9862.
(71) Fialkov, A. S. *Russ. J. Electrochem.* **2000**, *36*, 389.
(72) Escard, J. J.; Fialkov, A. S.; Leclerc, C.; Contour, J. P. *Catalysis* **1973**, *29*, 31.
(73) Hillenbrand, L. J.; Lacksonen, J. W. *J. Electrochem. Soc.* **1965**, *112*, 249.
(74) Coloma, F.; Sepulveda, A.; Fierro, J.; Rodriguez-Reinoso, F. *Appl. Catal., A* **1996**, *148*, 63.
(75) Shukla, A. K.; Ravikumar, M. K.; Roy, A.; Barman, S. R.; Sarma, D. D.; Aricò, A. S.; Antonucci, V.; Pino, L.; Giordano, N. *J. Electrochem. Soc.* **1994**, *141*, 1517.
(76) Shukla, A.; Ramesh, K.; Manoharan, R.; Sarode, P.; Vasudevan, S. *Ber. Bunsenges. Phys. Chem.* **1985**, *89*, 1261.
(77) Mason, M. G. *Phys. Rev. B* **1983**, *27*, 748.
(78) Eberhardt, W.; Fayet, P.; Cox, D. M.; Fu, Z.; Kaldor, A.; Sherwood, R.; Sondericker, D. *Phys. Rev. Lett.* **1990**, *64*, 780.
(79) Antolini, E.; Giorgi, L.; Cardellini, F.; Passalacqua, E. *J. Solid State Electrochem.* **2001**, *5*, 131.
(80) Goodenough, J. B.; Manoharan, R. *Chem. Mater.* **1989**, *1*, 391.
(81) McBreen, J.; Mukerjee, S. *J. Electrochem. Soc.* **1995**, *142*, 3399.
(82) Park, I.-S.; Par, K.-W.; Choi, J.-H.; Park, C. R.; Sung, Y.-E. *Carbon* **2007**, *45*, 28.
(83) Slanac, D. A.; Li, L.; Mayoral, A.; Yacaman, M. J.; Manthiram, A.; Stevenson, K. J.; Johnston, K. P. *Electrochim. Acta* **2012**, *64*, 35.
(84) Bogotski, V. S.; Snudkin, A. M. *Electrochim. Acta* **1984**, *29*, 757.
(85) Park, K.-C.; Jang, I.-Y.; Wongwiriyapan, W.; Morimoto, S.; Kim, Y.-J.; Jung, Y.-C.; Toya, T.; Endo, M. *J. Mater. Chem.* **2010**, *20*, 5345.
(86) Coloma, F.; Sepúlveda-Escribano, A.; Fierro, J. L. G.; Rodríguez-Reinoso, F. *Appl. Catal., A* **1997**, *150*, 165.
(87) Torres, G. C.; Jablonski, E. L.; Baronetti, G. T.; Castro, A. A.; de Miguel, S. R.; Scelza, O. A.; Blanco, M. D.; Peña Jiménez, M. A.; Fierro, J. L. G. *Appl. Catal., A* **1997**, *161*, 213.
(88) Aksoylu, A. E.; Freitas, M. M. A.; Figueiredo, J. L. *Appl. Catal., A* **2000**, *192*, 29.
(89) Prado-Burguete, C.; Linares-Solano, A.; Rodríguez-Reinoso, F.; Salinas-Martínez de Lecea, C. *J. Catal.* **1989**, *115*, 98.
(90) Liang, Y.; Zhang, H.; Yi, B.; Zhang, Z.; Tan, Z. *Carbon* **2005**, *43*, 3144.
(91) Perego, C.; Villa, P. *Catal. Today* **1997**, *34*, 281.
(92) Chochos, C. ; Gourdoupi, N. ; Triantafyllopoulos, N. ; Kallitsis, J. U.S. Patent 8,247,521 *B2*, 2012.
(93) Zhang, J. *PEM fuel cell electrocatalysts and catalyst layers: fundamentals and applications*; Springer: New York, 2008.
(94) Lavacchi, A.; Miller, H.; Vizza, F. *Nanotechnology in electrocatalysis for energy*; Springer: New York, 2013.
(95) Selvarani, G.; Vinod Selvaganesh, S.; Sridhar, P.; Pitchumani, S.; Shukla, A. K. *Bull. Mater. Sci.* **2011**, *34*, 337.
(96) Watanabe, M.; Uchida, M.; Motto, S. *J. Electroanal. Chem. Interfacial Electrochem.* **1987**, *229*, 395.
(97) Bang, J. H.; Han, K.; Skrabalak, S. E.; Kim, H.; Suslick, K. S. *J. Phys. Chem. C* **2007**, *111*, 10959.
(98) Xue, X. Z.; Liu, C. P.; Xing, W.; Lu, T. H. *J. Electrochem. Soc.* **2006**, *153*, E79.
(99) Patil, P. S. *Mater. Chem. Phs.* **1999**, *59*, 185.
(100) Shao, Y. Y.; Liu, J.; Wang, Y.; Lin, Y. H. *J. Mater. Chem.* **2009**, *19*, 46.
(101) Candelaria, S. L.; Shao, Y.; Zhou, W.; Li, X.; Xiao, J.; Zhang, J.−G.; Wang, Y.; Liu, J.; Li, J.; Cao, G. *Nano Energy* **2012**, *1*, 195.
(102) Trogadas, P.; Fuller, T. F.; Strasser, P. *Carbon* **2014**, *75*, 5.
(103) Augustine, R. L.; *Heterogeneous Catalysis for the Synthetic Chemist*; Marcel Dekker Incorporated: New York, 1996.
(104) Saha, M. S.; Neburchilov, V.; Ghosh, D.; Zhang, J. *WIREs Energy Environ.* **2013**, *2*, 31.
(105) Mansor, N.; Jorge, A. B.; Corà, F.; Gibbs, C.; Jervis, R.; McMillan, P. F.; Wang, X.; Brett, D. J. L. *J. Phys. Chem. C* **2014**, *118*, 6831.
(106) Zhou, Y.; Neyerlin, K.; Olson, T. S.; Pylypenko, S.; Bult, J.; Dinh, H. N.; Gennett, T.; Shao, Z.; O'Hayre, R. *Energy Environ. Sci.* **2010**, *3*, 1437.
(107) Limpattayanate, S.; Hunsom, M. *Renew. Energy* **2014**, *63*, 205.
(108) Yermakov, Y. I.; Surovikin, V. F.; Plaksin, G. V.; Semikolenov, V. A.; Likholobov, V. A.; Chuvilin, A. L.; Bogdanov, S. V. *React. Kinet. Catal. Lett.* **1987**, *33*, 435.
(109) Gamez, A.; Richard, D.; Gallezot, P. In Resume des Journees d'Etude Piles a Combustible; Paris, France, 1999; p 401.
(110) Kou, R.; Shao, Y.; Mei, D.; Nie, Z.; Wang, D.; Wang, C.; Viswanathan, V. V.; Park, S.; Aksay, I. A.; Lin, Y.; Wang, Y.; Liu, J. *J. Am. Chem. Soc.* **2011**, *133*, 2541.
(111) Siburian, R. *Int. Res. J. Pure Appl. Chem.* **2014**, *4*, 541.
(112) Wu, J.; Yuan, X.-Z.; Martin, J. J.; Wang, H.; Zhang, J.; Shen, J.; Wu, S.; Merida, W. *J. Power Sources* **2008**, *184*, 104.
(113) Knights, S. D.; Colbow, K. M.; St-Pierre, J.; Wilkinson, D. P. *J. Power Sources* **2004**, *127*, 127.
(114) Virkar, A. V.; Zhou, Y. *J. electrochem. Soc.* **2007**, *154*, B540.
(115) Garland, N. Fuel Cells Plenary; 2008 DOE Hydrogen Program Merit Review and Peer Evaluation Meeting, 2008.
(116) Paulus, U. A.; Wokaun, A.; Scherer, G. G.; Schmidt, T. J.; Stamenkovic, V.; Markovic, N. M.; Ross, P. N. *Electrochim. Acta* **2002**, *47*, 3787.
(117) Ralph, T. R.; Hogarth, M. P. *Platinum Met. Rev.* **2002**, *46*, 3.
(118) Passalacqua, E.; Vivaldi, M.; Giordano, N.; Anotonucci, P. L.; Kinoshita, K. *Proceedings of the 27th Intersociety Energy Conversion Engineering Conf.*; 1992; Vol. *929294*, pp 3.425−3.431.

DOI: 10.1021/cr500519c
Chem. Rev. 2015, 115, 3433−3467

(119) Schulenburg, H.; Müller, E.; Khelashvili, G.; Roser, T.; Bönnemann, H.; Wokaun, A.; Scherer, G. G. *J. Phys. Chem. C* **2009**, *113*, 4069.
(120) Thompsett, D. In *handbook of fuel cells—fundamentals, technology and applications*; Vielstich, W., Lamm, A., Gasteiger, H. A., Eds.; John Wiley & Sons: New York, 2003; Chapter 37.
(121) Debe, M. K. *Nature* **2012**, *486*, 43.
(122) Gomes, J. F.; Profeti, D.; Deiner, L. J. *ChemElectroChem* **2013**, *1*, 655.
(123) Roques, J.; Anderson, A. B.; Murthi, V. S.; Mukerjee, S. *J. Electrochem. Soc.* **2005**, *152*, E193.
(124) Salgado, J. R. C.; Antolini, E.; Gonzalez, E. R. *J. Power Sources* **2005**, *141*, 13.
(125) Rao, C. V.; Reddy, A. L. M.; Ishikawa, Y.; Ajayan, P. M. *Carbon* **2011**, *49*, 931.
(126) Russell, A. E.; Rose, A. *Chem. Rev.* **2004**, *104*, 4613.
(127) Hansen, T. W.; Wagner, J. B.; Hansen, P. L.; Dahl, S.; Topsøe, H.; Jacobsen, C. J. H. *Science* **2001**, *294*, 1508.
(128) Hansen, P. L.; Wagner, J. B.; Helveg, S.; Rostrup-Nielsen, J. R.; Clausen, B. S.; Topsøe, H. *Science* **2002**, *295*, 2053.
(129) Hofmann, S.; Sharma, R.; Ducati, C.; Du, G.; Mattevi, C.; Cepek, C.; Cantoro, M.; Pisana, S.; Parvez, A.; Cervantes-Sodi, F.; Ferrari, A. C.; Dunin-Borkowski, R.; Lizzit, S.; Petaccia, L.; Goldoni, A.; Robertson, J. *Nano Lett.* **2007**, *7*, 602.
(130) Gontard, L. C.; Chang, L.-Y.; Hetherington, C. J. D.; Kirkland, A. I.; Ozkaya, D.; Dunin-Borkowski, R. E. *Angew. Chem., Int. Ed.* **2007**, *46*, 3683.
(131) Nørskov, J. K.; Bligaard, T.; Hvolbæk, B.; Bild-Pedersen, F.; Chorkendorff, I.; Christensen, C. H. *Chem. Soc. Rev.* **2008**, *37*, 2163.
(132) Meier, J.; Schiøtz, J.; Liu, P.; Nørskov, J. K.; Stimming, U. *Chem. Phys. Lett.* **2004**, *390*, 440.
(133) Bing, Y.; Liu, H.; Zhang, L.; Ghosh, D.; Zhang, J. *Chem. Soc. Rev.* **2010**, *39*, 2184.
(134) Jacob, T.; Goddard, W. A., III *ChemPhysChem* **2006**, *7*, 992.
(135) Haynes, C. L.; McFarland, A. D.; Smith, M. T.; Hulteen, J. C.; Van Duyne, R. P. *J. Phys. Chem. B* **2002**, *106*, 1898.
(136) Hao, E.; Schatz, G. C.; Hupp, J. T. *J. Fluoresc.* **2004**, *14*, 331.
(137) Somorjai, G. A.; *Chemistry in two dimensions: surfaces*; Conrnell University Press: Ithaca, NY, 1981.
(138) Zhang, H.; Jin, M.; Xiong, Y.; Lim, B.; Xia, Y. *Acc. Chem. Res.* **2013**, *46*, 1783.
(139) Olveira, S.; Forster, S. P.; Seeger, S. J. *Nanotechnology* **2014**, *2014*, 324089.
(140) Liu, X.; Wang, D.; Li, Y. *Nano Today* **2012**, *7*, 448.
(141) Rao, C. N. R.; Muller, A.; Cheetham, A. K. *The Chemistry of Nanomaterials: synthesis, properties and applications*; Wiley-VCH: Weinheim, Germany, 2004.
(142) Peng, X.; Manna, L.; Yang, W.; Wickham, J.; Scher, E.; Kadavanich, A.; Alivisatos, A. P. *Nature* **2000**, *404*, 59.
(143) Gudiksen, M. S.; Lauhon, L. J.; Wang, J.-F.; Smith, D. C.; Lieber, C. M. *Nature* **2002**, *415*, 617.
(144) Watanabe, K.; Menzel, D.; Nilius, N.; Freud, H.−J. *Chem. Rev.* **2006**, *106*, 4301.
(145) Burda, C.; Chen, X.; Narayanan, R.; El-Sayed, M. A. *Chem. Rev.* **2005**, *105*, 1025.
(146) Lee, H.; Habas, S. E.; Kweskin, S.; Butcher, D.; Somorjai, G. A.; Yang, P.-D. *Angew. Chem., Int. Ed.* **2006**, *45*, 7824.
(147) Stamenkovic, V. R.; Fowler, B.; Mun, B. S.; Wang, G. F.; Ross, P. N.; Lucas, C. A.; Markovic, N. M. *Science* **2007**, *315*, 493.
(148) Chen, J.; Lim, B.; Lee, E. P.; Xia, Y. *Nano Today* **2009**, *4*, 81.
(149) Narayanan, R.; El-Sayed, M. A. *Nano Lett.* **2004**, *4*, 1343.
(150) Falicov, L. M.; Somojai, G. A. *Proc. Natl. Acad. Sci. U.S.A.* **1985**, *82*, 2207.
(151) Rolison, D. R. *Science* **2003**, *299*, 1698.
(152) Chen, M. S.; Goodman, D. W. *Catal. Today* **2006**, *111*, 22.
(153) Bond, G. C. *Platinum Met. Rev.* **1975**, *19*, 126.
(154) Somorjai, G. A.; Blakely, D. W. *Nature* **1975**, *258*, 580.
(155) Wang, J.-X.; Inada, H.; Wu, L.; Zhu, Y.; Choi, Y.; Liu, P.; Zhou, W.−P.; Adzic, R. R. *J. Am. Chem. Soc.* **2009**, *131*, 17298.
(156) Xia, Y.; Yang, P.; Sun, Y.; Wu, Y.; Mayers, B.; Gates, B.; Yin, Y.; Kim, F.; Yan, H. *Adv. Mater.* **2003**, *15*, 353.
(157) Narayanan, R.; El-Sayed, M. A. *J. Phys. Chem. B* **2005**, *109*, 12663.
(158) Quan, Z.; Wang, Y.; Fang, J. *Acc. Chem. Res.* **2013**, *46*, 191.
(159) Xiong, L.; Manthiram, A. *J. Electrochem. Soc.* **2005**, *152*, A697.
(160) Kim, J. W.; Heo, J. H.; Hwang, S. J.; Yoo, S. J.; Jang, J.-H.; Ha, J.-S.; Jang, S.; Lim, T.-H.; Nam, S. W.; Kim, S-K. *Int. J. Hydrogen, Energy* **2011**, *36*, 12088.
(161) Mukerjee, S.; Srinivasan, S.; Soriaga, M. P.; McBreen, J. *J. Phys. Chem.* **1995**, *99*, 4577.
(162) Zheng, J.; Fu, R.; Tian, T.; Wang, X.; Ma, J. *Int. J. Hydrogen Energy* **2012**, *37*, 12994.
(163) Zhang, H.; Lin, D.; Xu, G.; Zheng, J.; Zhang, N.; Li, Y.; Chen, B.-H. *Int. J. Hydrogen Energy* **2015**, *40*, 1742.
(164) Gan, L.; Yu, R.; Luo, J.; Cheng, Z.; Zhu, J. *J. Phys. Chem. Lett.* **2012**, *3*, 934.
(165) Yang, H.; Alonso-Vante, N.; Léger, J.-M.; Lamy, C. *J. Phys. Chem. B* **2004**, *108*, 1938.
(166) Luo, J.; Njoki, P. N.; Lin, Y.; Wang, L.; Zhong, C. J. *Electrochem. Commun.* **2006**, *8*, 581.
(167) Kadirgan, F.; Kanna, A. M.; Atilan, T.; Beyhan, S.; Ozenler, S. S.; Suzer, S.; Yörür, A. *Int. J. Hydrogen Energy* **2009**, *34*, 9450.
(168) Golikand, A. N.; Asgari, M.; Lohrasbi, E. *Int. J. Hydrogen Energy* **2011**, *36*, 13317.
(169) Xiong, L.; He, T. *Electrochem. Commun.* **2006**, *8*, 1671.
(170) Wang, C.; Markovic, N. M.; Stamenkovic, V. R. *ACS Catal.* **2012**, *2*, 891.
(171) Paulus, U. A.; Wokaun, A.; Scherer, G. G.; Schmidt, T. J.; Stamenkovic, V.; Radmilovic, V.; Markovic, N. M.; Ross, P. N. *J. Phys. Chem. B* **2002**, *106*, 4181.
(172) Anderson, A. B.; Roques, J.; Mukerjee, S.; Murthi, V. S.; Markovic, N. M.; Stamenkovic, V. *J. Phys. Chem. B* **2005**, *109*, 1198.
(173) Wang, C.; Chi, M.-F.; Wang, G.-F.; van der Vliet, D.; Li, D.-G.; More, K.; Wang, H.-H.; Schlueter, J. A.; Markovic, N. M.; Stamenkovic, V. R. *Adv. Funct. Mater.* **2011**, *21*, 147.
(174) Matanović, I.; Garzon, F. H.; Henson, N. J. *J. Phys. Chem. C* **2011**, *115*, 10640.
(175) Oezaslan, M.; Hasché, F.; Strasser, P. *J. Electrochem. Soc.* **2012**, *159*, B394.
(176) Jeon, T.−Y.; Yoo, S. J.; Cho, Y.−H.; Kang, S. H.; Sung, Y.−E. *Electrochem. Commun.* **2010**, *12*, 1796.
(177) Schuster, R.; Ertal, G. Electrochemical Nanostructuring of Surfaces. In *Catalysis and Electrocatalysis at nanoparticle surfaces*; Wieckowski, A., Savinova, E. R., Vayenas, C. G., Eds.; Marcel Dekker: New York, 2003; Chapter 6.
(178) Maillard, F.; Schreier, S.; Hanzlik, M.; Savinova, E. R.; Weinkauf, S.; Stimming, U. *Phys. Chem. Chem. Phys.* **2005**, *7*, 385.
(179) Chen, M.; Liu, J.-P.; Sun, S.-H. *J. Am. Chem. Soc.* **2004**, *126*, 8394.
(180) Ahrenstorf, K.; Heller, H.; Kornowski, A.; Broekaert, J. A. C.; Weller, H. *Adv. Funct. Mater.* **2008**, *18*, 3850.
(181) Lamer, V. K.; Dinegar, R. H. *J. Am. Chem. Soc.* **1950**, *72*, 4847.
(182) Kim, H. U.S. Patent 7,625,637 *B2*, 2009.
(183) Sevonkaev, I.; Privman, V.; Goia, D. *J. Solid State Electrochem.* **2013**, *17*, 279.
(184) Gago, A. S.; Habrioux, A.; Alonso-Vante, N. *Nanotechnol. Rev.* **2012**, *1*, 427.
(185) Sun, S.-H.; Murray, C. B.; Weller, D.; Folks, L.; Moser, A. *Science* **2000**, *287*, 1989.
(186) Shevchenko, E. V.; Talapin, D. V.; Rogach, A. L.; Kornowski, A.; Haase, M.; Weller, H. *J. Am. Chem. Soc.* **2002**, *124*, 11480.
(187) Wang, C.; Chi, M. F.; Li, D.-G.; van der Vliet, D.; Wang, G.-F.; Lin, Q.-Y.; Mitchell, J. F.; More, K. L.; Markovic, N. M.; Stamenkovic, V. R. *ACS Catal.* **2011**, *1*, 1355.
(188) Wang, C.; van der Vliet, D.; Chang, K. C.; You, H. D.; Strmcnik, D.; Schlueter, J. A.; Markovic, N. M.; Stamenkovic, V. R. *J. Phys. Chem. C* **2009**, *113*, 19365.

DOI: 10.1021/cr500519c
Chem. Rev. 2015, 115, 3433−3467

(189) Ahrenstorf, K.; Albrecht, O.; Heller, H.; Kornowski, A.; Gorlitz, D.; Weller, H. *Small* **2007**, *3*, 271.
(190) Park, J.; Joo, J.; Kwon, S. G.; Jang, Y.; Hyeon, T. *Angew. Chem., Int. Ed.* **2007**, *46*, 4630.
(191) Porter, D. A.; Easterling, K. E. *Phase transformations in metals and alloys*, 2nd ed.; Chapman & Hall: London, 1992.
(192) Mullin, J. W. *Crystallization*, 3rd ed.; Oxford University Press: Oxford, 1997.
(193) Sugimoto, T.; Shiba, F.; Sekiguchi, T.; Itoh, H. *Colloid Surf. A: Physicochem. Eng. Asp.* **2000**, *164*, 183.
(194) Volmer, M.; Weber, A.; hem, Z. *Phys. C* **1926**, *227*, 119.
(195) Volmer, M.; *Kinetic der Phasbildung, Dresden, Steinfopff, Leipzig*, 1939.
(196) Becker, R.; Doring, W. *Ann. Phys.* **1935**, *24*, 719.
(197) Peng, X.-G.; Wickham, J.; Alivisatos, A. P. *J. Am. Chem. Soc.* **1998**, *120*, 5343.
(198) Reiss, H. *J. Chem. Phys.* **1951**, *19*, 482.
(199) Rao, Ch. V.; Viswanathan, B. *J. Phys. Chem. C* **2009**, *113*, 18907.
(200) Okaya, K.; Yano, H.; Uchida, H.; Watanabe, M. *ACS Appl. Mater. Interfaces.* **2010**, *2*, 888.
(201) Cuenya, R. R. *Thin Solid Films* **2010**, *518*, 3127.
(202) Bönnemann, H.; Nagabhushana, K. S. *J. New Mater. Electrochem. Systems* **2004**, *7*, 93.
(203) Bönnemann, H.; Nagabhushana, K. S. *Chem. Ind.* **2004**, *58*, 271.
(204) Zhou, J.; Ralston, J.; Sedev, R.; Beattie, D. A. *J. Colloid Interface Sci.* **2009**, *331*, 251.
(205) L. D. Pachón, L. D.; Rothenberg, G. *Appl. Organometal. Chem.* **2008**, *22*, 288.
(206) Ozkar, S.; Finke, R. G. *J. Am. Chem. Soc.* **2002**, *124*, 5796.
(207) Jeon, T.−Y.; Yoo, S. J.; Cho, Y.−H.; Lee, K.−S.; Kang, S. H.; Sung, Y. E. *J. Phys. Chem. C* **2009**, *113*, 19732.
(208) Zhang, H.; Jin, M.; Xia, Y. *Chem. Soc. Rev.* **2012**, *41*, 8035.
(209) Neto, A. O.; Verjulio-Silva, R. W. R.; Linardi, M.; Spinacé, E. V. *Int. J. Electrochem. Sci.* **2009**, *4*, 954.
(210) Guo, J.-W.; Zhao, T. S.; Prabhuram, J.; Wong, C. W. *Electrochim. Acta* **2005**, *50*, 1973.
(211) Ozkar, S.; Finke, R. G. *J. Am. Chem. Soc.* **2002**, *124*, 5796.
(212) Tsai, M.-C.; Yeh, T.-K.; Tsai, C.-H. *Int. J. Hydrogen Energy* **2011**, *36*, 8261.
(213) Sarkar, A.; Manthiram, A. *J. Phys. Chem. C* **2010**, *114*, 4725.
(214) Zhu, H.; Li, X.; Wang, F. *Int. J. Hydrogen Energy* **2011**, *36*, 9151.
(215) Sarkar, A.; Kerr, J. B.; Cairns, E. J. *ChemPhysChem* **2013**, *14*, 2132.
(216) Li, B.; Chan, S. H. *Int. J. Hydrogen Energy* **2013**, *38*, 3338.
(217) Almeida, T. S.; Kokoh, K. B.; De Andrade, A. R. *Int. J. Hydrogen Energy* **2011**, *36*, 3803.
(218) Kim, J.-W.; Heo, J. H.; Hwang, S.-J.; Yoo, S.-J.; Jang, J.-H.; Ha, J.-S.; Jang, S.; Lim, T.−H.; Nam, S. W.; Kim, S.−K. *Int. J. Hydrogen Energy* **2011**, *36*, 12088.
(219) Benedicte, T. *Platinum Metals Rev.* **2004**, *48*, 62.
(220) Wu, Y.; Cai, S.; Wang, D.; He, W.; Li, Y. *J. Am. Chem. Soc.* **2012**, *134*, 8975.
(221) Semagina, N.; Kiwi-Minsker, L. *Catal. Rev.* **2009**, *51*, 147.
(222) Li, H.; Sun, G.; Gao, Y.; Jiang, Q.; Jia, Z.; Xin, Q. *J. Phys. Chem. C* **2007**, *111*, 15192.
(223) Shimazaki, Y.; Kobayashi, Y.; yamada, S.; Miwa, T.; Konno, M. *J. Colloid Interface Sci.* **2005**, *292*, 122.
(224) Abedini, A.; Daud, A. R.; Hamid, M. A. A.; Othman, N. K.; Saion, E. *Nanoscale Res. Lett.* **2013**, *8*, 474.
(225) Rusnaeni, N.; Purwanto, W. W.; Nasikin, M.; Hendrajaya, L. *J. Appl. Sci.* **2010**, *10*, 2899.
(226) Oh, H. S.; Oh, J. G.; Hong, Y. G.; Kim, N. *Electrochem. Acta* **2007**, *52*, 7278.
(227) Kristian, N.; Yu, Y.; Lee, J.−M.; Liu, X.; Wang, X. *Electrochim. Acta* **2010**, *56*, 1000.
(228) Ren, G.; Shi, H.; Xing, Y. *Nanotechnology* **2007**, *18*, 385604.
(229) Gan, L.; Cui, C.; Rudi, S.; Strasser, P. *Top. Catal.* **2014**, *57*, 236.
(230) Lu, J.; Low, K.−B.; Lei, Y.; Libera, J. A.; Nicholls, A.; Stair, P. C.; Elam, J. W. *Nat. Commun.* **2014**, *5*, 3264.
(231) Li, W.; Xin, Q.; Yan, Y. *Int. J. Hydrogen Energy* **2010**, *35*, 2530.
(232) Gan, L.; Heggen, M.; Rudi, S.; Strasser, P. *Nano Lett.* **2012**, *12*, 5423.
(233) Bezerra, C. W. B.; Zhang, L.; Liu, H.; Lee, K.; Marques, A. L. B.; Marques, E. P.; Wang, H.; Zhang, J. *J. Power Sources* **2007**, *173*, 891.
(234) Singh, B.; Dempsey, E. *ECS J. Solid State Sci. Technol.* **2012**, *1*, M25.
(235) Sheng, W.; Lee, S. W.; Crumlin, E. J.; Chen, S.; Yang, S.-H. *J. Electrochem. Soc.* **2011**, *158*, B1398.
(236) Chandan, A.; Hattenberger, M.; El-kharouf, A.; Du, S.; Dhir, A.; Self, V.; Pollet, B. G.; Ingram, A.; Bujalski, W. *J. Power Sources* **2013**, *231*, 264.
(237) Antolini, E.; Passos, R. R.; Ticianelli, E. A. *Electrochim. Acta* **2002**, *48*, 263.
(238) Beard, B. C.; Ross, P. N., Jr. *J. Electrochem. Soc.* **1990**, *137*, 3368.
(239) Salgado, J. R. C.; Antolini, E.; Gonzalez, E. R. *J. Phys. Chem. B* **2004**, *108*, 17767.
(240) Santiago, E. I.; Varanda, L. C.; Villullas, H. M. *J. Phys. Chem. C* **2007**, *111*, 3146.
(241) Xiong, L.; Kannan, A. M.; Manthiram, A. *Electrochem. Commun.* **2002**, *4*, 898.
(242) Tseng, C. J.; Lo, S. T.; Lo, S. C.; Chu, P. P. *Mater. Chem. Phys.* **2006**, *100*, 385.
(243) Beard, B. C.; Ross, P. N., Jr. *J. Electrochem. Soc.* **1986**, *133*, 1839.
(244) Yano, H.; Inukai, J.; Uchida, H.; Watanabe, M.; Panakkattu, K. B.; Kobayashi, T.; Chung, J. H.; Oldfield, E.; Wieckowski, A. *Phys. Chem. Chem. Phys.* **2006**, *8*, 4932.
(245) Marković, N. M.; Schmidt, T. J.; Stamenković, V.; Ross, P. N. *Fuel Cells* **2001**, *1*, 105.
(246) Wroblowa, H. S.; Pan, Y. C.; Razumney, J. *J. Electroanal. Chem.* **1976**, *69*, 195.
(247) Kinoshita, K. *Electrochemical Oxygen Technology*; John Wiley & Sons: New York, 1992.
(248) Markovic, N. M.; Gasteiger, H. A.; Ross, P. N. *J. Electrochem. Soc.* **1997**, *144*, 1591.
(249) Zhang, J.; Vukmirovic, M. B.; Sasaki, K.; Nilekar, A. U.; Mavrikakis, M.; Adzic, R. R. *J. Am. Chem. Soc.* **2005**, *127*, 12480.
(250) Koh, S.; Strasser, P. *J. Am. Chem. Soc.* **2007**, *129*, 12624.
(251) Mukerjee, S.; Srinivasan, S. *J. Electroanal. Chem.* **1993**, *357*, 201.
(252) Toda, T.; Igarashi, H.; Uchida, H.; Watanabe, M. *J. Electrochem. Soc.* **1999**, *146*, 3750.
(253) Sung, Y.; Hwang, J.; Chung, J. S. *Int. J. Hydrogen Energy* **2011**, *36*, 4007.
(254) Jayasayee, K.; Rob Van Veen, J. A.; Manivasagam, T. G.; Celebi, S.; Hensen, E. J. M.; de Bruijn, F. A. *Appl. Catal. B Environ.* **2012**, *111*−*112*, 515.
(255) Yano, H.; Kataoka, M.; Yamashita, H.; Uchida, H.; Watanabe, M. *Langmuir* **2007**, *23*, 6438.
(256) Kinoshita, K. *J. Electrochem. Soc.* **1900**, *137*, 845.
(257) Hwang, J. T.; Chung, J. S. *Electrochim. Acta* **1993**, *38*, 2715.
(258) Maghsodi, A.; Milani Hoseini, M. R.; Dehghani Mobarakeh, M.; Kheirmand, M.; Samiee, L.; Shoghi, F.; Kameli, M. *Appl. Surf. Sci.* **2011**, *257*, 6353.
(259) Remona, A. M.; Phani, K. L. N. *J. Fuel Cell Sci. Technol.* **2011**, *8*, 011001.
(260) Álvarez, G.; Alcaide, F.; Miguel, O.; Calvillo, L.; Lázaro, M. J.; Quintana, J. J.; Calderón, J. C.; Pastor, E. *J. Solid State Electrochem.* **2010**, *14*, 1027.
(261) Mani, P.; Srivastava, R.; Strasser, P. *J. Power Sources* **2011**, *196*, 666.
(262) Oezaslan, M.; Strasser, P. *J. Power Sources* **2011**, *196*, 5240.

DOI: 10.1021/cr500519c
Chem. Rev. 2015, 115, 3433−3467

(263) Koh, S.; Yu, C.; Mani, P.; Srivastava, R.; Strasser, P. *J. Power Sources* **2007**, *172*, 50.
(264) Koh, S.; Toney, M. F.; Strasser, P. *Electrochim. Acta* **2007**, *52*, 2765.
(265) Strasser, P.; Koh, S.; Mani, P.; Ratndeep, S. U.S. Patent 7,994,089 B2, 2007.
(266) Gan, L.; Heggen, M.; O'Malley, R.; Theobald, B.; Strasser, P. *Nano Lett.* **2013**, *13*, 1131.
(267) Guo, D.-J.; Ding, Y. *Electroanalysis* **2012**, *24*, 2035.
(268) Tang, Y.; Cheng, W. *Langmuir* **2013**, *29*, 3125.
(269) Guo, S.; Zhang, S.; Su, D.; Sun, S. *J. Am. Chem. Soc.* **2013**, *135*, 13869.
(270) Wu, J.; Yang, H. *Acc. Chem. Res.* **2013**, *46*, 1848.
(271) Zhong, C.-J.; Luo, J.; Fang, B.; Wanjala, B. N.; Njoki, P. N.; Loukrakpam, R.; Yin, J. *Nanotechnology* **2010**, *21*, 062001.
(272) Tao, A. R.; Habas, S.; Yang, P. D. *Small* **2008**, *4*, 310.
(273) Yang, H.; Teng, X. W.; Maksimuk, S. In Corain, B., Schmid, C. G., Toshima, N., Eds.; *Metal Nanoclusters in Catalysis and Materials Science: The Issue of Size Control. Part II: Methodologies*; Elsevier: Amsterdam, 2008.
(274) Bönnemanna, H.; Khelashvili, G. *Appl. Organometal. Chem.* **2010**, *24*, 257.
(275) Zhou, X.; Gan, Y.; Du, J.; Tian, D.; Zhang, R.; Yang, C.; Dai, Z. *J. Power Sources* **2013**, *232*, 310.
(276) Peng, Z.-M.; Yang, S.-C.; Yang, H. In *Metallic Nanomaterials*; Kumar, C., Ed.; Wiley-VCH Verlag: Weinheim, Germany, 2009; Vol. *1*, Chapter 10.
(277) Cui, C.; Gan, L.; Heggen, M.; Rudi, S.; Strasser, P. *Nat. Mater.* **2013**, *12*, 765.
(278) Wang, C.; Xu, C.; Zeng, H.; Sun, S. *Adv. Mater.* **2009**, *21*, 3045.
(279) Li, W.; Chen, Z.; Xu, L.; Yan, Y. *J. Power Sources* **2010**, *195*, 2534.
(280) Marquardt, D.; Barthel, J.; Braun, M.; Ganter, C.; Janiak, C. *CrystEngComm* **2012**, *14*, 7607.
(281) Dutta, I.; Carpenter, M. K.; Balogh, M. P.; Ziegelbauer, J. M.; Moylan, T. E.; Atwan, M. H.; Irish, N. P. *J. Phys. Chem. C* **2010**, *114*, 16309.
(282) Lin, R.; Cao, C.; Zhao, T.; Huang, Z.; Li, B.; Wieckowski, A.; Ma, J. *J. Power Sources* **2013**, *223*, 190.
(283) Bhlapibul, S.; Pruksathorn, K.; Piumsomboon, P. *Renewable Energy* **2012**, *41*, 262.
(284) Wanjala, B. N.; Luo, J.; Loukrakpam, R.; Fang, B.; Mott, D.; Njoki, P. N.; Engelhard, M.; Naslund, H. R.; Wu, J. K.; Wang, L.; Malis, O.; Zhong, C.-J. *Chem. Mater.* **2010**, *22*, 4282.
(285) Yu, S.; Lou, Q.; Han, K.; Wang, Z.; Zhu, H. *Int. J. Hydrogen Energy* **2012**, *37*, 13365.
(286) Zhang, J.; Yang, H.; Fang, J.; Zou, S. *Nano Lett.* **2010**, *10*, 638.
(287) Wu, J.; Gross, A.; Yang, H. *Nano Lett.* **2011**, *11*, 798.
(288) Wu, J.; Zhang, J.; Peng, Z.; Yang, S.; Wagner, F. T.; Yang, H. *J. Am. Chem. Soc.* **2010**, *132*, 4984.
(289) Carpenter, M. K.; Moylan, T. E.; Kukreja, R. S.; Atwan, M. H.; Tessema, M. M. *J. Am. Chem. Soc.* **2012**, *134*, 8535.
(290) Zhang, C.; Hwang, S. Y.; Trout, A.; Peng, Z. *J. Am. Chem. Soc.* **2014**, *136*, 7805.
(291) Wu, J.; Qi, L.; You, H.; Gross, A.; Li, J.; Yang, H. *J. Am. Chem. Soc.* **2012**, *134*, 11880.
(292) Koenigsmann, C.; Santulli, A. C.; Gong, K.; Vukmirovic, M. B.; Zhou, W.; Sutter, E.; Wong, S. S.; Adzic, R. R. *J. Am. Chem. Soc.* **2011**, *133*, 9783.
(293) Zhang, Y.; Han, T.; Fang, J.; Xu, P.; Li, X.; Xu, J.; Liu, C.-C. *J. Mater. Chem. A* **2014**, *2*, 11400.
(294) Qian, Y.; Wen, W.; Adcock, P. A.; Jiang, Z.; Hakim, N.; Saha, M.; Mukerjee, S. *J. Phys. Chem. C* **2008**, *112*, 1146.
(295) Chen, C.; Kang, Y.; Huo, Z.; Zhu, Z.; Huang, W.; Xin, H. L.; Snyder, J. D.; Li, D.; Herron, J. A.; Mavrikakis, M.; Chi, M.; More, K. L.; Li, Y.; Markovic, N. M.; Somorjai, G. A.; Yang, P.; Stamenkovic, V. R. *Science* **2014**, *343*, 1339.
(296) Zhang, G.; Shao, Z.-G.; Lu, W.; Xie, F.; Qin, X.; Yi, B. *Electrochim. Acta* **2013**, *103*, 66.
(297) Han, L.; Liu, H.; Cui, P.; Peng, Z.; Zhang, S.; Yang, J. *Nature* **2014**, *4*, 6414.
(298) Wang, D.; Yu, Y.; Xin, H. L.; Hovden, R.; Ercius, P.; Mundy, J. A.; Chen, H.; Richard, J. H.; Muller, D. A.; Disalvo, F. J.; Abruña, H. D. *Nano Lett.* **2012**, *12*, 5230.
(299) Lu, W.; Liu, Q.; Sun, Z.; He, J.; Ezeolu, C.; Fang, J. *J. Am. Chem. Soc.* **2008**, *130*, 6983.
(300) Ferrando, R.; Jellinek, J.; Johnston, R. L. *Chem. Rev.* **2008**, *108*, 845.
(301) Yuan, Q.; Wang, X. *Nanoscale* **2010**, *2*, 2328.
(302) Carbonea, L.; Cozzoli, P. D. *Nano Today* **2010**, *5*, 449.
(303) Yin, Y.; Alivisatos, A. P. *Nature* **2005**, *437*, 664.
(304) Mullen, T. J.; Dameron, A. A.; Saavedra, H. M.; Williams, M. E.; Weiss, P. S. *J. Phys. Chem. C* **2007**, *111*, 6740.
(305) Maksimuk, S.; Teng, X.; Yang, H. *J. Phys. Chem. C* **2007**, *111*, 14312.
(306) Zhang, G.; Shao, Z.-G.; Lu, W.; Xiao, H.; Xie, F.; Qin, X.; Li, J.; Liu, F.; Yi, B. *J. Phys. Chem. C* **2013**, *117*, 13413.
(307) Guo, S. J.; Li, J.; Dong, S. J.; Wang, E. K. *J. Phys. Chem. C* **2010**, *114*, 15337.
(308) Ataee-Esfahani, H.; Wang, L.; Yamauchi, Y. *Chem. Commun.* **2010**, *46*, 3684.
(309) Wang, L.; Yamauchi, Y. *Chem.-Asian J.* **2010**, *5*, 2493.
(310) Wang, L.; Nemoto, Y.; Yamauchi, Y. *J. Am. Chem. Soc.* **2011**, *133*, 9674.
(311) Alexandridis, P.; Tsianou, M. *Eur. Polym. J.* **2011**, *47*, 569.
(312) Piao, Y.; Jang, Y.; Shokouhimehr, M.; Lee, I. S.; Hyeon, T. *Small* **2007**, *3*, 255.
(313) Rioux, R. M.; Song, H.; Grass, M.; Habas, S.; Niesz, K.; Hoefelmeyer, J. D.; Yang, P.; Somorjai, G. A. *Top. Catal.* **2006**, *39*, 167.
(314) Lee, E. P.; Peng, Z. M.; Cate, D. M.; Yang, H.; Campbell, C. T.; Xia, Y. *J. Am. Chem. Soc.* **2007**, *129*, 10634.
(315) Lee, E. P.; Chen, J.-Y.; Yin, Y.-D.; Campbell, C. T.; Xia, Y.-N. *Adv. Mater.* **2006**, *18*, 3271.
(316) Song, H.; Kim, F.; Connor, S.; Somorjai, G. A.; Yang, P.-D. *J. Phys. Chem. B* **2005**, *109*, 188.
(317) Chen, J.-Y.; Herricks, T.; Xia, Y.-N. *Angew. Chem., Int. Ed.* **2005**, *44*, 2589.
(318) Maksimuk, S.; Teng, X. W.; Yang, H. *Phys. Chem. Chem. Phys.* **2006**, *8*, 4660.
(319) Teng, X.-W.; Yang, H. *Nano Lett.* **2005**, *5*, 885.
(320) Yin, A.-X.; Min, X.-Q.; Zhang, Y.-W.; Yan, C.-H. *J. Am. Chem. Soc.* **2011**, *133*, 3816.
(321) Huang, X.-Q.; Tang, S.-H.; Zhang, H.-H.; Zhou, Z.-Y.; Zheng, N.-F. *J. Am. Chem. Soc.* **2009**, *131*, 13916.
(322) Huang, X.-Q.; Tang, S.-H.; Mu, X.-L.; Dai, Y.; Chen, G.-X.; Zhou, Z.-Y.; Ruan, F.-X.; Yang, Z.-L.; Zheng, N.-F. *Nat. Nanotechnol.* **2011**, *6*, 28.
(323) Subhramannia, M.; Pillai, V. K. *J. Mater. Chem.* **2008**, *18*, 5858.
(324) Zhang, X.-Y; Dong, D.-H; Li, D.; Williams, T.; Wang, H.-T; Webley, P. A. *Electrochem. Commun.* **2009**, *11*, 190.
(325) Zhang, X.-Y.; Li, D.; Dong, D.-H; Wang, H.-T; Webley, P. A. *Mater. Lett.* **2010**, *64*, 1169.
(326) Ataee-Esfahani, H.; Wang, L.; Nemoto, Y.; Yamauchi, Y. *Chem. Mater.* **2010**, *22*, 6310.
(327) Antolini, E.; Perez, J. *J. Mater. Sci.* **2011**, *46*, 4435.
(328) Yamauchi, Y.; Takai, A.; Komatsu, M.; Sawada, M.; Ohsuna, T.; Kuroda, K. *Chem. Mater.* **2008**, *20*, 1004.
(329) Mirkovic, T.; Zacharia, N. S.; Scholes, G. D.; Ozin, G. A. *ACS Nano* **2010**, *4*, 1782.
(330) Kuroda, Y.; Yamauchi, Y.; Kuroda, K. *Chem. Commun.* **2010**, *46*, 1827.
(331) Gu, D.; Schüth, F. *Chem. Soc. Rev.* **2014**, *43*, 313.
(332) Chen, H. M.; Liu, R.-S. *J. Phys. Chem. C* **2011**, *115*, 3513.
(333) Hu, J.; Chen, M.; Fang, X.; Wu, L. *Chem. Soc. Rev.* **2011**, *40*, 5472.
(334) Sui, Y. C.; Skomski, R.; Sorge, K. D.; Sellmyer, D. J. *Appl. Phys. Lett.* **2004**, *84*, 1525.

DOI: 10.1021/cr500519c
Chem. Rev. 2015, 115, 3433−3467

(335) Cheng, F.; Ma, H.; Li, Y.; Chen, J. *Inorg. Chem.* **2007**, *46*, 788.
(336) Vitos, L.; Ruban, A. V.; Skriver, H. L.; Kollár, J. *Surf. Sci.* **1998**, *411*, 186.
(337) Yang, J.; Hu, W.; Chen, S.; Tang, J. *J. Phys. Chem. C* **2009**, *113*, 21501.
(338) Baletto, F.; Ferrando, R. *Rev. Mod. Phys.* **2005**, *77*, 371.
(339) Baletto, F.; Ferrando, R.; Fortuneli, A.; Montalent, F.; Mottet, C. *J. Chem. Phys.* **2002**, *116*, 3856.
(340) Biacchi, A. J.; Schaak, R. E. *ACS Nano* **2011**, *5*, 8089.
(341) Wang, C.; Daimon, H.; Onodera, T.; Koda, T.; Sun, S. *Angew. Chem., Int. Ed.* **2008**, *47*, 3588.
(342) Ahmadi, T. S.; Wang, Z. L.; Green, T. C.; Henglein, A.; El Sayed, M. A. *Science* **1996**, *272*, 1924.
(343) Wang, Z.-L. *J. Phys. Chem. B* **2000**, *104*, 1153.
(344) Wang, C.; Daimon, H.; Lee, Y.; Kim, J.; Sun, S. *J. Am. Chem. Soc.* **2007**, *129*, 6974.
(345) Ren, J. T.; Tilley, R. D. *J. Am. Chem. Soc.* **2007**, *129*, 3287.
(346) Kang, Y.; Murray, C. B. *J. Am. Chem. Soc.* **2010**, *132*, 7568.
(347) Markovic, N. M.; Gasteiger, H. A.; Ross, P. N. *J. Phys. Chem.* **1995**, *99*, 3411.
(348) Guo, S.; Zhang, S.; Sun, S. *Angew. Chem., Int. Ed.* **2013**, *52*, 8526.
(349) Adzic, R. R.; Zhang, J.; Sasaki, K.; Vukmirovic, M. B.; Shao, M.; Wang, J.-X.; Nilekar, A. U.; Mavrikakis, M.; Valerio, J. A.; Uribe, F. *Top. Catal.* **2007**, *46*, 249.
(350) Brankovic, S. R.; Wang, J. X.; Adzic, R. R. *Surf. Sci.* **2001**, *474*, L173.
(351) Zhang, J.; Vukmirovic, M. B.; Xu, Y.; Mavrikakis, M.; Adzic, R. R. *Angew. Chem., Int. Ed.* **2005**, *44*, 2132.
(352) Nilekar, A. U.; Xu, Y.; Zhang, J.; Vukmirovic, M. B.; Sasaki, K.; Adzic, R. R.; Mavrikakis, M. *Top. Catal.* **2007**, *46*, 276.
(353) Xu, Y.; Ruban, A. V.; Mavrikakis, M. *J. Am. Chem. Soc.* **2004**, *126*, 4717.
(354) Cai, Y.; Adzic, R. R. *Adv. Phys. Chem.* **2011**, *2011*, 530397.
(355) Xu, D.; Liu, Z.; Yang, H.; Liu, Q.; Zhang, J.; Fang, J.; Zou, S.; Sun, K. *Angew. Chem., Int. Ed.* **2009**, *48*, 4217.
(356) Hammer, B.; Nørskov, J. K. *Adv. Catal.* **2000**, *45*, 71.
(357) Shao, M.; Liu, P.; Zhang, J.; Adzic, R. R. *J. Phys. Chem. B* **2007**, *111*, 6772.
(358) Sasaki, K.; Naohara, S. H.; Cai, Y.; Choi, Y. M.; Liu, P.; Vukmirovic, M. B.; Wang, J. X.; Adzic, R. R. *Angew. Chem., Int. Ed.* **2010**, *49*, 8602.
(359) Cai, Y.; Ma, C.; Zhu, Y.; Wang, J. X.; Adzic, R. R. *Langmuir* **2011**, *27*, 8540.
(360) Zhang, J.; Sasaki, K.; Sutter, E.; Adzic, R. R. *Science* **2007**, *315*, 220.
(361) Stamenkovic, V.; Schmidt, T. J.; Ross, P. N.; Markovic, N. M. *J. Phys. Chem. B* **2002**, *106*, 11970.
(362) Stamenkovic, V. R.; Mun, B. S.; Arenz, M.; Mayrhofer, K. J. J.; Lucas, C. A.; Wang, G.; Ross, P. N.; Markovic, N. M. *Nat. Mater.* **2007**, *6*, 241.
(363) Stamenkovic, V. R.; Mun, B. S.; Mayrhofer, K. J. J.; Ross, P. N.; Markovic, N. M. *J. Am. Chem. Soc.* **2006**, *128*, 8813.
(364) Stamenkovic, V.; Schmidt, T. J.; Ross, P. N.; Markovic, N. M. *J. Electroanal. Chem.* **2003**, *554*, 191.
(365) Nilekar, A. U.; Mavrikakis, M. *Surf. Sci.* **2008**, *602*, L89.
(366) Toda, T.; Igarashi, H.; Watanabe, M. *J. Electroanal. Chem.* **1999**, *460*, 258.
(367) Jalan, V.; Taylor, E. J. *J. Electrochem. Soc.* **1983**, *130*, 2299.
(368) Mukerjee, S.; Srinivasan, S.; Soriaga, M. P.; McBreen, J. *J. Electrochem. Soc.* **1995**, *142*, 1409.
(369) Malheiro, A. R.; Perez, J.; Villullas, H. M. *J. Electrochem. Soc.* **2009**, *156*, B51.
(370) Okaya, K.; Yano, H.; Kakinuma, K.; Watanabe, M.; Uchida, H. *ACS Appl. Mater. Interfaces* **2012**, *4*, 6982.
(371) Okaya, K.; Yano, H.; Uchida, H.; Watanabe, M. *ACS Appl. Mater. Interfaces* **2010**, *2*, 888.
(372) Khamskii, E. *Crystallization from solutions*; Consultants Bureau: New York, 1969.
(373) Kashchiev, D. *Nucleation: Basic theory with applications*; butterworth Heinemann: Oxford, 2000.
(374) Chambers, S. A. *Surf. Sci. Rep.* **2000**, *39*, 105.
(375) Liu, A. W. K.; Santos, M. B. *Thin films: heteroepitaxial systems*; World Scientific: Singapore, 1999.
(376) Wang, D.; Xin, H. L.; Hovden, R.; Wang, H.; Yu, Y.; Muller, D. A.; Disalvo, F. J.; Abruña, H. D. *Nat. Mater.* **2013**, *12*, 81.
(377) Wang, D.; Zhuang, L.; Lu, J.-T. *J. Phys. Chem. C* **2007**, *111*, 16416.
(378) Wang, D.; Lu, S.-F.; Jiang, S.-P. *Chem. Commun.* **2010**, *46*, 2058.
(379) Wang, D.; Lu, S.-F.; Jiang, S.-P. *Electrochim. Acta* **2010**, *55*, 2964.
(380) Wang, D.; Subban, C. V.; Wang, H.; Rus, E.; Disalvo, F. J.; Abruña, H. D. *J. Am. Chem. Soc.* **2010**, *132*, 10218.
(381) Wang, D.; Xin, H.-L.; Yu, Y.; Wang, H.; Rus, E.; Muller, D. A.; Abruña, H. D. *J. Am. Chem. Soc.* **2010**, *132*, 17664.
(382) Wang, G.; Wu, H.; Wexler, D.; Liu, H.; Savadogo, O. *J. Alloys Compd.* **2010**, *503*, L1.
(383) Choi, R.; Choi, S.; Choi, C. H.; Nam, K. M.; Woo, S. I.; Par, J. T.; Han, S. W. *Chem.—Eur. J.* **2013**, *19*, 8190.
(384) Liu, L.; Samjeske, G.; Nagamatsu, S.; Sekizawa, O.; Nagasawa, K.; Takao, S.; Imaizumi, Y.; Yamamoto, T.; Uruga, T.; Iwasawa, Y. *J. Phys. Chem. C* **2012**, *116*, 23453.
(385) Luo, M.; Wei, L.; Wang, F.; Han, K.; Zhu, H. *J. Power Sources* **2014**, *270*, 34.
(386) Zhu, H.; Luo, M.; Zhang, S.; Wei, L.; Wang, F.; Wang, Z.; Wei, Y.; Han, K. *Int. J. Hydrogen Energy* **2013**, *38*, 3323.
(387) Stassi, A.; Gatto, I.; Monforte, G.; Baglio, V.; Passalacqua, E.; Antonucci, V.; Aricò, A. S. *J. Power Sources* **2012**, *208*, 35.
(388) Aricò, A. S.; Stassi, A.; Gatto, I.; Monforte, G.; Passalacqua, E.; Antonucci, V. *J. Phys. Chem. C* **2010**, *114*, 15823.
(389) Gatto, I.; Stassi, A.; Passalacqua, E.; Aricò, A. S. *Int. J. Hydrogen Energy* **2013**, *38*, 675.
(390) Aricò, A. S.; Baglio, V.; Di Blasi, A.; Modica, E.; Antonucci, P. L.; Antonucci, V. *J. Electroanal. Chem.* **2003**, *557*, 167.
(391) Park, J.-I.; Kim, M.-G.; Jun, Y.-W.; Lee, J.-S.; Lee, W.-R.; Cheon, J. *J. Am. Chem. Soc.* **2004**, *126*, 9072.
(392) Lee, W.-R.; Kim, M.-G.; Choi, J.-R.; Park, J.-I.; Ko, S.-J.; Oh, S.-J.; Cheon, J. *J. Am. Chem. Soc.* **2005**, *127*, 16090.
(393) Shao, M.; Sasaki, K.; Marinkovic, N. S.; Zhang, L.; Adzic, R. R. *Electrochem. Commun.* **2007**, *9*, 2848.
(394) Sarkar, A.; Manthiram, A. *J. Phys. Chem. C* **2010**, *114*, 4725.
(395) Sarkar, A.; Murugan, A. V.; Manthiram, A. *Langmuir* **2010**, *26*, 2894.
(396) Brouzgou, A.; Song, S. Q.; Tsiakaras, P. *Appl. Catal. B Environ.* **2012**, *127*, 371.
(397) Kulesza, P. J.; Pieta, I. S.; Rutkowska, I. A.; Wadas, A.; Marks, D.; Klak, K.; Stobinski, L.; Cox, J. A. *Electrochim. Acta* **2013**, *110*, 474.
(398) Sauthoff, G. *Intermetallics*; VCH-Wiley: Weinheim, 1995.
(399) Pfeiler, W. *Alloy Physics: A Comprehensive Reference*; Wiley-VCH: Weinheim, 2007.
(400) Jalan, V.; Taylor, E. J. *J. Electrochem. Soc.* **1983**, *130*, 2299.
(401) Xiong, L.; Manthiram, A. *J. Mater. Chem.* **2004**, *14*, 1454.
(402) Noh, S. H.; Seo, M. H.; Seo, J. K.; Fischer, P.; Han, B. *Nanoscale* **2013**, *5*, 8625.
(403) Kim, J.; Lee, S. W.; Carlton, C.; Shao-Horn, Y. *Electrochem. Solid-State Lett.* **2011**, *14*, B110.
(404) Wang, W. H.; Tian, X. L.; Chen, K.; Cao, G. Y. *Colloid Surf. A Physicochem. Eng. Asp.* **2006**, *273*, 35.
(405) Massalski, T. B.; Murray, J. L.; Bennett, L. H.; Baker, H. *Binary Alloy Phase Diagrams*; American Society for Metals: Metals Park, OH, 1986.
(406) Kumbhar, A.; Spinu, L.; Agnoli, F.; Wang, K. Y.; Zhou, W. L.; O'Connor, C. J. *IEEE Trans. Magn.* **2001**, *37*, 2216.
(407) Hyun, M. S.; Kim, S. K.; Lee, B.; Peck, D.; Shul, Y.; Jung, D. *Catal. Today* **2008**, *132*, 138.
(408) Shimazaki, Y.; Kobayashi, Y.; Yamada, S.; Miwa, T.; Konno, M. *J. Colloid Interface Sci.* **2005**, *292*, 122.

DOI: 10.1021/cr500519c
Chem. Rev. 2015, 115, 3433−3467

(409) Deivaraj, T. C.; Lee, J. Y. *J. Power Sources* **2005**, *142*, 43.
(410) Bönnemann, H.; Richards, R. M. *Eur. J. Inorg. Chem.* **2001**, 2455.
(411) Yang, S.-C.; Peng, Z.-M.; Yang, H. *Adv. Funct. Mater.* **2008**, *18*, 1.
(412) Maksimuk, S.; Yang, S.-C.; Peng, Z.-M.; Yang, H. *J. Am. Chem. Soc.* **2007**, *129*, 8684.
(413) Travitsky, N.; Ripenbein, T.; Golodnitsky, D.; Rosenberg, Y.; Burshtein, L.; Peled, E. *J. Power Sources* **2006**, *161*, 782.
(414) Solla-Gullon, J.; Rodes, A.; Montiel, V.; Aldaz, A.; Clavilier, J. *J. Electroanal. Chem.* **2003**, *554*, 273.
(415) Lide, D. R. *CRC Handbook of Chemistry and Physics*, 88th ed.; CRC Press/Taylor and Francis: Boca Raton, FL, 2008.
(416) Lee, Y. H.; Lee, G.; Shim, J. H.; Hwang, S.; Kwak, J.; Lee, K.; Song, H.; Park, J. T. *Chem. Mater.* **2006**, *18*, 4209.
(417) Liu, Z.; Ada, E. T.; Shamsuzzoha, M.; Thompson, G. B.; Nikles, D. E. *Chem. Mater.* **2006**, *18*, 4946.
(418) Elkins, K. E.; Vedantam, T. S.; Liu, J. P.; Zeng, H.; Sun, S. H.; Ding, Y.; Wang, Z.-L. *Nano Lett.* **2003**, *3*, 1647.
(419) Biggs, T.; Cortie, M. B.; Witcomb, M. J.; Cornish, L. A. *Platinum Metals Rev.* **2003**, *47*, 142.
(420) Watanabe, M.; Tsurumi, K.; Mizukami, T.; Nakamura, T.; Stonehart, P. *J. Electrochem. Soc.* **1994**, *141*, 2659.
(421) Liu, Z.-F.; Jackson, G. S.; Eichhorn, B. W. *Angew. Chem., Int. Ed.* **2010**, *49*, 3173.
(422) Ji, X.; Lee, K. T.; Holden, R.; Zhang, L.; Zhang, J.; Botton, G. A.; Couillard, M.; Nazar, L. F. *Nat. Chem.* **2010**, *2*, 286.
(423) Ghosh, T.; Vukmirovic, M. B.; Disalvo, F. J.; Adzic, R. R. *J. Am. Chem. Soc.* **2010**, *132*, 906.
(424) Prabhudev, S.; Bugnet, M.; Bock, C.; Botton, G. A. *ACS Nano* **2013**, *7*, 6103.
(425) Zhang, S.; Hao, Y.; Su, D.; Doan-Nguyen, V. V. T.; Wu, Y.; Li, J.; Sun, S.; Murray, C. B. *J. Am. Chem. Soc.* **2014**, *136*, 15921.
(426) Hernández-Fernández, P.; Rojas, S.; Ocón, P.; Gómez de la Fuente, J. L.; San Fabián, J.; Sanza, J.; Peña, M. A.; García-García, F. J.; Terreros, P.; Fierro, J. L. G. *J. Phys. Chem. C* **2007**, *111*, 2913.
(427) Oezaslan, M.; Hasché, F.; Strasser, P. *J. Electrochem. Soc.* **2012**, *159*, B444.
(428) Zhang, K.; Yue, Q.; Chen, G.; Zhai, Y.; Wang, L.; Wang, H.; Zhao, J.; Liu, J.; Jia, J.; Li, H. *J. Phys. Chem. C* **2011**, *115*, 379.
(429) Greeley, J.; Stephens, I. E. L.; Bondarenko, A. S.; Johansson, T. P.; Hansen, H. A.; Jaramillo, T. F.; Rossmeisl, J.; Chorkendorff, I.; Norskov, J. K. *Nat. Chem.* **2009**, *1*, 552.
(430) Wells, P. P.; Qian, Y.; King, C. R.; Wiltshire, R. J. K.; Crabb, E. M.; Smart, L. E.; Thompsett, D.; Russell, A. E. *Faraday Discuss.* **2008**, *138*, 273.
(431) Ball, S. C.; Hudson, S. L.; Leung, J. H.; Russell, A. E.; Thompsett, D.; Theobald, B. R. C. *ECS Trans.* **2007**, *11*, 1247.
(432) Ball, S. C.; Theobald, B.; Thompsett, D.; Hudson, S. *ECS Trans.* **2006**, *1*, 141.
(433) Cui, C.; Gan, L.; Li, H.−H.; Yu, S.−H.; Heggen, M.; Strasser, P. *Nano Lett.* **2012**, *12*, 5885.
(434) Wagner, F. T. DOE Hydrogen and Fuel Cells Program: FY 2012 Annual Progress Report, V.D.12 High-Activity Dealloyed Catalysts, General Motors, LLC (GM).
(435) Jha, N.; Ramesh, P.; Bekyarova, E.; Tian, X.; Wang, F.; Itkis, M. E.; Haddon, R. C. *Sci. Rep.* **2013**, *3*, 2257.
(436) US-DRIVE: Fuel Cell Target Tables, http://www.uscar.org/commands/files_download.php?files_id=279; 07-27-2011.

DOI: 10.1021/cr500519c
Chem. Rev. 2015, 115, 3433−3467